Development of Minimally-Invasive Optical Methods to Individualize the Doses Used for Therapeutic Applications of Light

THÈSE N^{O} 4831 (2010)

PRÉSENTÉE LE 26 NOVEMBRE 2010

À LA FACULTÉ SCIENCES DE BASE

INSTITUT DES SCIENCES ET INGENIERIE CHIMIQUES

PROGRAMME DOCTORAL EN PHOTONIQUE

ÉCOLE POLYTECHNIQUE FÉDÉRALE DE LAUSANNE

POUR L'OBTENTION DU GRADE DE DOCTEUR ÈS SCIENCES

PAR

Filippo PIFFARETTI

acceptée sur proposition du jury:

Prof. O. Martin, président du jury
Dr G. Wagnières, directeur de thèse
Prof. Y. Barrandon, rapporteur
Prof. C. Pournaras, rapporteur
Prof. T. van Leeuwen, rapporteur

ÉCOLE POLYTECHNIQUE
FÉDÉRALE DE LAUSANNE

Suisse
2010

Abstract

Despite the experience gained over several decades in various types of light-based medical treatments, the optimization of the corresponding therapeutic protocols and accurate forecasting of their outcome have not yet been achieved in many cases. The difficulty often arises from the heterogeneity of living tissues, their variable optical properties, and from the heterogeneous distribution of the photoactive or photosensitive substances - whether naturally present in the tissue or artificially adde.

Our work focuses on the *individualization and control of irradiation parameters*, in order for the physician to be able to elicit a predictable clinical response in the irradiated tissues. In this thesis, we present three separate studies in which we tried to evaluate the possibility of individualizing and optimizing the corresponding clinical outcomes by measuring or monitoring certain, particular parameters.

In a first clinical study, performed at the medical practice of Dr Vezzola, MD, in Saló, Italy, the *human eye's retinal reflectance* was measured and mapped, in the framework of subthreshold thermal laser therapy, using an excitation wavelength identical to that of the treatment laser, *i.e.* at $810\,nm$. The specific goal of this study was to correlate the *occurrence of retinal burns* with the *measured infrared retinal reflectance*. This study was performed using a modified fundus camera to record infrared reflectance images of the retina, and by recording the slit-lamp based laser therapy parameters (irradiation parameters and spot location) in such a way so as to overlay the map of the laser treatment spots on the corresponding

reflectance fundus image. The clinical study demonstrated the expected existence of *spatial variations in light reflectance* at 810 nm (probably due to changes of the tissue absorption), which we then tried to relate to the *occurrences of retinal burns* observed during the laser treatment. The analysis of the results obtained with the applied conditions, did *not* however show a clear correlation between the local retina reflectance, the laser beam parameters, and the occurrence of retinal burns. Therefore we postulate that either the absorbing structures of the retina cannot be seen with the imaging device we used, possibly due to *its limited resolution*, or *other important elements* play a role in the laser-tissue interactions during this type of lasers-light interaction with the local retinal tissue.

The second study was pre-clinical, performed at EPFL, and aimed at monitoring in real-time the *tissular oxygen concentration* during photodynamic therapy (PDT). It was performed *in vivo* on the *chicken embryo's chorio-allantoic membrane* (CAM) model, which was submitted to aminolevulinic acid (ALA)-based PDT. The molecular oxygen, which is thought to be an essential actor in the cascade of reactions leading to the tissular PDT effect, is actually the main molecule responsible for the *photosensitizer's* (PS) triplet state quenching. Therefore, the *delayed fluorescence lifetime of the photosensitizer*, protoporphyrin IX (PpIX), was measured with a specially designed and assembled, optical fiber-based, time-resolved spectrofluorometer, and used as a *proxy for tissular* $p\mathrm{O}_2$. Simultaneously, vascular damages caused by PDT were characterized and quantified, to check for correlation between the two parameters. Using the PS's delayed fluorescence lifetime to evaluate tissular $p\mathrm{O}_2$ proved to be a quite reasonable strategy, due to the fact that *it is possible to measure the* $p\mathrm{O}_2$ *at the location of the PS molecule*. The study's results demonstrate a robust, linear correlation between *tissular* $p\mathrm{O}_2$ *reduction* and *vascular damage extent*. They also suggest that the amount of oxygen consumed during PDT could be a useful, measurable parameter for assessing and/or controlling the PDT's therapeutic effect.

The third, clinical, study aimed at measuring the *fluorescence photobleaching of the PpIX photosensitizer due to PDT*. This study was performed at the "Hôpitaux Universitaires de Genève - HUG", in Geneva, Switzerland, in collaboration with Dr Denis Salomon, MD, and Dr Behrooz Kasraee, MD, in the framework of

a series of *standard clinical PDT treatments of aktinic keratoses (AK), which is a pre-cancerous skin lesion.* The lesions' fluorescence intensity was quantified with a specially adapted quantitative imaging device, using a homogeneous and constant intensity fluorescence excitation light. The specific goal was to check for a relation between the *extent of photobleaching* of the PS (in this case PpIX, which was induced by the administration of Metvix®) and *the clinical outcome* (disappearance of AK) evaluated several months after the treatment. The study's results show that the amount of photobleached PS is strongly and linearly correlated to the fluorescence measured before the treatment. Likewise, the preliminary assessment of the clinical outcomes confirms the existence of a correlation of these outcomes with the PS's fluorescence bleaching, thus making it possible, in principle, to select and optimize the PDT's irradiation parameters before starting the treatment. The results of this study demonstrate the relevance of measuring the PS's photo-bleaching for optimizing PDT and forecasting of its outcome.

Keywords: Optic nerve head, Retina, Infrared fundus reflectance, Monitoring, Thermal laser, 810 nm, Tissular, Oxygen, *In vivo*, Lifetime, PpIX, Luminescence, Delayed fluorescence, Subthreshold, PDT, CAM, ALA, Tissular Oxygen, Vascular effect, AK, Photobleaching

Sommario

Precise previsioni degli effetti terapeutici indotti in seguito all'interazione con una radiazione luminosa restano tuttora difficili. Nonostante la grande esperienza accumulata nell'utilizzo della luce in diverse applicazioni cliniche, l'ottimizzazione dei corrispondenti protocolli terapeutici non é ancora stata raggiunta. La difficoltà nasce dalla conformazione eterogenea dei tessuti, dalle diverse caratteristiche ottiche e dalle diverse e particolari concentrazioni delle sostanze responsabili dell'assorbimento della radiazione. L'oggetto e l'obiettivo alla base dei progetti qui sviluppati consiste *nell'individualizzazione dei parametri d'irradiazione* permettendo così di ottenere, in modo sistematico, sempre la stessa risposta dai tessuti irradiati. In questa tesi sono state studiate tre situazioni, rispettivamente, tre parametri differenti per verificare se attraverso la loro misura e il loro controllo si potessero omogeneizzare e ottimizzare i risultati clinici.

Il primo progetto, portato a termine presso lo studio medico del Dr Vezzola, consiste in uno *studio clinico* nel quadro di un *trattamento laser termico* della retina. L'assorbimento del fondo retinico, valutato tramite la misura della *quantità di luce riflessa* in seguito a un'eccitazione a medesimo spettro del laser di trattamento ($810\,nm$), é stato caratterizzato e mappato. L'obiettivo specifico era di valutare l'occorrenza delle bruciature retiniche durante il trattamento laser in funzione della quantità di luce riflessa dallo stesso fondo retinico. Un fluorangiografo standard é stato dunque modificato in modo tale da poter registrare la riflessione del fondo retinico anche nello spettro infrarosso. Parallelamente, durante la terapia laser,

somministrata attraverso una lampada a fessura, i parametri d'irradiazione laser e la localizione dello spot laser sono stati registrati. In questo modo il coefficente di riflessione retinico, corrispondente alla zona irradiata da ogni singlo spot laser, ha potuto essere studiato precisamente. I risultati hanno dimostrato l'esistenza di *significative variazioni spaziali* del coefficiente di riflessione dovute probabilmente ad un assorbimento eterogeneo della radiazione luminosa. Tuttavia lo studio ha dimostrato che *non* esiste una chiara correlazione tra: il coefficiente di riflessione retinico, i parametri d'irradiazione e l'occorrenza di bruciature retiniche. Detto ciò si presume che, in questo tipo di trattamento, esistano *altri elementi* che giocano un ruolo chiave nell'interazione tra tessuto e radiazione laser; alternativamente si può pensare che le strutture responsabili dell'assorbimento non siano visibili attraverso le nostre misure, data la *limitata risoluzione* delle immagini infrarosso.

Il secondo studio, eseguito presso l'EPFL, su un modello animale *in vivo* trattato con ALA ("Chick Chorio-Allantoic Model", CAM), aveva come obiettivo, il controllo, in tempo reale e durante la terapia fotodinamica (PDT), della concentrazione dell'ossigeno molecolare ($p\mathrm{O}_2$) contenuto nei tessuti. Infatti, l'ossigeno molecolare, oltre ad essere l'attore principale nelle reazioni a catena che portano all'effetto PDT, é il principale responsabile della riduzione del tempo di vita dello stato elettronico di tripletto del fotosensibilizzatore (PS), la protoporfirina IX (PpIX). Di conseguenza, uno speciale spettrofluorimetro risolto nel tempo, basato su una singola fibra ottica, é stato costruito per poter misurare *il tempo di vita della fluorescenza ritardata* del PS e così valutare la $p\mathrm{O}_2$ nei tessuti. Contemporaneamente, l'effetto vascolare indotto dalla PDT é stato caratterizzato e quantificato, permettendo di verificare la correlazione esistente tra questi due parametri. La strategia adottata si é rivelata essere particolarmente interessante, grazie all'insita possibilità di ottenere *misure della pO_2 all'esatta corrispondenza spaziale* del PS. I risultati dello studio mostrano una correlazione consolidata tra la *riduzione della pO_2* e l'importanza dei *danni vascolari indotti.* La quantità di ossigeno consumata durante la PDT potrebbe essere dunque un parametro utile (e misurabile) per verificare, monitorare, e asservire l'irradiazione PDT e così ottimizzare gli effetti terapeutici.

Il terzo studio clinico, aveva come obiettivo la misura del *fotodecadimento del fotosensibilizzatore (PS)* durante la PDT. Lo studio é stato eseguito in collaborazione

con “les Hôpitaux Universitaires de Genève - HUG” nell’ambito di una serie di trattamenti clinici standard per il trattamento di *lesioni cutanee pre-cancerogene* (aktinic keratosis). L’intensità della fluorescenza del PS, accumulato nelle lesioni, é stata misurata tramite un’apparecchiatura costruita appositamente e caratterizzata da un’illuminazione della zona analizzata rigorosamente costante ed omogenea. L’obiettivo specifico era di studiare la correlazione esistente tra il *fotodecadimento del PS* (PpIX; indotto, in questo caso, attraverso la somministrazione di Metvix®) ed *i risultati clinici* valutati a diversi mesi dal trattamento. I risultati mostrano un robusta correlazione tra il *fotodecadimento* del PS e la fluorescenza misurata *prima* dell’illuminazione PDT. Allo stesso modo, i risultati clinici preliminari confermano l’esistenza di una tendenza verso una robusta correlazione tra il fotodecadimento e gli effetti terapeutici indotti. Con ció, diviene possibile selezionare e ottimizzare i parametri d’illuminazione della terapia PDT *prima o durante* il trattamento. Nel caso specifico del trattamento di lesioni di aktinic keratosis, il risultato di questo studio fornisce una chiara indicazione della pertinenza nell’utilizzo del *fotodecadimento* del PS per *l’ottimizzazione* dei protocolli PDT e per prevederne gli effetti terapeutici.

Parole chiave: Nervo ottico, Retina, Riflessione infrarossa, Monitoraggio, Laser termico, Sotto soglia, 810 nm, *In vivo*, Tempo di vita, PpIX, Luminescenza, Fluorescenza ritardata, PDT, CAM, ALA, Ossigeno tissulare, Effetto vascolare, AK, Fotodecadimento

– No man should escape our universities without knowing how little he knows. –

J. Robert Oppenheimer

Ai miei genitori Wilma e Giuseppe, pur restando dietro le quinte, mi hanno sempre sostenuto. Alla mia compagna, Michela, sempre attenta e sempre presente!

Contents

List of Figures

LIST OF FIGURES

List of Tables

Glossary

AK Actinic keratosis; pathological condition of the skin usually caused or stimulated by daylight

ALA 5-aminolaevulinic acid; precursor of heme

AMD Age-related Macular Degeneration; The leading cause of blindness in the United States and most Western countries. Degenerative pathology of the macular region of the retina, responsible for central vision

BK Dr Behrooz Kasraee, MD

CAM Chorioallantoic membrane, animal model

CW Continuous wave; electromagnetic wave of constant amplitude and frequency

DF Delayed fluorescence; radiative emission characterized with same spectroscopy as prompt fluorescence but having characteristic phosphorescence lifetimes

DMSO Dimethyl sulfoxide; organic solvent, readily passes through skin

DSO Digital storage oscilloscope

EDD Embryo development day

HRL Hydrodynamic rebalancing laser; innovative infrared (810 nm) laser protocol. This laser protocol is still under clinical evaluation

IC Internal conversion; non-radiative transition from a higher electronic state to a lower one

IR Infrared radiation; radiation having wavelengths in the range from 0.7 to 300 μm

IRR Infrared reflectance

ISC Intersystem crossing; electron transition form the singlet to the triplet state

MAL ALA-methylester; ALA derivative having better skin penetration kinetics than ALA

MD Medical doctor

PDT Photodynamic therapy; treatment modality which takes advantage of the photochemical interactions induced by the synergy between excitation light, tissular oxygen, and a light sensitive drug

PF Prompt fluorescence; spin-allowed radiative transition

PMT Photomultiplier tube, device characterized by several multiplying stages which enable to analyze weak emission

PPIX Protoporphyrin IX; photo active molecule produced endogenously for example during the biosynthesis heme

PRP Pan-retinal photocoagulation; commun laser protocol to treat proliferative diabetic retinopathy

PS Photosensitizer; photoactive substance

RPE Retinal pigmented epithelium; pigmented hystological layer of the inner retina

TTT Transpupillary thermotherapy; infrared (810 nm) laser therapy used to treat subfoveal choroidal neovascularisation

Introduction

1

General Objectives of the Thesis

The Biomedical Photonics Group at EPFL (Previously known as the EPFL Photomedicine Group.) is active in the field of clinical photodetection of cancers and light based therapies. Specific research interests and goals in this field focus mostly in the context of clinical applications, on optimizing the irradiation parameters, improving the selectivity of photosensitizers, the reliability of light based diagnosis, and generally ameliorating the efficacy of light based therapies.

The Group's research efforts aim at clinical, pre-clinical, and fundamental studies. In particular, we seek to get a better understanding of the mechanisms involved, to optimize the influence of specific parameters for successful photodiagnostics or for light based therapies. This strategy is due to the fact that, currently, intra- and inter- patient fluctuations, false positive or false negative detections, and lesion recurrences, still characterize the outcome of many light-based clinical applications.

The present thesis aimed at studying the possibility of individualizing and optimizing the irradiation parameters used in certain phototherapies, by measuring or monitoring, during the treatment, certain particular tissular properties. In this work, we considered three different applications and, respectively, three different tissular parameters.

The first, clinical, study aimed to analyze the influence of the near infra-red optical absorbance of the eye fundus, on the appearance of retinal burns during a subthereshold laser therapy. This was done in the hope to prevent side effects, by adapting the irradiance of the thermal laser to the local fundus reflectance.

The second, pre-clinical, study aimed to monitor the tissular molecular oxygen depletion during photodynamic therapy (PDT), a parameter known to play an important role in the

PDT effect induced in the tissue.

The third, clinical, study seeked to measure the photosensitizer (PS) photobleaching during PDT, also a parameter related to the induced PDT effect. In these two studies, measuring the considered parameter was done in the hope that its knowledge could help to reduce intra-, and inter-patient fluctuations in PDT outcome, and possibly also help optimizing and individualizing the PDT protocol itself.

2

Selected Concepts of Photomedicine

Photobiology is the study of how light - usually natural sunlight - interacts with living organisms or tissues and of physiological processes stemming from such interactions, *e.g.* photosynthesis and animal vision. Photomedicine may be considered as a sub-discipline of medicine, taking advantage of appropriate, available photobiological knowledge to study and develop the use of light - usually from an artificial source such as a lamp or a laser - for diagnosing or treating certain pathological conditions in human organs or tissues.

In this chapter, we present certain aspects of the aforementioned disciplines needed to understand the work and results reported in this thesis: an overview on optical properties of biological tissues (§2.1), an overview on light-tissue interactions (§2.2), and an overview on the physical basis of luminescence (§2.3). To conclude this introduction, we present a somewhat more detailed overview on Protoporphyrin IX, a photosensitizer used in this work (§2.4).

2.1 Tissue Optics

To study how light interacts with matter, particularly with biological tissues, we need knowledge of the studied (bio-)material's optical properties. We introduce, hereunder, the standard parameters used to characterize how illuminated biological tissues influence the propagation of the light irradiating them. Four principal interactions can be identified: reflection, refraction, absorption, and scattering. Four fundamental microscopic parameters, corresponding to these 4 light-matter interaction types characterize the optical properties of biological tissues: the absorption coefficient μ_a, the scattering coefficient μ_s, the refraction index n, and the

phase function ϕ (see Table 2.1). Mathematical modeling of the above-mentioned light-tissue interactions relies on these four (tissular) microscopic optical parameters.

The absorption and scattering coefficients μ_a and μ_s are defined to be the probability of absorption, respectively scattering, per unit path-length. Their inverse is actually the mean free path before occurrence of an absorption, respectively a scattering, event. The refraction index n, defined as the ratio of light speed in a vacuum relative to that speed in the tissue, is the main parameter responsible for light refraction and reflection. The last fundamental microscopic parameter, the phase function $\phi(\mathbf{s}, \mathbf{s}')$, describes the probability density of a photon to be scattered from direction $\mathbf{s}$ to direction $\mathbf{s}'$. Therefore, this parameter characterizes the geometric dispersion of the scattered light. By definition an *isotropic* scattering matter is characterized by $\phi(\mathbf{s}, \mathbf{s}') = \frac{\mathbf{1}}{\mathbf{4\pi}}$ (See Equation 2.1)

$$\int_{4\pi} \phi(\mathbf{s}, \mathbf{s}') \mathbf{d}\omega = \mathbf{1} \tag{2.1}$$

Using these four fundamental microscopic parameters, we can derive other, dependent quantities, often used in practice, such as the *total extinction coefficient*: $\mu_t = \mu_a + \mu_s$, and its inverse: $L_t = 1/\mu_t$, which is the *mean free optical path* of incident photons in a turbid media. Another useful parameter is the scattering distribution in a turbid media, described by the anisotropy factor g, obtained by computing the mean *cosine* of the scattering angle. The value of g, in a scale from -1 to 1, characterizes the direction of the scattering: a value of: $g = 1$ denotes *purely forward* scattering, while: $g = -1$ corresponds to *purely backward* scattering and: $g = 0$ denotes isotropic scattering. For example, in most biological tissue, the value of g ranges from 0.7 to 0.99 [16], indicating that photons are preferably scattered in the forward direction. Using g, we can compute a *reduced* scattering coefficient : $\mu'_s = (1 - g)\mu_s$, which takes into account the anisotropy of scattering in the studied media.

Nevertheless, in usual, real situations, where samples of bulk tissue are analyzed, the microscopic parameters are difficult to evaluate, as these situations are characterized by the occurrence of *multiple* scattering/absorption events. As a consequence, to characterize the optical properties of thick or massive samples, three *macroscopic* parameters are defined, : the *effective attenuation coefficient* μ_{eff}, is equal to the inverse of the tissue depth at which the incident spatial irradiance is attenuated by a factor $1/e$ (36%); the *diffuse reflectance* R is computed as the proportion of the light backscattered by the tissue; similarly, the *diffuse transmission* T is computed as the ratio of the light transmitted by the tissue relative to the light transmitted by an 100% transmission sample. It then becomes possible to evaluate the

Fundamental microscopic parameters			
μ_a		Absorption coefficient	$[cm^{-1}]$
μ_s		Scattering coefficient	$[cm^{-1}]$
n		Refraction index	
$\phi(\mathbf{s}, \mathbf{s}')$		Phase function	
Dependent microscopic parameters			
μ_t	$= \mu_a + \mu_s$	Total extinction coefficient	$[cm^{-1}]$
L_t	$= (\mu_t)^{-1}$	Free optical path length	$[cm]$
a	$= \mu_s/\mu_t$	Albedo	
g	$= \int_{4\pi} \phi(\mathbf{s}, \mathbf{s}') \cos(\omega) d\omega$	Anisotropy factor	
μ_s'	$= (1-g)\mu_s$	Reduced scattering coefficient	$[cm^{-1}]$
Macroscopic parameters			
μ_{eff}	$= \sqrt{3\mu_a(\mu_a + \mu_s')}$	Effective attenuation coefficient	$[cm^{-1}]$
d	$= 1/\mu_{eff}$	Effective penetration depth	$[cm]$
R		Diffuse reflectance	
T		Diffuse transmittance	

Table 2.1: Optical parameters used to characterize light-tissue interactions. The fundamental, microscopic parameters are the absorption coefficient (μ_a), the scattering coefficient (μ_s), the refraction index n, and the phase function (ϕ), from which all other parameters are deduced.

microscopic parameters from the macroscopic ones by using specific, theoretical models of light propagation. For example, the following relation between μ_{eff} and the microscopic parameters μ_a and μ_s' is obtained, in the context of the diffusion approximation by [27]:

$$\mu_{eff} = \sqrt{3\mu_a(\mu_a + \mu_s')} \tag{2.2}$$

The microscopic parameters of different tissues have been studied by numerous groups [25], whose measurements do not always allow for the adoption of a consensus value, for some tissue/parameter combinations.

In Table 2.2, we report these parameters for the outermost skin layer (the human epidermis),

showing their dependence on the wavelength. The reported values also support the wavelength-dependency of the effective penetration depth of light in massive samples.

Optical Parameter	Wavelenght [nm]	
$[cm^{-1}]$	400	630
μ_a	15	2
μ_s	900	70
μ'_s	300	20
g	0.74	0.8

Table 2.2: Typical microscopic optical parameters for the human skin epidermis [23]

Typical values for the effective penetration depth ($1/\mu_{eff}$) for tissues like the skin (See Figure 2.1(a)) varies from several hundreds of μm to some mm in the red and near infrared ($600 - 900\,nm$). Blue light ($\approx 400\,nm$), by contrast, will only penetrate several tens of μm. It is worth noting that, in the clinical field, the penetration depth is now frequently defined as the depth where the incident light is decreased by one order of magnitude (*i.e.* $I = 0.1 \times I_0$) rather than the theoretically correct factor of $1/e$ (*i.e.* $I = 0.36 \times I_0$). As a consequence, "decadic" penetration depths defined in this way are much larger: thus, in normal skin, we would have a "decadic" penetration of : $300 - 400\,\mu m$ at 400 nm and $6 - 7\,mm$ at 600 nm [2, 26].

Different studies were conducted to find out the main parameters influencing the penetration depth. Obeid et al. [17], for example, while studying the penetration of red light in the skin (at $630\,nm$), observed a significant - and expected - correlation with the so-called *Fitzpatrick skin type*[1]. In this case the penetration depth ranging form $600\,\mu m$ to $1500\,\mu m$ is probably limited by absorption of the melanin, which is found in different concentration in the six skin "types".

Indeed, light absorption plays an important role in photomedical applications, the major light-absorbing molecules in mammalian tissues being: oxy- and deoxy-hemoglobin, melanin, myoglobin and water, see Figure 2.1(b). Examination of these absorption spectra helps to define the optical therapeutic window to find a strategy to efficiently treat the target lesions.

[1]The Fitzpatrick skin type scale, developed in 1975 by T.B. Fitzpatrick, classifies the response of the different types of skin to UV light, on a 0-100 scale, divided in 6 types. It describes several lumped properties: genetic, reaction to solar UV light and tanning habits. For example: "Type II (scores 8-16): white; fair; red or blond hair; blue, hazel or green eyes; Usually burns, tans with difficulty"

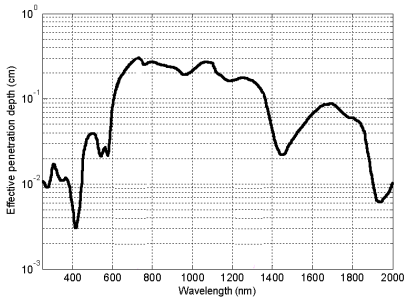

(a) Effective penetration depth in breast tissue

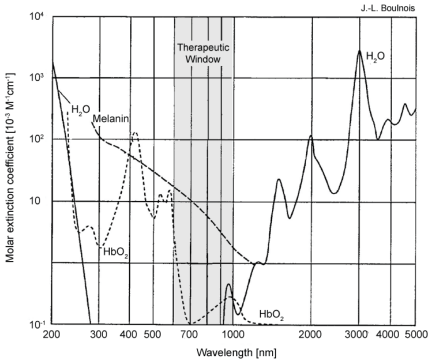

(b) Principal absorbers in biological tissue

Figure 2.1: (a) Typical penetration depth of light in the skin as a function of light wavelength, adaptated form Vo-Dinh and Masters [27]. (b) Absorption spectra of commonly found absorbing molecules in living tissues, showing the "therapeutic optical window" between 600 and 1000 nm [3].

2.2 Light-Tissue Interactions

This discussion focuses on some of the different types of phenomenae which can be observed when light is applied to biological tissue. For convenience a laser light source is considered to support the following discussion, due to its monochromaticity, short pulse duration, and high radiance. However, similar observations can be inferred for non-coherent light sources, provided that these sources allow for the tissue irradiance and exposure times, needed to observe all the different types of possible light-tissue interactions [4].

Tissue characteristics as well as parameters of the laser irradiation may lead to a diversity of outcomes. The laser light delivered is characterized by its wavelength (in nm), duration or exposure time (in s), and tissue irradiance in (W/cm^2). Among these, for a given amount of applied energy density, the exposure time appears as a crucial discriminant between different types of interactions.

Following the invention of the laser by Maiman [13], many studies were conducted to investigate its potential effects on tissues, using all kinds of laser systems and tissue targets. Eventually a consensus emerged and resulted in five main categories of interaction types, still in use today: photochemical interactions, thermal interactions, photoablation, plasma induced ablation, and photodisruption. The domains (in terms of exposure time and power density), where these five basic interaction types are usually observed are shown in Figure 2.2.

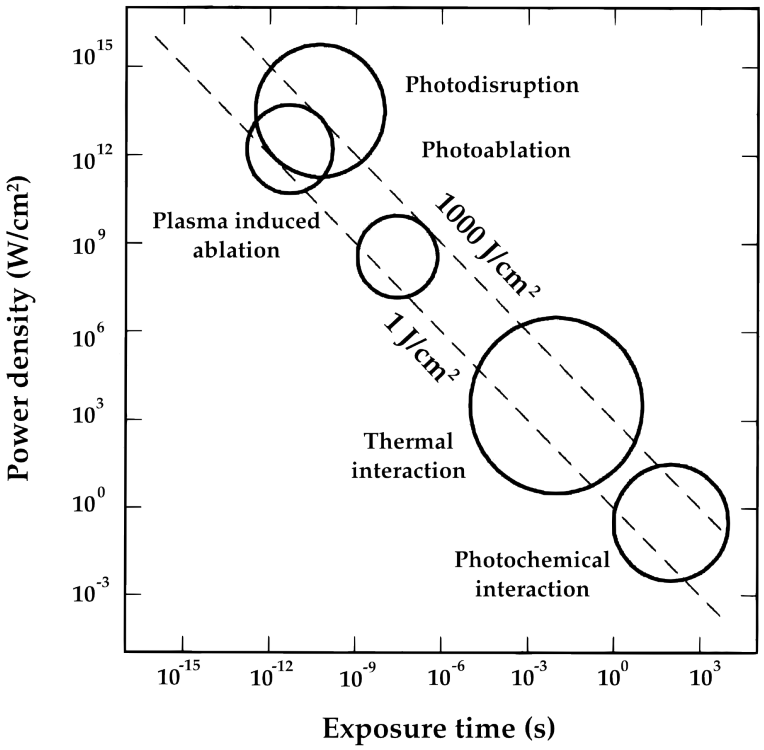

Figure 2.2: Map of laser tissue interactions. (The ordinate expresses the applied power density or irradiance in W/cm^2. The abscissa represents the exposure time in seconds. Two diagonals show constant radiant energy densities at $1\,J/cm^2$ and $1000\,J/cm^2$, respectively) The circles give a rough estimate of the associated laser parameters. Adapted from Boulnois [3]

These characteristic domains fall roughly between two parallel diagonal lines, corresponding to constant radiant energy density of 1 J/cm^2 and $1000\,J/cm^2$, respectively. According to this chart, and at these energy levels, the exposure time scale can be roughly divided into five sections [16]:

- photochemical interactions, from several thousands seconds down to $1\,s$;
- thermal interactions, from several tens of seconds down to several μs;
- photoablation, from $1\,\mu s$ down to $1\,ns$ and
- plasma-induced ablation and photodisruption, for exposure times shorter than $1\,ns$ (in this case we can observe an overlap, depending on optical dose).

Hereunder, we will focus specifically on *thermal interactions*, which are at the core of the

work described in Part I, and on *photochemical interactions*, which are essential for the work reported in Parts II and III.

2.2.1 Thermal Interactions

When discussing thermal interactions, the principal effect sought is the heating of the irradiated sample. In general, photothermal processes originate via a two step precess. First the excitation light is absorbed and the energy of photons is transfered to the electronic, and/or vibrational, and/or rotational, excited states of the irradiated molecules. Successively, these excited molecules de-excites (with decay lifetimes form 10^{-13} to $10^{-12}\,s$), through non-radiative de-excitation (thermalization), giving their energy to adjacent molecules, increasing the system's kinetic energy, and by definition, also the temperature of the irradiated tissues. The two-step reaction, leading to local temperature increase, can be schematically represented as [3]:

$$\begin{aligned} &\textit{Absorption} && A + h\nu \rightarrow A^* \\ &\textit{Thermal relaxation} && A^* + M(E_{cin}) \rightarrow A + M(E_{cin} + \Delta E_{cin}) \end{aligned}$$

where A represent the target molecule, which is promoted, following photon absorption, to an electronically and/or vibrationally excited state A^*. Thereafter, by collision or inelastic scattering, the kinetic energy of an adjacent partner molecule (M) is increased through the transfer of the excess internal energy of A^*.

Thanks to the numerous possible thermal decay pathways, a photothermal process is highly efficient. Moreover, by comparing the typical energies of laser photons (Er:YAG laser: 0.35 eV; Nd:YAG laser: 1.2 eV; ArF laser: 6.4 eV) with the kinetic energy of a molecule at room temperature (0.025 eV) we see that the absorption of a single photon can easily lead to a very large and quick temperature increase.

The peak value of the temparature reached, and the period during which the increased tissue temperature is maintained, will actually define the tissue response to light radiation. In practice, independently form the administration mode (through continuous wave (CW) laser radiation or pulsed laser), carefull adaptation of the exposure time may lead to four main different outcomes: coagulation, vaporization, carbonization, and melting.

As an example, the histological appearance of coagulated tissue is illustrated in figure 2.3, where 120 pulses from an Er:YAG laser were applied to an excised cornea. Coagulated tissue

appears significantly darker than other tissue, when staining the tissue with hematoxylin and eosin. During the process of coagulation, temperatures reach at least $60\,°C$, and coagulated tissue becomes necrotic [16]

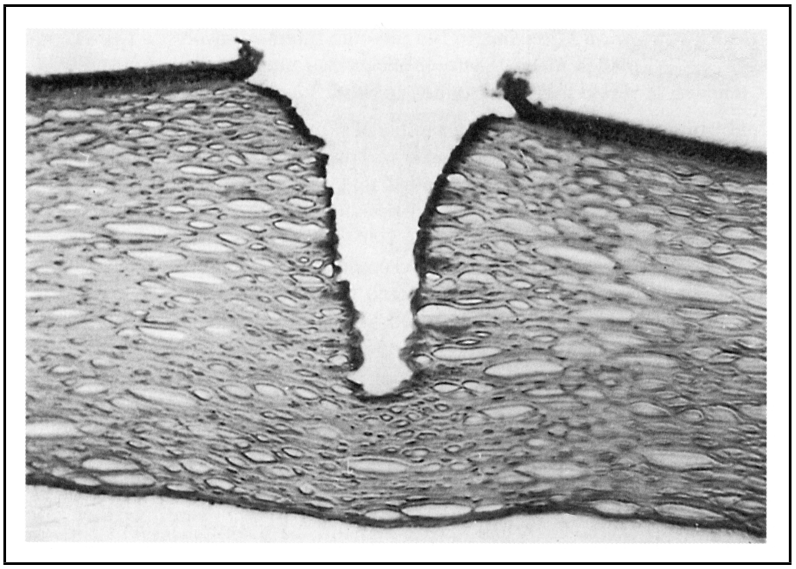

Figure 2.3: Human cornea coagulated with 120 pulses from an Er:YAG laser. Figure adapted from [16](pulse duration: $90\,\mu s$, pulse energy $5\,mJ$, repetition rate: $1\,Hz$, bar: $100\,\mu m$)

By carefully examining Figure 2.3 we may see that the irradiated tissue is being affected at the absorption location, but also, that the thermal effect affects deeper structures. These irreversible structural changes, induced by the photothermal process, reflect tissue thermogenesis caused by thermal conduction of the absorbed incident power. In order to minimize thermal damage to the zones adjacent to the irradiation location, and obtain a smaller necrotic zone, it is important to adjust the irradiation exposure time. The scaling parameter for this time-dependent thermal conduction process is called the *thermal relaxation time*, τ_T, obtained by equating the characteristic optical penetration light depth L ($L = \frac{1}{\alpha}$) to the characteristic, time-dependent, thermal penetration depth, z_T ($z_T(t) = \sqrt{4\kappa t}$). The optical penetration depth and thermal penetration depth, are respectively the parameters that characterize the distance at which a light irradiation and a temperature drop by a factor of 36% ($1/e$) is observed. Consequently, τ_T is defined as the threshold time needed to confine the temperature increase to a depth on the order of the optical penetration depth (see Equation 2.3).

$$L = \sqrt{4\kappa\tau_T} \tag{2.3}$$

where κ (cm^2/s) is the tissue diffusivity, a lumped physical parameter characterizing the material's thermal response (which depends on thermal conductivity, specific heat and density). For example, the diffusivity of liquid water is $\kappa \approx 1.4 \times 10^{-3}\, cm^2/s$.

Therefore, a clinical thermal laser application has to be carefully designed in order to provoque strictly localized effects (thermal confinement). This is especially important in opthalmologic laser treatments of the retina, where the usual target tissue, the retinal pigmented epithelium (RPE), is immediately adjacent to the visual photoreceptors layer, which is only a few tens of μm away. Thus, to avoid iatrogenic blind spots in the field of view of the treated patient, the diffusion of heat away from the absorption site has to be carefully controlled.

Along these lines, retinal *subthreshold* laser therapies were recently introduced: they consist in application of thermal laser radiations, inducing a well localized temperature increase, deemed useful to promote the healing effect, but simultaneously avoiding any thermal denaturation of the photoreceptor layers (*i.e.* "retinal burns").

2.2.2 Photochemical Interactions

A light-tissue interaction is considered as being "photochemical" when it can empirically be observed that light has caused chemical effects and/or reactions within the tissue, its compartments or its macromolecules. One of the best examples was created by evolution itself, *the photosynthesis*. For a photochemical interaction to exist, a specific chromophore must be present in the tissue (the chlorophyll in the vegetal tissue, in the case of photosynthesis) which will usually act as the catalytist of some specific chemical reaction or set of reactions (the production of carbo-hydrates from water and carbon dioxyde, in the case of photosynthesis). As shown in Figure 2.2 photochemical interactions are usually induced at very low power densities (typically $1\, W/cm^2$) and long exposure times (ranging from tens of seconds to several minutes), and photochemical processes can thus be initiated with simple, non-coherent light sources or even by daylight (*e.g.* photosynthesis, sun-tanning). Hence, to obtain a desired photochemical reaction, without undesirable, *thermal* side-effects, low power densities and long exposure times are preferred.

Photochemical interactions are at the root of most mechanisms involved in *photodynamic therapy* (PDT). PDT is a treatment modality which takes advantage of the effects induced by light in the tissue, tissular oxygen, and a light sensitive drug, the photosensitizer (PS) [5]. A PS, with known spectral properties, is administered to the target tissue, where the above mentioned photochemical reactions are triggered by applying light from a source spectrally

matched to the PS's absorption spectra. This results in the formation of cytotoxic products, mainly reactive oxygen species (ROS), which may destroy, or provoque the death of target cells, organs or tissue components.

From a photochemical perspective (see Figure 2.4) the energy of the absorbed light photon, promotes the photosensitizer molecule to an electronically excited singlet state (^{1}PS). From there, three routes are available: the radiative or non-radiative relaxations of the excited singlet molecule to its ground state (^{0}PS), and intersystem crossing of the excited singlet to an excited triplet state (^{3}PS*) which, finally, may in turn, either relax to the ground state (by non-radiative or radiative routes), or take part in one of several sets of photochemical reactions, with the tissular substrate and tissular oxygen (See §2.3 for details).

The radiative decays of the excited singlet and excited triplet states of the PS are called fluorescence and phosphorescence, respectively. Typical lifetimes of fluorescence are of the order of nanoseconds, whereas phosphorescence may last several milliseconds, up to seconds. Thus, excited triplet PS molecules, which do not immediately relax to the ground state, may interact with the surrounding environment and molecules during a relatively long time period: according to Foote [7], this mainly takes place by two competing photochemical pathways, known as Type I and Type II mechanisms (Fig. 2.4). They are characterized by either the generation of free radicals or radical-ions (Type I), or the transfer of energy to tissular oxygen molecules, which are excitated to their highly reactive singlet state, noted here as $^1O_2$ for short (Type II).

In Type I reactions, the triplet state PS interacts with any nearby molecule - other than oxygen - producing free neutral or ionized radicals. Further reaction of these radicals with triplet oxygen may lead to the formation of hydrogen dioxide or superoxide anions.

In Type II reactions, the triplet state PS directly reacts with molecular triplet oxygen $^3O_2$ which is promoted to its excited singlet state $^1O_2$. Such triplet-triplet reactions are highly favored [10].

Both, type I and type II photochemical reactions occur in parallel, and both may produce ROS that will interact with cells, inducing apoptosis, or leading directly to necrosis via oxidative processes. The relative importance of the two reaction paths depends on several parameters, the nature of the photosensitizer used and the oxygen concentration being the most important [7, 18]. Nevertheless, for most photosensitizers employed in PDT, type II photochemical reactions represent the dominant process [9, 28]. This is the case for Protoporphyrin IX [5, 24], the photosensitizer used in the experiments developed in Parts II and III of the present work.

2.3 Physico-Chemical Aspects of Luminescence

In Parts II and III of this thesis, we seek to monitor two specific parameters, the PS's delayed fluorescence (DF) lifetime and the PS's fluorescence photobleaching, respectively, in view of optimizing the clinical outcome of PDT. In this section of our introduction, we offer an overview of some aspects of luminescence, necessary to understand these two parameters.

Luminescence is the phenomenon of light emission by a system. Depending on the nature of the excitation mechanism (which promoted the system from its ground to its excited state), this light emitting phenomenon is called chemiluminescence, bioluminescence, electroluminescence, cathodoluminescence, or photoluminescence. In the studies presented here, we are mainly interested in *photo*luminescence, as the system (the PS) is excited with visible light. Photoluminescence, in turn, can be categorized as fluorescence or phosphorescence, depending on the nature of the system's excited state: Fluorescence corresponds to the decay of a short-lived, excited singlet state, while phosphorescence is caused by the decay of a longer-lived, excited triplet state. The various molecular processes related to luminescence are conveniently represented in a so-called Jablonski diagram, see Figure 2.5. In this diagram, some of the electronic (thick horizontal lines) and vibrational (thin horizontal lines) energy levels, or states, of a specific molecule are represented, as well as some of the relevant state transitions (*i.e.* energy conversions).

We will focus here on only two physico-chemical process, the "quenching" of an excited state and the "photobleaching", both relevant for this work.

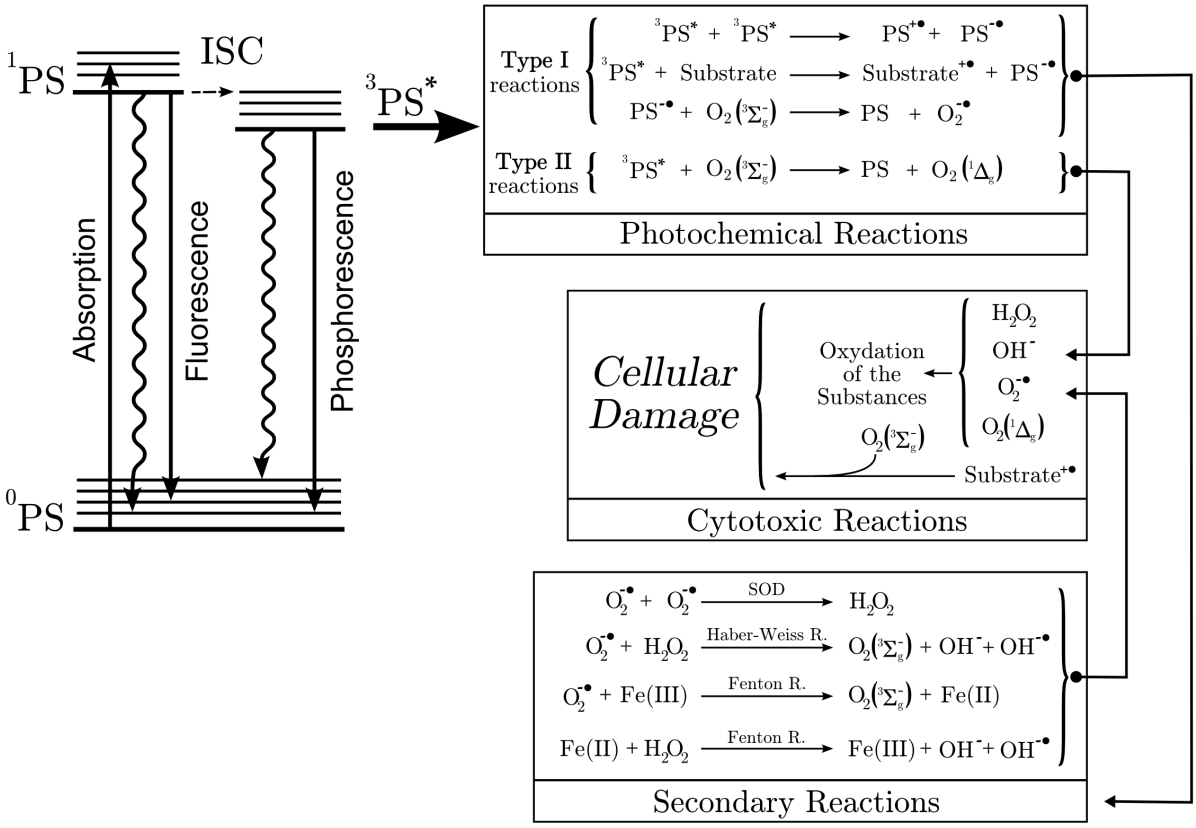

Figure 2.4: Photochemical reaction pathways of an irradiated photosensitizer molecule, PS: If the excited PS molecule does not relax through fluorescence, phosphorescence or non-radiative decay, it may take part in a number of photochemical reactions, following either the Type I or Type II initial mechanisms, with the substrate or tissular oxygen, in its triplet ground state $O_2(^3\Sigma_g^-)$. This results in the production of reactive oxygen species (ROS), causing dose-dependent cellular damage. The most important ROSs are: H_2O_2, hydrogen peroxide; $O_2(^1\Delta_g)$, singlet oxygen (excited state); $O_2^{-\bullet}$, superoxide anion; and $OH^{-\bullet}$, the hydroxyl radical. Other species involved: SOD, superoxide dismutase; $X^{+/-}$, anion/cation species; $X^{\bullet}$, radical species. Adapted from a figure published by [20].

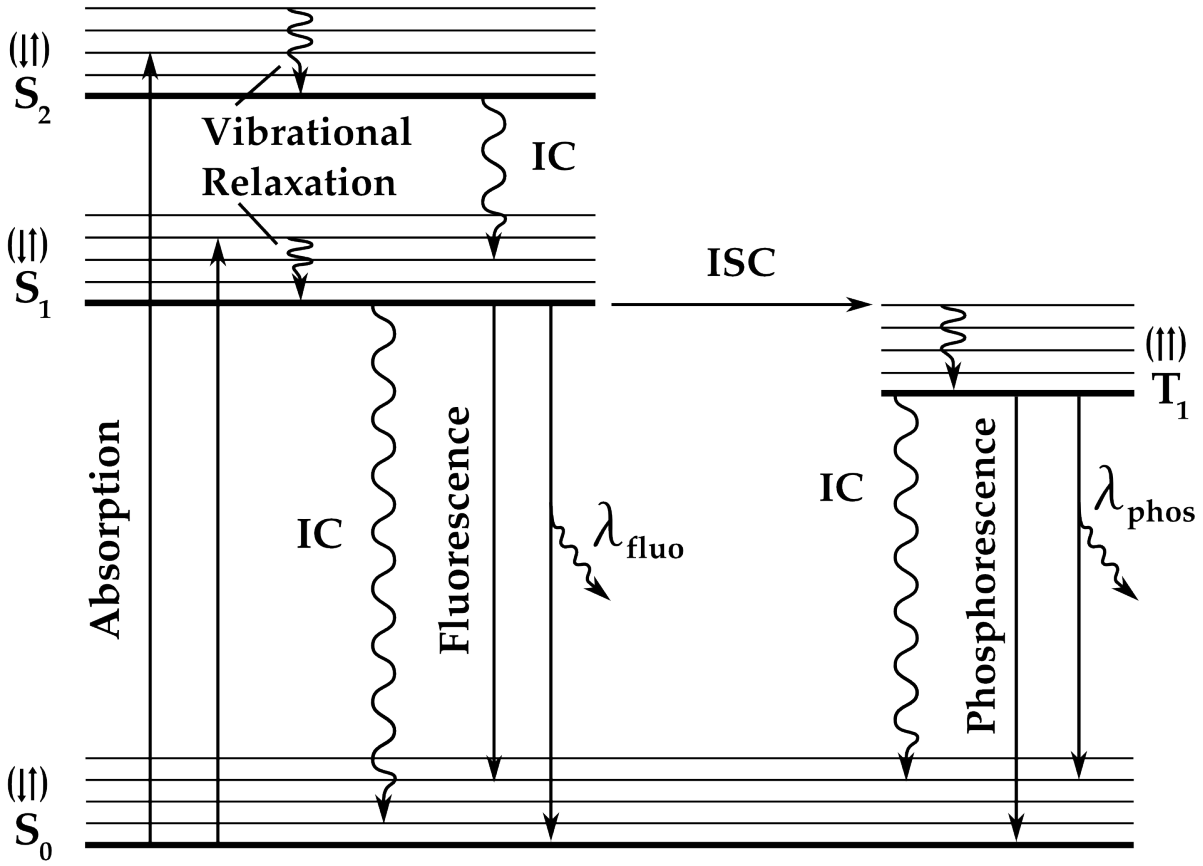

Figure 2.5: Jablonski diagram of a luminescent molecule. The diagram indicates, with thick horizontal lines, the ground state (S_0), the first and second electronically excited singlet states (S_1 and S_2), and the first (electronically) excited triplet state (T_1) of the molecule, each with its vibrational levels (thin lines). Transitions between the energy levels are depicted by vertical arrowṡ: straight arrows for radiative transitions, wavy arrows for non-radiative decays. The molecule is promoted to an electronically excited singlet states by the absorption of light, possibly relaxing very rapidly ($< 10^{-12}\,s$) to its vibrational ground state ("vibrational relaxation"). Internal conversion (IC) is the non-radiative transition from a higher electronic state to a lower one. Fluorescence is the radiative transition of a molecule from a higher electronic singlet state to its ground state S_0. Typically, these transitions occur within $10^{-9}\,s$. Intersystem crossing (ISC) describes the transition between an excited singlet state of the molecule and its triplet state. Such transitions are quantum mechanically "forbidden" and therefore "long-lived" ($\approx 10^{-3}\,s$). The emission of light resulting from the radiative de-excitation of the triplet called phosphorescence.

2.3.1 Quenching of Excited States

For a normally luminescent molecule, total or partial replacement of its (luminescent) radiative relaxation route by a radiationless (non-luminescent) decay, due to its interacting with an adequate species - the quencher - through electronic energy or charge transfer, is known as "quenching" (of the luminescence). Thus, any molecule causing a decrease in the luminescence intensity of a PS (or, more generally, a fluorophore) is considered as a "quencher" [10, 15].

Quenching resulting from collisional encounters between the PS and quencher is called collisional or dynamic quenching. In this case, upon contact with the quencher, the excited fluorophore returns to its ground state, without emission of photons or structural change of the fluorophore - the latter in contrast with certain other types of quenching mechanisms - [19]. This quenching phenomenon has been widely studied and is still used to characterize processes in many biochemical applications. For example, in photodynamic therapy (see §2.2.2), the triplet state of the PS is dynamically quenched by tissular molecular O_2, which leads to the production of the useful, cytotoxic ROSs such as $^1O_2$. A fundamental characteristic of dynamic quenching is the existence of a relationship between quencher concentration and: (i) the intensity of the radiative decay, (ii) the lifetime of the excited state being quenched. Dynamic quenching is described by the well-known Stern-Volmer equation 2.4:

$$F_0/F = \tau_0/\tau = 1 + k_q\tau_0[\mathrm{Q}] \tag{2.4}$$

where F_0, τ_0 and F, τ are the intensity and lifetime of the radiative decay in the absence, respectively the presence of quencher. k_q is the bimolecular quenching constant, and [Q] is the concentration of quencher.

In Part II of this thesis, a specific instrument was developed to measure the lifetime of the PS's triplet state during PDT, in view of evaluating the tissular oxygen concentration, oxygen being a known quencher.

2.3.2 Photobleaching

Photobleaching is defined as an irreversible photochemical destruction of a fluorophore. As a rule, photobleaching represents a limitating factor in many optical based diagnostic methods and therapeutic treatments. Note, however, that in certain photomedical applications, such

as *fluorescence recovery after photobleaching*, the induced local destruction of a specific fluorophore is used to analyze the lateral diffusion and the association and disassociation coefficients characterizing the binding of proteins to cellular structures.

During PDT, ROSs (*e.g.* $^1O_2$) generated by the photochemical reactions, are thought to be the main responsible, not only for induced tissue effects, but also for the observed photobleaching of the PS. Consequently, under certain conditions, the photobleaching may be linearly correlated with the induced tissular effect [6, 24, 29]. One important condition to meet, in order to observe this relation, is that molecular oxygen has to be abundantly present in the treated tissue, to avoid being a limiting factor in the PDT effect.

In Part III of this thesis, we check if the clinical outcome of PDT, performed on a superficial skin condition (actinic keratosis), can be predicted by measuring the amount of photobleached PS.

2.4 Protoporphyrin IX

In view of optimizing PDT, various photosensitizing drugs have been developed. On the other hand, two classes of photosensitizers can be distinguished: exogenous PSs and endogenously induced fluorochromes, i.e fluorochromes that are not directly administered to the patient but generated by the patient's organism after application of a precursor, either topically or systemically. PpIX is such an endogenous photosensitizer. The build-up of PpIX in the patient's body is promoted by administering a specific precursor, 5-aminolaevulinic acid (ALA), either systemically, or topically to the target tissue. PpIX is considered as an efficient PS, thanks to the high observed $^1O_2$ quantum yield [21], with a high sensitizing potential. It can be used for treating many conditions in different body locations. On the other hand, PpIX is an intermediate species in the biosynthesis of heme, the iron-containing constituent of hemoglobin. PpIX is therefore produced and present in almost all mammalian cells. It is to be noted that a chronic, excessive accumulation of PpIX leads to different severe condition, one among these is called erythropoietic protoporphyria [22], causing permanent light sensitization and liver disfunction. Luckily, a transient, selective accumulation of PpIX in a target organ does not present adverse effects other than transient photosensitization of the administered zone. Moreover the clearance of the accumulated excess of PpIX is relatively fast (less than 48h).

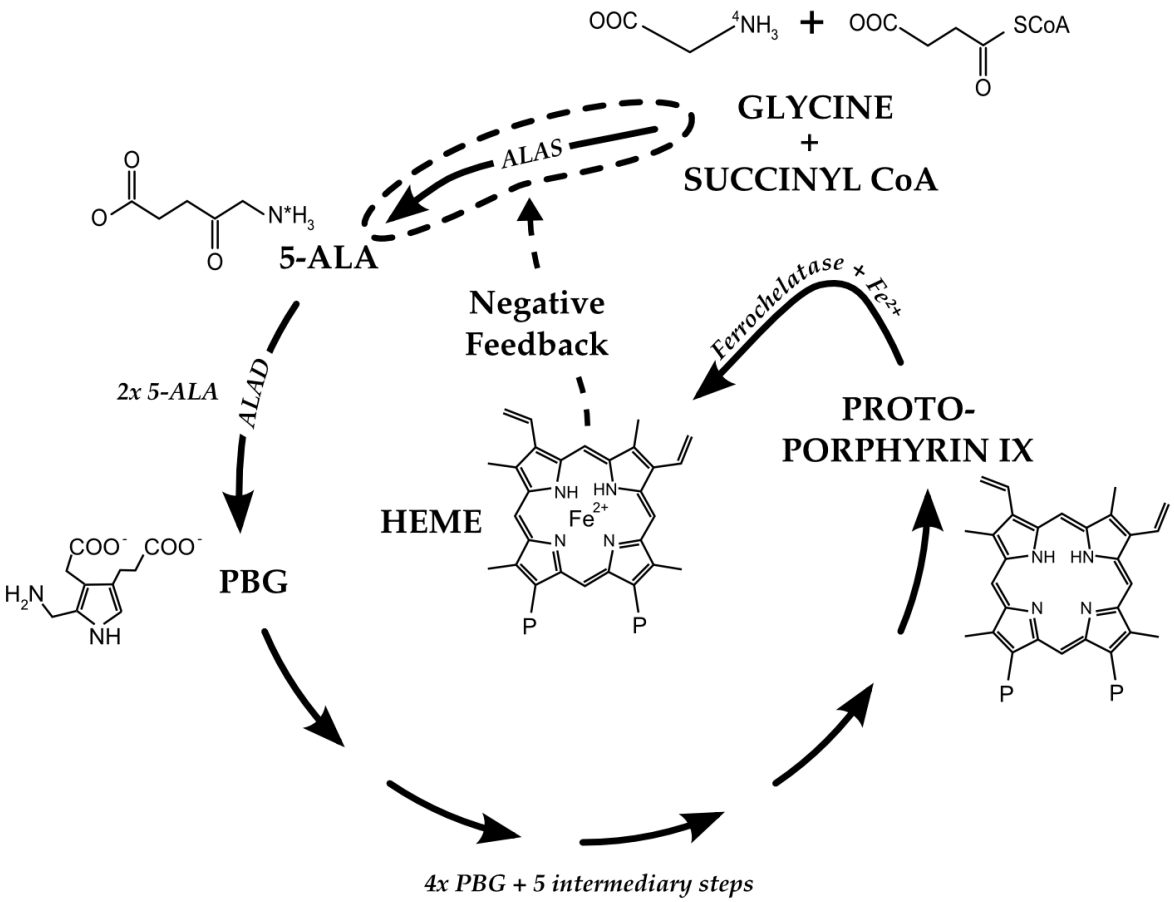

Figure 2.6: Heme's simplified biosynthesis. A first enzyme, 5-aminolevulinate synthase (ALAS), catalyzes the reaction of glycine with succinyl CoA, giving one molecule of 5-aminolevulinic acid (5-ALA). This is followed by the condensation of two 5-ALA molecules, catalyzed by the enzyme 5-aminolevulinate dehydratase (ALAD), into one molecule of porphobilinogen (PBG). An enzymatic cascade of reactions then converts four molecules of PBG, in several steps, into one molecule of protoporphyrin IX (PpIX). Heme is produced when the enzyme ferrochelatase inserts a ferrous iron into PpIX. To note the negative feedback exerted by the presence of Heme on the first catalysis reaction leeding to the biosynthesis of 5-ALA. A: acetate; P: propionate. Adapted and simplified from [8].

2.4.1 Biosynthesis of Protoporphyrin IX

PpIX is produced during the biosynthesis cycle of heme. This cycle is depicted in the simplified Figure 2.6.

The initial step is the condensation of glycine and succinyl coenzyme A (succinyl CoA) to 5-ALA (ALA for short) in the mitochondrion. The ALA molecule passes into the cytoplasm where it is first dimerized to PBG, 4 molecules of which undergo various chemical reactions, regulated by enzymes, to produce, in several steps, the phototoxic PpIX. The last step is the chelation, enabled by the enzyme ferrochelatase, of a ferrous iron ion (Fe^{2+}) into the porphyrin ring, resulting in the non-fluorescent heme molecule. The heme molecule is then further transformed to hemoglobin. On the other hand, ALA production is regulated by heme through a negative feedback mechanism, *i.e.* a cellular increase of the concentration of heme (itself derived from ALA, through the PpIX) inhibits the normal, biologic pathway of ALA production.

ALA (Levulan®) is one of the most common, photomedically approved, precursor of PpIX. Several derivatives of ALA are also in medical use, such as, for example, its methyl ester (MAL, Metvix®) and its hexyl ester (HAL, Hexvix®). Exogenously administered ALA (or one of its derivatives) appears to "fool" the negative feedback mechanism of heme production. Thus, the external application of ALA can lead to a temporary accumulation of PpIX. The amount of accumulated PpIX depends on the cell type or pathology. For instance certain, neoplastic cells show a higher accumulation of PpIX after administration of exogenous ALA than healthy ones. The resulting fluorescence intensity contrast between healthy tissues and lesions is used in ALA-induced PpIX fluorescence, for detection of dysplasia and early neoplasia [11, 12, 14].

2.4.2 Spectral Properties of Protoporphyrin IX

Studying the PpIX's emission and excitation spectra (see Fig. 2.7), they show that this PS may be excited at several wavelength. In particular we observe a small but significant absorption in the red spectrum ($630 - 635\,nm$). As described in §2.1, this portion of the spectrum is of high interest due to the high penetration of red light ($6 - 7\,mm$) in soft tissues. Thus, PDT might be efficiently administrated also to relatively deep seated structures in the tissues.

Simultaneously, the possibility to efficiently excite PpIX with shorter wavelengths, is of interest if the lesions are confined to the superficial layers of the target tissue. Thus the PDT selectivity could be further enhanced. Different studies have, for example, analyzed the induced

pain during PDT in function of the PDT illumination wavelength. It was shown that at shorter wavelength ($405\,nm$) the pain experienced by the patients was significantly reduced even if the photochemotherapeutic dose is kept constant [1].

To conclude, PpIX's many useful properties explain why it is considered as a excellent photosensitizer, which is used in a number of clinical applications.

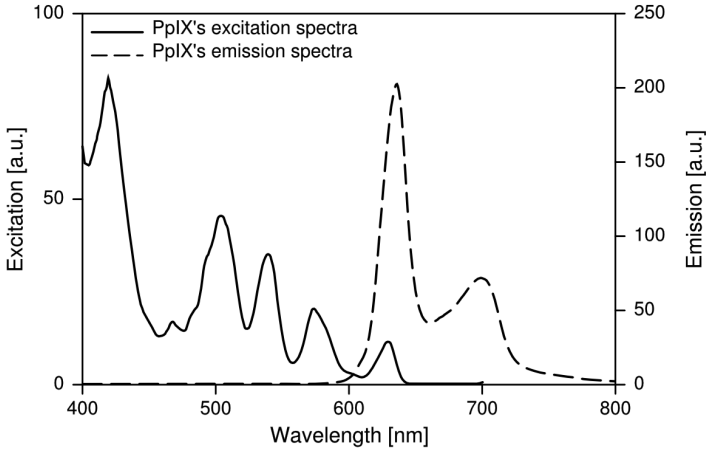

Figure 2.7: PpIX's emission (Ex. at 405 nm) and excitation (Em. at $\approx$ 700 nm) spectra

2.5 Applications of Selected Concepts

We have briefly introduced some of the relevant aspects of photomedicine necessary to understand the work developpes in this thesis. We will now present the three different developed topics. Part I presents a clinical study aiming to improve the control over a subthreshold thermal laser therapy. In this study the reflectance of the eye fundus was measured to verify whether a correlation exists with the aptitude to create "retinal burns".

Part II, present a pre-clinical *in vivo* study where we evaluates whether of the PpIX's delayed fluorescence is a valuable parameter to control and predict the PDT vascular effect in the chick chorioallantoic membrane model.

Finally, the third project, a clinical study, analyses the PpIX's fluorescence photobleaching during a superficial PDT skin treatment, see Part III. The aim, of this study was to evaluate whether the photobleaching is a valuable parameter to predict the clinical outcome of PDT treatment for actinic keratosis.

References

[1] J. Barge, T. Glanzmann, H. van den Bergh, and G Wagnières. Correlation between ppix fluorescence and both tissular effects and pain induced by pdt on normal skin using fluorescence imaging. *IPA*, 2007. Abstract. 22

[2] V. Barun, A. Ivanov, A. Volotovskaya, and V. Ulashchik. Absorption spectra and light penetration depth of normal and pathologically altered human skin. *Journal of Applied Spectroscopy*, 74(3):430–439, 2007. doi: http://dx.doi.org/10.1007/s10812-007-0071-2. 8

[3] J. L. Boulnois. Photophysical processes in recent medical laser developments: A review. *Lasers in Medical Science*, 1(1):47–66, 1986. doi: http://dx.doi.org/10.1007/BF02030737. xvii, 9, 10, 11

[4] F. Cammarata and M. Wautelet. Medical lasers and laser-tissue interactions. *Physics Education*, 34(3):156–161, 1999. URL `http://stacks.iop.org/0031-9120/34/156`. 9

[5] A. Curnow, J C. Haller, and S G. Bown. Oxygen monitoring during 5-aminolaevulinic acid induced photodynamic therapy in normal rat colon. comparison of continuous and fractionated light regimes. *J Photochem Photobiol B*, 58(2-3):149–55, November 2000. ISSN 1011-1344. 13, 14

[6] J. S. Dysart and M. S. Patterson. Photobleaching kinetics, photoproduct formation, and dose estimation during ala induced ppix pdt of mll cells under well oxygenated and hypoxic conditions. *Photochem Photobiol Sci*, 5(1):73–81, January 2006. ISSN 1474-905X. 19

[7] C. S. Foote. Definition of type i and type ii photosensitized oxidation. *Photochem Photobiol*, 54(5):659, November 1991. ISSN 0031-8655. 14

[8] N. Fotinos, M. A. Campo, F. Popowycz, R. Gurny, and N. Lange. 5-aminolevulinic acid derivatives in photomedicine: Characteristics, application and perspectives. *Photochem Photobiol*, 82(4):994–1015, 2006. ISSN 0031-8655. 20

[9] T. Ito. Cellular and subcellular mechanisms of photodynamic action: the 1o2 hypothesis as a driving force in recent research. *Photochem Photobiol*, 28(4-5):493–508, 1978. ISSN 0031-8655. 14

[10] J. R. Lakowicz. *Principles of Fluorescence Spectroscopy*. Springer, 3rd ed. edition, 1983. ISBN 0-387-31278-1. 14, 18

[11] A Leunig, C S Betz, M Mehlmann, H Stepp, S Arbogast, G Grevers, and R Baumgartner. Detection of squamous cell carcinoma of the oral cavity by imaging 5-aminolevulinic acid-induced protoporphyrin ix fluorescence. *Laryngoscope*, 110(1): 78–83, January 2000. ISSN 0023-852X. 21

[12] Blaise Lovisa, Patrice Jichlinski, Daniela Aymon, Bernd-Claus Weber, Hubert van den Bergh, and Georges Wagnieres. Bladder cancer detection by fluorescence imaging with hexvix: optimization of the excitation light during high magnification cystoscopy. volume 7368, page 73681I. SPIE, 2009. doi: 10.1117/12.831565. URL `http://link.aip.org/link/?PSI/7368/73681I/1`. 21

[13] T. H. Maiman. Optical and microwave-optical experiments in ruby. *Phys. Rev. Lett.*, 4(11):564–566, Jun 1960. doi: 10.1103/PhysRevLett.4.564. 9

[14] A Marti, P Jichlinski, N Lange, J-P Ballini, L Guillou, H J Leisinger, and P Kucera. Comparison of aminolevulinic acid and hexylester aminolevulinate induced protoporphyrin ix distribution in human bladder cancer. *J Urol*, 170(2 Pt 1):428–32, August 2003. ISSN 0022-5347. 21

[15] W. Melhuish. Nomenclature, symbols, units and their usage in spectrochemical analysis—vi molecular luminescence spectroscopy. *Spectrochimica Acta*, 37(3):259–272, 1982. 18

[16] M. H. Niemz. *Laser-Tissue Interactions: Fundamentals and Applications*, volume XVI of *Biological and Medical Physics, Biomedical Engineering*. Springer, 3rd enlarged edition, 2004. ISBN 978-3-540-72191-8. 6, 10, 12

[17] A. N. Obeid, D. M. Boggett, N. J. Barnett, G. Dougherty, and P. Rolfe. Depth discrimination in laser doppler skin blood flow measurement using different lasers. *Med Biol Eng Comput*, 26 (4):415–9, July 1988. ISSN 0140-0118. 8

[18] M. Ochsner. Photophysical and photobiological processes in the photodynamic therapy of tumours. *Journal of Photochemistry and Photobiology. B, Biology*, 39(1):1–18, 5 1997. 14

[19] L. K. Patterson, G. Porter, and M. R. Topp. Oxygen quenching of singlet and triplet states. *Chemical Physics Letters*, 7 (6):612–614, 1970. doi: DOI:10.1016/0009-2614(70)87019-1. 18

[20] K. Plaetzer, B. Krammer, J. Berlanda, F. Berr, and T. Kiesslich. Photophysics and photochemistry of photodynamic therapy: Fundamental aspects. *Lasers in Medical Science*, 24(2):259–68, 3 2009. doi: 10.1007/s10103-008-0539-1. 16

[21] R. W. Redmond and J. N. Gamlin. A compilation of singlet oxygen yields from biologically relevant molecules. *Photochem Photobiol*, 70(4):391–475, October 1999. ISSN 0031-8655. 19

[22] U. B. Rüfenacht, L. Gouya, X. Schneider-Yin, H. Puy, B. W. Schäfer, R. Aquaron, Y. Nordmann, E. I. Minder, and J. C. Deybach. Systematic analysis of molecular defects in the ferrochelatase gene from patients with erythropoietic protoporphyria. *Am J Hum Genet*, 62(6):1341–52, June 1998. ISSN 0002-9297. 19

[23] Elena Salomatina, Brian Jiang, John Novak, and Anna N Yaroslavsky. Optical properties of normal and cancerous human skin in the visible and near-infrared spectral range. *J Biomed Opt*, 11(6):064026, 2006. ISSN 1083-3668. 8

[24] C. Sheng, P. J. Hoopes, T. Hasan, and B. W. Pogue. Photobleaching-based dosimetry predicts deposited dose in ala-ppix pdt of rodent esophagus. *Photochem Photobiol*, 83 (3):738–48, 2007. ISSN 0031-8655. 14, 19

[25] V. Tuchin. *Tissue Optics: Light Scattering Methods and Instruments for Medical Diagnosis, Second Edition (SPIE Press Monograph Vol. PM166)*. SPIE Publications, 2nd edition, 2002. 7

REFERENCES

[26] M. C. van Gemert and A. J. Welch. Clinical use of laser-tissue interactions. *IEEE Eng Med Biol Mag*, 8(4):10–3, 1989. ISSN 0739-5175. 8

[27] T. Vo-Dinh and B. R. Masters. Biomedical photonics handbook. *Journal of Biomedical Optics*, 9(5):1110–1111, 2004. doi: 10.1117/1.1776177. URL `http://link.aip.org/link/?JBO/9/1110/1`. 7, 9

[28] K. R. Weishaupt, C. J. Gomer, and T. J. Dougherty. Identification of singlet oxygen as the cytotoxic agent in photoinactivation of a murine tumor. *Cancer Res*, 36(7 PT 1):2326–9, July 1976. ISSN 0008-5472. 14

[29] B. Wilson, M. Patterson, and L. Lilge. Implicit and explicit dosimetry in photodynamic therapy: a new paradigm. *Lasers in Medical Science*, 12(3):182–199, 1997. doi: http://dx.doi.org/10.1007/BF02765099. 19

Part I

Clinical Reflectance Imaging of the Eye Fundus at 810 nm to Optimize the Treatment of the Retina by Hydrodynamic Rebalancing Laser

3

Introduction

3.1 A brief Overview of Lasers in Ophthalmology

The laser has become a standard tool for the treatment and diagnostic of various conditions affecting the eye, including the retina [16, 18, 21, 23, 24, 26, 27]. Many retinal conditions can be more or less efficiently treated by delivering suitable laser light: age-related macular degeneration (AMD) [1, 18], diabetic retinopathy, retinal tears [2, 3], macular edema [7] and intraocular tumors [4, 19]. In certain cases (*e.g.* retinal tears), the laser is used to perform a mechanical welding of the retinal layers. In some other pathologies (*e.g.* diabetic retinopathy), the periphery of the retina is denatured, in order to increase the amount of oxygen in the treated area and in the macular region, thereby preserving central vision. In many ophthalmologic laser treatements, photothermal reactions is the main interaction modality, as it is the case during pan-retinal photocoagulation (PRP) which is used to treat for instance diabetic retinopathy [8, 10, 15, 20].

Photothermal regimes and thus photocoagulation can cause undesired modifications of the irradiated tissue (*e.g.* retinal burns). If such burns occur in the retinal layers (see Figure 3.1), they can produce a transient whitish lesion, and may result in a permanent local scotoma (*i.e.* area of diminished vision) in the patient's field of view. Even though retinal burns are still the endpoint for different laser therapies [14], it was shown that clinical efficacy is not always related to the extent or appearance of those tissue modifications [6, 12, 13, 17].

Large variations in the optical properties of the retina in the visible and/or the near infrared have been demonstrated by other groups [4, 5, 9, 11, 25]. In order to improve the laser treatment safety by preventing the retinal burns, we had in mind to reduce the laser irradiation time or

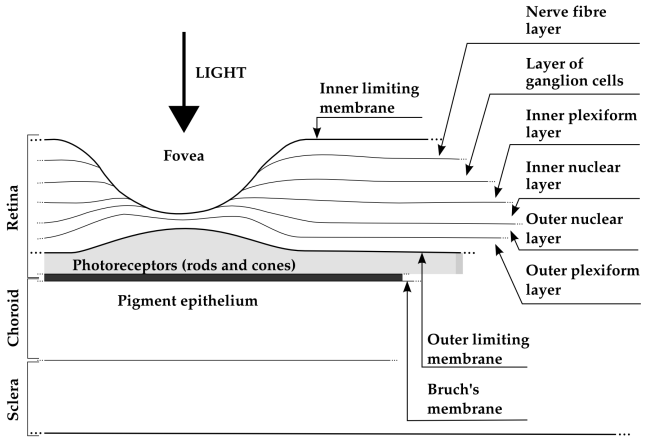

Figure 3.1: Histological layers of the human eye fundus (adapted from Polyak [22])

the laser irradiance if the local retinal area presents a strong absorbtion. We tried to validate this strategy during the retinal treatment with a new and promising subthreshold infrared ($810\,nm$) laser therapy, namely the hydrodynamic rebalancing laser (HRL).

3.2 Objectives of this Work

The present work aimed at investigating if the observed side effects ("retinal burns") during HRL therapy were correlated with the presence of highly absorbing structures in the fundus tissue. In order to reach this goal, a standard fundus camera was modified to record the eye fundus reflectance at the same wavelength as the treatment laser ($810\,nm$).

The presence of highly absorbing structures was evaluated by recording an infrared reflectance image ($810\,nm$) just before the onset of HRL treatment. During HRL treatment, the exact retinal location and the irradiation parameters of each HRL laser spot were recorded. Additionally, the clinician reported each laser spot that led to the formation of "retinal burns".

Knowing the exact position of the infrared laser spots we could study the local infrared reflectance of the fundus and so evaluate the correlation with the aptitude to create "retinal burns".

Thanks to the vivid collaboration between the Biomedical Photonics-EPFL laboratory and the two medical doctors: Dr Vezzola and Dr Sickenberg we designed, a clinical study in order to investigate whether the HRL could be optimized. In Chapter 4, we present the results of this clinical study, performed in the private clinical practice of Dr Vezzola in Saló, Italy.

References

[1] D. V. Alfaro. *Age-Related Macular Degeneration: A Comprehensive Textbook*. Lippincott Williams & Wilkins, 1 edition, 2005. 27

[2] A. S. Banker and W. R. Freeman. Retinal detachment. *Ophthalmol Clin North Am*, 14(4):695–704, December 2001. ISSN 0896-1549. 27

[3] H. Y. Cho, Y. T. Kim, and S. W. Kang. Laser photocoagulation as adjuvant therapy to surgery for large macular holes. *Korean J Ophthalmol*, 20(2):93–8, June 2006. ISSN 1011-8942. 27

[4] B. P Connolly, C. D. Regillo, R. C. Eagle, C. L. Shields, J. A. Shields, and H. Moran. The histopathologic effects of transpupillary thermotherapy in human eyes. *Ophthalmology*, 110(2):415–20, February 2003. ISSN 0161-6420. 27

[5] F. C. Delori and K. P. Pflibsen. Spectral reflectance of the human ocular fundus. *Applied Optics*, 28(6):17, 3 1989. 27

[6] G. Dorin. Subthreshold and micropulse diode laser photocoagulation. *Semin Ophthalmol*, 18(3):147–53, September 2003. ISSN 0882-0538. 27

[7] S. S. Hayreh. Management of central retinal vein occlusion. *Ophthalmologica*, 217(3):167–88, 2003. ISSN 0030-3755. 27

[8] Y. J. Hu. Pain relief during panretinal photocoagulation for diabetic retinopathy. *Eye (Lond)*, [Epub ahead of print], March 2010. ISSN 1476-5454. 27

[9] M. R. Jerath, D. Kaisig, H. G. Rylander III, and Ashley J. Welch. Calibrated real-time control of lesion size based on reflectance images. *Appl. Opt.*, 32(7):1200–1209, 1993. URL `http://ao.osa.org/abstract.cfm?URI=ao-32-7-1200`. 27

[10] R. S. Kaiser, M. G. Maguire, J. E. Grunwald, D. Lieb, B. Jani, A. J. Brucker, A. M. Maguire, A. C. Ho, and S. L. Fine. One-year outcomes of panretinal photocoagulation in proliferative diabetic retinopathy. *Am J Ophthalmol*, 129(2):178–85, February 2000. ISSN 0002-9394. 27

[11] C. N. Keilhauer and F. C. Delori. Near-infrared autofluorescence imaging of the fundus: visualization of ocular melanin. *Invest Ophthalmol Vis Sci*, 47(8):3556–64, August 2006. ISSN 0146-0404. 27

[12] P. Lanzetta, G. Dorin, A. Pirracchio, and F. Bandello. Theoretical bases of non-ophthalmoscopically visible endpoint photocoagulation. *Semin Ophthalmol*, 16(1):8–11, March 2001. ISSN 0882-0538. 27

[13] M. L. Laursen, F. Moeller, B. Sander, and A. K. Sjoelie. Subthreshold micropulse diode laser treatment in diabetic macular oedema. *Br J Ophthalmol*, 88(9):1173–9, 9 2004. 27

[14] M. A. Mainster. Decreasing retinal photocoagulation damage: principles and techniques. *Semin Ophthalmol*, 14(4):200–9, December 1999. ISSN 0882-0538. 27

[15] A. L. McKenzie. Physics of thermal processes in laser-tissue interaction. *Phys Med Biol*, 35(9):1175–209, September 1990. ISSN 0031-9155. 27

[16] G. A. Moo-Young. Lasers in ophthalmology. *West J Med*, 143 (6):745–50, December 1985. ISSN 0093-0415. 27

[17] C. M. Moorman and A. M. Hamilton. Clinical applications of the micropulse diode laser. *Eye (Lond)*, 13 (Pt 2):145–50, April 1999. ISSN 0950-222X. 27

[18] M. B. Parodi, G. Virgili, and J. R. Evans. Laser treatment of drusen to prevent progression to advanced age-related macular degeneration. *Cochrane Database Syst Rev*, 1(3):CD006537, 2009. ISSN 1469-493X. 27

[19] R. Parrozzani, B. Boccassini, V. De Belvis, P. P. Radin, and E. Midena. Long-term outcome of transpupillary thermotherapy as primary treatment of selected choroidal melanoma. *Acta Ophthalmol*, [Epub ahead of print], September 2008. ISSN 1755-3768. 27

[20] Y. M. Paulus, A. Jain, R. F. Gariano, B. V. Stanzel, M. Marmor, M. S. Blumenkranz, and D. Palanker. Healing of retinal photocoagulation lesions. *Invest Ophthalmol Vis Sci*, 49(12): 5540–5, December 2008. ISSN 1552-5783. 27

[21] J. S. Pollack, J. E. Kim, J. S. Pulido, and J. M. Burke. Tissue effects of subclinical diode laser treatment of the retina. *Arch Ophthalmol*, 116(12):1633–9, December 1998. ISSN 0003-9950. 27

[22] S.L. Polyak. *The Retina*. Chicago: University of Chicago Press, 1941. p. 201. xvii, 28

[23] F. Ricci, F. Missiroli, F. Regine, M. Grossi, and G. Dorin. Indocyanine green enhanced subthreshold diode-laser micropulse photocoagulation treatment of chronic central serous chorioretinopathy. *Graefes Arch Clin Exp Ophthalmol*, 247(5):597–607, May 2009. ISSN 1435-702X. 27

[24] J. Roider. Laser treatment of retinal diseases by subthreshold laser effects. *Semin Ophthalmol*, 14(1):19–26, March 1999. ISSN 0882-0538. 27

[25] J. Sandeau, J. Kandulla, H. Elsner, R. Brinkmann, G. Apiou-Sbirlea, and R. Birngruber. Numerical modelling of conductive and convective heat transfers in retinal laser applications. *J Biophotonics*, 1(1):43–52, March 2008. ISSN 1864-0648. 27

[26] S. H. Sarks, J. J. Arnold, J. P. Sarks, M. C. Gilles, and C. J. Walter. Prophylactic perifoveal laser treatment of soft drusen. *Aust N Z J Ophthalmol*, 24(1):15–26, February 1996. ISSN 0814-9763. 27

[27] M. Sculpher. A preliminary economic evaluation of the diode laser in ophthalmology. *Lasers in Medical Science*, 8(3):163–169, 1993. doi: http://dx.doi.org/10.1007/BF02547872. 27

4

HRL Monitoring (Submitted Paper)

Pilot study: Reflectance Imaging of the Human Eye Fundus at 810 nm to Optimize the Hydrodynamic Rebalancing Laser Treatment of Retinal Disease

Filippo Piffaretti, Jean-Pierre Ballini, Roberto Perotti, Edoardo Vezzola, Michael Sickenberg, Georges Wagnières

Federal Institute of Technology Lausanne (EPFL)
Lausanne, Switerland

Keywords: Optic nerve head, Retina, Infrared fundus reflectance, Monitoring, Thermal laser, Near infrared, 810 nm, Subthreshold

Abbreviation: (AMD) Age-related macular degeneration, (PRP) Pan-retinal photocoagulation, (RPE) Retinal pigmented epithelium,(TTT) Transpupillary thermotherapy, (HRL) Hydrodynamic rebalancing laser, (ONH) Optic nerve head, (IR) Infrared, (IRR) Infrared reflectance

Abstract

In the *Hydrodynamic Rebalancing Laser* (HRL) treatment of eye disease, the prediction of the exact response of the retinal tissue to the thermal diode laser (810 nm) is not trivial. HRL is a novel ophthalmic therapy based on the administration of focused, sub-threshold near infrared radiation to selected spots of the eye's fundus. We are interested in the parameters responsible for the heterogeneity of tissue responses. Variation of the tissular optical absorbance at the laser's wavelength was hypothesized to be a main cause of the observed uneven tissue response, including the undesired occurence of burns. We therefore studied the normalized *fundus reflectance* at 810 nm with a standard fundus camera, whose response was extended to the near-infrared spectral region. Thus, for each laser spot, we recorded the location (with a resulotion of about $20\,\mu m$), the irradiation parameters and the tissue response, in order to discover any measurable correlation between tissue response and the value of the local, normalized, infrared fundus reflectance.

The results do not show any clear correlation. There may be several reasons for this, one being that the geometrical resolution of the reflectance images, taken with our infrared fundus camera, is not sufficient to see "small" (typically $10\,\mu m$ in diameter) absorption centers. Moreover, due to the weak absorbance of the fundus, and to the significant scattering of the near infrared laser light, it is not easy to distinguish between reflected and scattered light. Although local variations of the fundus optical absorption almost certainly play an important role in the occurrence of burns, other tissue parameters, that influence heat diffusion, and thus the temperature increases induced by the laser, also had to be discussed and analyzed in the framework of our experimental results. We conclude that standardizing the results of HRL therapy, or any similar infrared diode laser-based therapy, by adapting the laser pulses to local optical properties will require more sophisticated technologies. Including imaging the retina's reflectance with an improved resolution.

4.1 Introduction

The laser has become a standard tool for the treatment and diagnostic of various conditions affecting the eye including the retina [58, 63, 68, 71, 72, 75, 76]. Many retinal conditions such as age-related macular degeneration (AMD) [2, 63], diabetic retinopathy, retinal tears [5, 17], macular edema[34] and intra ocular tumors [18, 64] can be more or less efficiently treated by delivering suitable laser light. In certain cases (*e.g.* retinal tears) the laser is just used to perform a mechanical welding of the retinal layers. Other laser therapies include the treatment of secondary cataract with pulsed YAG lasers, the treatment of glaucoma, and the correction of vision. In some other pathologies (*e.g.* diabetic retinopathy) the periphery of the retina is denatured as the oxygen amount delivered to the inner retina of those treated areas increases and thereby potentially helps to preserve central vision. In some cases, the mechanisms that lead to improvement of the vision are not yet fully understood and are the object of much ongoing research. Despite the observed treatment efficacy, a deeper understanding of the mechanism of the treatments is still needed for further optimization.

The regimes and types of laser-tissue interactions commonly used in these retinal treatments are either photochemical or photothermal. Photochemical reactions take place, for example, during the treatment of exudative AMD by photodynamic therapy [78, 84, 87]. Photothermal reactions are, instead, the main interaction modality during pan-retinal photocoagulation (PRP) [36, 41, 57, 65] which is used to treat for instance diabetic retinopathy. Photothermal regimes and, more particularly, photocoagulation can cause undesired modifications of the irradiated tissue, among which retinal burns. If such burns are induced in the neuronal layers, they can produce a transient whitish lesion, significantly increasing light scattering, and may result in a permanent local scotoma in the patient's field of view.

Even though the denaturation of the neuronal layers are still common in different laser therapies [51], the clinical efficacy was shown to be independent from the extent or appearance of those tissue modifications [9, 24, 47, 48, 60]. Several new irradiation protocols in ophthalmology, known as "subthreshold protocols" which also rely on somewhat different laser sources have been developed. They aim at a controlled and limited temperature increase of the neuronal retinal layers and seek to avoid retinal burns [25, 47, 57].

[1]The thermal relaxation time, τ_T, of a tissue is a time-scaling parameter of the thermal conduction process. It is obtained by equating the characteristic optical penetration depth, L, to the time-dependent characteristic thermal penetration depth, $z_T(t) = \sqrt{4kt}$, where k is the tissue thermal diffusivity of the tissue. Thus:

The temperature increase can be restricted to the irradiated tissues if the laser irradiation period is kept much shorter than the tissue's thermal relaxation time. [1] For example, several groups [4, 15, 16] have studied what is sometimes designated as *micropulse laser thermotherapy*, whereby repetitive short laser (Nd-YLF laser $527\,nm$, $1.7\,\mu s$) pulses at a large irradiance (0.2-0.4 MW/cm^2) are administered to selectively treat the retinal pigmented epithelium (RPE). Even though the highly absorbing RPE cells are directly in contact with the photoreceptors and the neuronal layers, irradiation times of the order of a few μs allow to photomechanically destroy them while while inducing light changes to the nearby photoreceptors. Analysis of the results obtained with these methods indicates an amelioration of the clinical outcome and a reduction of side effects.

Another example of such subthreshold therapies is *transpupillary thermotherapy* (TTT). It was evaluated for the treatment of subfoveal choroidal neovascularisation in AMD [32, 38, 53, 62, 64, 73], as well as non-exsudative AMD [27, 56, 63, 89]. For this treatment, a near infrared (IR, $810\,nm$) diode laser was chosen because of its high tissue penetration and the relatively weak absorption of melanin and macular pigments at this wavelength. These characteristics enable to target deeper structures, typically $100 - 300\,\mu m$ below the photoreceptors and the neuronal layers of the retina, therefore preserving them, even during long irradiation periods, thanks to the limited heat diffusion, from the deep-seated absorbing centers. Long (usually $60\,s$) laser pulses with small irradiance (2-8 W/cm^2) are used to significantly increase the temperature in the neighbourhood of the sub-macular choroidal neovascularisation [23, 43, 52]. This heating induces vessel damage and thrombosis to the pathological neovascularisation. Morover, the weak absorption of hemoglobin at this wavelenght allows for macular irradiation even in the presence of retinal and subretinal hemorrhage, which, once again helps to preserve the neuronal layers.

The treatment of the retina by "*hydrodynamic rebalancing laser* (HRL)" therapy [67, 79] is yet another approach presenting similarities with TTT. HRL consists of the administration of 70 to 200 laser spots (at $810\,nm$) in selected locations of the retina that are *not* vital for sight, thus excluding the optic nerve. Direct treatment of the macula, as is the case in TTT, would not be safe. (see figure 4.5). Clinical observations (Dr. E. Vezzola and Dr. M. Sickenberg, private communications) suggest that the best clinical outcome is achieved by administering laser pulses near the upper limit of the subthreshold regime.

[1] $\tau_T = L^2/4k$.

There laser treatment is performed with a conventional slit-lamp and a Goldmann contact lens [55], which gives access to a large field of view and helps to avoid excessive movement of the patient's eye. HRL makes use of a CW near infrared laser (810 nm), with power levels from 0.4 to 1.0 W, a constant spot diameter of $\varnothing$ 100 μm on the retina and irradiation pulses ranging from 50 to 200 ms [67].

Historically the developments of HRL treatment modalities is based on the clinical observation by Walter [86], who noticed significant modifications of the temporal border of the optic nerve head (ONH). He observed that in certain diseases processes and with advancing age there is a progressive degeneration of the para-disc retinal pigment epithelium, followed by a vasoproliferation of the disc vessels followed by a slow diffusion of serous fluids between the pigment epithelium and the inner limiting membrane of Bruch.

The process of degeneration and effusion of the proteinaceous material in the serum tend to pool either in micro or macroscopically observable areas to produce small detachments of the retinal pigment epithelium. As this degenerative process extends over a period of years, there is a slow but progressive degeneration of the pigment epithelium, followed by liberation of vasoproliferative which responsible for the formation of pathological neovessels.

These abnormalities were present in several patients affected by different pathologies. This led to the working hypothesis that numerous macular diseases have a pathological origin associated with the ONH's disk leakage of extravascular fluids. Vezzola then proposed a new 810 nm laser treatment to restore the hydrodynamic balance within the posterior pole.

Although the mechanistic processes at the base of HRL therapy are not well understood, a reasonable hypothesis seems that the laser acts in such a manner that it reduces some of the typical effects induced by aging and/or ocular hypertension [1, 31, 35, 44, 59]. This hypothesis is supported by work performed by Sickenberg et al. [79], who studied the initial stages of fluorescein angiography, performed on patients with chorioretinal neovascularisation (wet AMD). Fluorescence angiography with fluorescein and a scanning laser ophthalmoscope demonstrated a small but measurable ONH's leakage in some of the patients. It was not at all clear whether these leaks had a physiological or pathological cause, but these observations suggested that the leakage was related to a rupture of the hemato-retinal barrier or to direct leaking of cerebrospinal fluids into the retinal space.

Several thousands patients have now been treated by HRL therapy, with a good safety profile. These treatments were associated with "unpredictable" retinal burns, in 2-3%

of the laser spots. Albeit much more rare, small haemorrhages were observed in 2‰ of the laser spots. These side effects were categorized as "unpredictable" because their occurrence could not be correlated with the effective laser parameters or the average fundus absorbance as perceived by the clinician (E. Vezzola, personal communication). Therefore, a reasonable hypothesis was to attribute these side effects to a heterogeneous distribution of "deep-seated optical absorbing centers" in the eye's fundus. This assumption was supported by the fact that firing the HRL laser on large pigmented structures of the choroid (choroidal nevi) frequently led to such side effects. Also, both small deep-seated absorbing centers of the eye's fundus and choroidal pigmented structures, are frequently difficult to localize, even under near infrared fundus inspection.

Large variations in the optical properties of the retina, in the visible and/or the near infrared, have been demonstrated by other groups [18, 20, 39, 42, 74]. Thus the present study aimed at investigating if the observed side effects of HRL were correlated to the presence of highly absorbing structures in the fundus tissue. A logical strategy to prevent the occurrence of the described side effects and, consequently, to improve the safety of the HRL treatment, would then consist of reducing the laser spots irradiation time or the laser irradiance, at locations of the retina presenting a strong absorption. Direct *in vivo* measurements of the eye's fundus absorption is not possible, which is why clinical diagnosis, including inspection of the retina, make use of fundus reflectometry. Thus, measuring the fundus reflectance, in particular when executed at the wavelenght of the treatment laser, could possibly help to evaluate spatial variations of the fundus absorption, in an approach similar to that used by de Graaf et al. [19], Ludwig et al. [49], Naess et al. [61]. This strategy was applied in the present study.

4.2 Materials and Methods

4.2.1 Study Design

As mentionned previously, HRL treatement elicits a small percentage of "unpredictable" responses from fundus tissue, even when the laser's irradiation parameters are kept constant. Given our working hypothesis, which links this heterogeneity in the tissue reaction to the pigmentation density and its distribution in the eye's fundus, our study focused on the frequency of induced retinal burns as a function of the local tissue absorbance - as "deduced" from its reflectance - measured at the laser spot location.

For this, one near infrared (810 nm) reflectance (IRR) image of the fundus was taken before the laser therapy. During the therapy, a video camera was focused on the eye fundus.

Whenever a laser pulse was administered by the clinician, the corresponding video image, showing the precise laser spot position, was captured and recorded. Simultaneously, the laser power and irradiation time used were recorded, in order to draw up an accurate cartography of the HRL treatment. The map of the laser spot positions and irradiation parameters was then superimposed on the initial IRR fundus image.

During the treatment, the clinician was asked to assess whether the laser-tissue interaction created or not a visible retinal "burn". Each laser spot was thus characterized and tagged with the clinician's observation, thus allowing us to establish wether a correlation existed between the local fundus reflectance and the laser tissue response.

The study took place in April and June 2008 and all measurements were done in Salò, Italy. 35 patients (for a total of 46 eyes treated by HRL) took part in the study. Of these, 16 patients (for a total of 20 eyes treated by HRL), with ages ranging from 22 to 78 years ($\mu_{age} = 50.75 \pm 16.12$ years), provided the data effectively used in the study (see §4.3).

All these patients gave their informed consent to be part of the study. Their enrolement only implied to take two supplementary images and to record the laser parameters, in addition to the usual HRL treatment. In the "standard" procedure, 3 fundus images are taken to planify the HRL treatment: a standard color picture, a red-free picture and a fluorescein angiogram. In the framework of the present study, supplementary fundus images were taken as follows: one infrared image just before the HRL session, to measure the fundus reflectance, and one white-light image just after each administered laser spot, to record the spot location.

4.2.2 HRL Treatment

HRL treatments are routinely performed in several private practice since, up to June 2010, more than 5000 patients had been treated. A typical HRL treatment session consists of a series of $100 - 200$ laser shots, with the laser beam focused on the RPE. According to the clinical observations, treatment efficacy is maximal (data not published) when using laser pulses at the upper limit of the subthreshold regime. During the treatment, shots aimed at the macula and the optic nerve head, are carefully avoided. The laser treatement is administered via a solid state, CW, ophthalmologic laser source ($810\,nm$), coupled to a standard slit lamp.

The irradiation parameters are chosen by the clinician, depending on the apparent fundus pigmentation and clarity of the ocular media of each patient. To evaluate these irradiation parameters, a test laser pulse is shot on a temporal, periferical zone of the eye fundus (A similar procedure is also used during

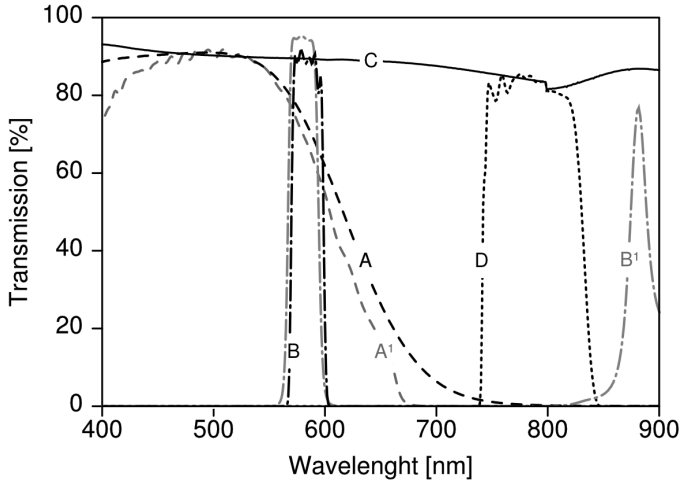

Figure 4.1: Optical transmission of the standard filters (A^1, B^1), and of the replacement and additional filters (A, B, C, D), used in the ophthalmoscope. A^1: Original Canon® EOS-D1 CCD filter; B^1: Original redfree filter; A: X-Nite CCD filter, used for balanced color images; C: New CCD filter, used for IRR images; B: Replacement redfree filter; D: IRR image excitation filter.

PRP, to find, in that case, laser parameters adequate for creating mild retinal burns).

In this study, the laser spot diameter on the retina was kept constant to $\varnothing 100\,\mu m$ for all the treated patients and the laser power was set to 1 W - except in one particular case where the power was lowered to $0.4\ W$ -. This was at the clinician's demand, in view of keeping these laser spots at the limit of the subthreshold regime (the specific patient was affected by a severe myopic condition). The *maximum* irradiation time was chosen by the clinician and set between 50 and 200 ms. However, the laser firing system allowed the clinician to terminate irradiation before this preset, maximum time was reached, thus making it possible to "personalize" and modulate every single laser spot. Anyway the precise duration of the laser irradaition was measured as described in §4.2.3

4.2.3 Instrumentation

Acquisition of the IR Reflectance images

The setup used to record IR reflectance images relied on standard commercial apparatus, with minor modifications. It consists of a digital camera (Canon®, EOS-1D) attached to an ophthalmoscope (Canon®, CF-60UVi). The sets of filters in the camera and the ophthalmoscope were replaced as described hereunder (see figure 4.1).

The CCD filter of the camera was changed to improve its sensitivity in the near infrared. Thus the band-pass filter used for visible wavelengths (A^1), which was normally mounted in front of the CCD, was replaced by a clear glass window (C). The ophthalmoscope's filter set was modified to match the enhanced spectral sensibility of the camera. Thus the standard green band-pass filter (B^1) for removing parasitic transmission bands in the IR range, was replaced with an interferometric filter (B) (Chroma®, HQ585-30X) in order to enable the acquisition of the diagnostic "redfree" images with minimal noise. A visible-wavelengths band-pass filter (A), (LDP LCC®, X-NiteCC1), was used to acquire white-light balanced color images. Finally a near-infrared band-pass filter (D) (Chroma®, HQ790/95X) was used to filter out the flash light when acquiring the fundus IRR images. Note that the band-pass filter for the acquisition of the fluorescein angiograms was not modified. These minor modifications did not affect the effective resolution of the diagnostic system, which was found to be about 40 μm for the standard color pictures.

HRL treatment:
Data acquisition and processing

The setup is schematically shown in Fig. 4.2. The clinician (1) administered the HRL treatment to the patient's eye (3) using a standard slit-lamp (2) (Takagi®, SM-70N). To fire a laser pulse, the clinician pressed on the laser driving pedal switch (4). Additionally, the clinician was instructed to press a second pedal switch (4b) whenever he perceived an increased reflectance, *i.e.* a withening of the treated spot, thus tagging the laser spot as a retinal burn. A digital video camera (Optronics®, CS-450) was coupled to the slit-lamp (2) to record the position of each laser spot. Simultaneously the effective irradiance period (t_L) and the laser power (P_L), were measured with a calibrated fast photodiode (OSRAM®, BPX61, typical switching time 20 ns) integrated in the medical laser (5) (Optikon 2000 S.p.a., Elios, $\lambda = 810\,nm$). The photodiode signal was digitized and analysed with a data aquisition board (Acquitek, CH-3150) integrated to the PC (6).

Recording of the HRL treatment information (laser position, irradiation parameters and clinician's observations) was triggered by the fast photodiode, every time the clinician pressed on the laser driving pedal switch (4). Dashed-lines with arrows in figure 4.2 represent the driving signals. A self written software drove the aquisition of the data from the 3 different sources as shown by the solid-lines with arrows in figure 4.2.

The fast photodiode was calibrated with a standard power sensor (Coherent®, FieldMaster-GS LM-2) to give the effectively delivered power (P_L) and the irradiation time

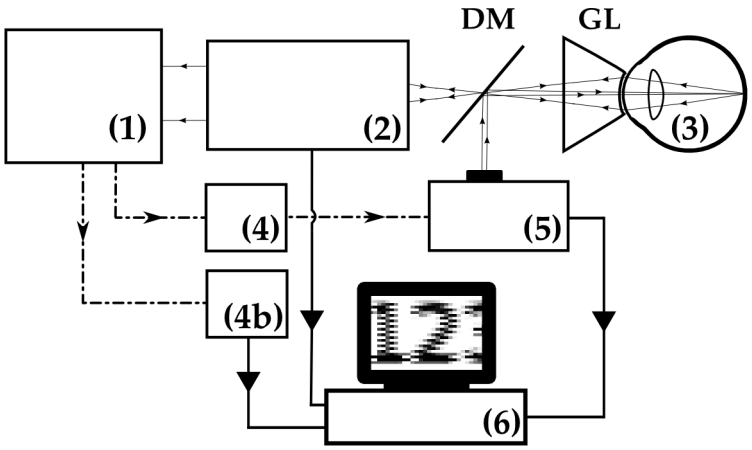

Figure 4.2: Schematic representation of the experimental HRL treatment setup, used in this study: at the beginning of the session, the clinician (1), examines the patient's eye (3) through the slit-lamp (2), which incorporates also the video camera; he then adjusts the treatment laser (5), setting the desired power and maximum irradiation time; to apply one laser pulse, he presses on the pedal switch (4a), which (i) starts the laser, whose beam is directed on the eye fundus by the dichroic mirror (DM) and the Goldman lens (GL), and, (ii) triggers the recording of the corresponding video image and laser parameters in the PC (6); the clinician releases pedal switch (4a) to stop the irradiation; if he observes the formation of a retinal burn, he tags the corresponding laser spot, by pressing pedal switch (4b).

(T_L) measured at full width half maximum of each laser spot. The calibration procedure showed that these measurements where characterized by a precision of about $\pm 10\%$. The image of the laser treatment site, acquired with the video camera attached to the slit-lamp, was recorded immediately at the beginning of the laser irradiation. The time needed for acquiring this image and transfering it to the PC was less than 40 ms (average file size ≈1 MB), which was shorter than the shortest irradiation period. Recording of all the measured HRL treatment parameters was done in less than 400 ms. This duration was compatible with the $\approx$ 2 Hz laser firing frequency typically used in the HRL laser treatment protocol.

Data Superimposition/Registration

A semi-automatic procedure was used to record the information and superimpose the slit-lamp pictures with the IRR images. In a first, automated step, the slit-lamp images, which reported the laser spot locations, were transformed, re-oriented and scaled to the images taken with the ophthalmoscope. In a second, manual step, the slit-lamp images reporting the HRL treatment position,

were registered with the corresponding IRR image. The registration process relied on the presence of at least a partial, characteristic vascular pattern in the slit-lamp images, which had to be found and identified in the wide field ophthalmoscopic IRR pictures. Both patterns were then manually registered, in a two step process: (i) with the help of a dedicated registration software (ImageJ®, Turboreg, [81]), assisting the manual registration, the slit-lamp images were registered with the top of the "redfree" fundus images, where the vessels appeared with a good contrast (see figure 4.3), thus providing a clear cartography of the HRL treatment; (ii) the HRL cartography was, again with the help of the mentioned software, registered with the top of the IRR image. According to this software's specifications, the precision of these computer-assisted registrations is in the subpixel range. In our case we estimated it to be on the order of 50 μm on the retina.

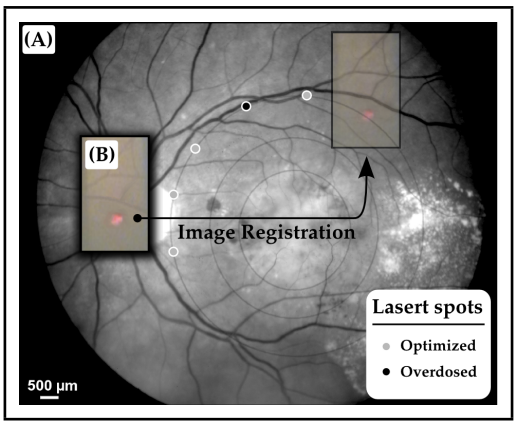

Figure 4.3: Image registration: HRL irradiation parameters and spot position (B), superimposition on the "red-free" image (A). White bar 500 μm on the retina

4.2.4 Eye Fundus Infrared Reflectance (IRR) Image Processing

Quantitative measurements of the fundus reflectance rely on the standardization and calibration of the fundus illumination. Even though the parameters of the flash, used for acquiring the IRR images, were kept constant for all patients, this did not result in a stable and homogeneous illumination of the fundus. The excitation heterogeneity was due, among others, to variations in the patients' pupil diameter, the optical properties of their eye media and the entrance angle of the excitation light, rather than to flash fluctuations. Therefore, the IRR images were normalized to the flash's image pattern, using a simple image processing method: for any specific case, the reflectance image was filtered with a low-pass filter ($< 3\,lp/mm$ on the retina) to extract the flash excitation pattern. The IRR image was then normalized by dividing the image itself by the flash excitation pattern, resulting in a normalized IRR image, corrected for illumination heterogeneity, over the whole image (see figure 4.4).

Such normalized images efficiently emphasize *variations* in local IR reflectance - at

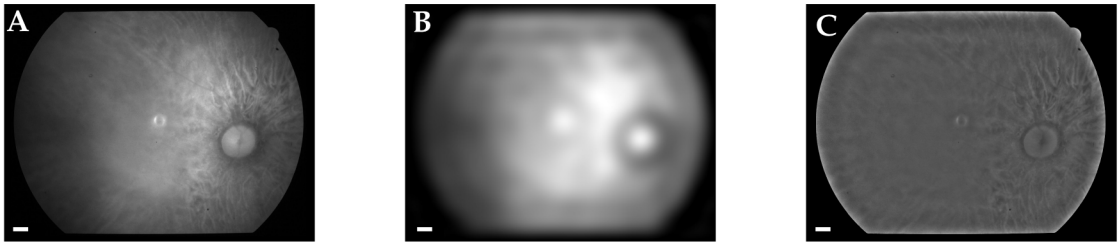

Figure 4.4: Correction of IR eye fundus images for the heterogeneity of the ophthalmoscope excitation light: (A) Raw IR fundus image at 810 nm; (B) Intensity pattern of the 810 nm excitation light flash; (C) Corrected IR fundus image obtained by dividing image (A) by image (B). White bar 1 mm on the retina

the price of the loss of information on the *absolute* local reflectance. Despite the latter shortcoming, detecting these variations in the fundus reflectance (*i.e.* in its absorbance) made possible the investigation of the assumed correlation between laser parameters, tissue properties and clinical outcome.

4.3 Results

As already mentionned, 35 patient (46 eyes) were treated by HRL in April and June 2008. A total of 5660 laser spots were placed in 46 retinas, causing 131 retinal burns (2.3%). No hemorrhage occurred. As retinal burns did not occur in all the cases, and, in some other cases, the slit-lamp images of interest did not present any visible vascular pattern (needed for the registration procedure) the study focused on the remaining, usable cases, *i.e.* on 20 treated eyes from 16 patients.

To be able to analyse and compare the results, also in function of their pathology, the 20 eyes were subdivided in 6 pathology-specific groups: Glaucoma (7 eyes), Papillary Atrophy (4 eyes), Age Related Macular Degeneration (4 eyes), Retinitis Pigmentosa (3 eyes), Myopic Retinopathy (1 eye) and Diabetic Retinopathy (1 eye). From the point of view of the ergonomy and adaptability of the measurements, the minor modifications brought to the standard medical device (required for image acquisition and laser data capture) did not significantly influence the medical practice working habits (the increase treatment time is about $\approx$ 10%). However, the HRL administration rhythm had to be reduced, to allow for a correct acquisition of all useful parameters. On the other hand, acquisition of the extra, initial IRR image became part of the routine diagnosis, thanks to the useful propensity of these images to highlight the presence of large, deep-seated absorbing structures, such as choroidal naevi.

We performed the registration procedure for all the laser shots tagged as “having

caused retinal burn" (*i.e.* about 2 to 4 per treated eye), plus a few "subthreshold" laser spots around them *i.e.* 5 to 10 "subthreshold" shots, located within 1 mm of each "burn-causing" shot. Data analysis started with the slit-lamp images reporting the retinal position of these nearby 5-to-10 subthreshold laser spots, selected for comparison purposes, as their proximity should reduce the influence on the optical absorbance, of other tissular parameters, including choroidal blood flow, accumulated chorio-retinal fluids and chorio-retinal thickness.

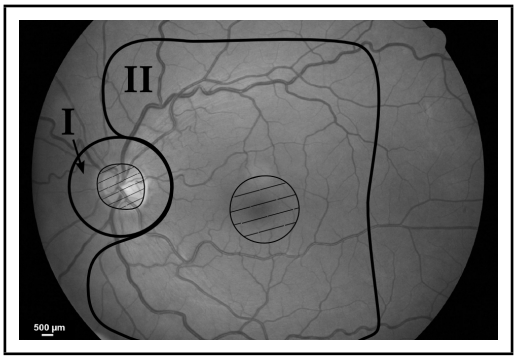

Figure 4.5: Subdivision of the retina in 2 treatment zones. The treated zones, I and II, are delimited with dark lines. The macular and ONH zones, circled and hatched with light lines, are to be spared.

In addition, the retina was divided in two zones (see Fig. 4.5), in view of grouping the fired laser spots in relatively homogeneous retinal zones: zone I was defined to be an annular region around the ONH; zone II was delineated by the inferior and superior retinal arcades. During the study, the laser spot diameter ($\varnothing 100\,\mu m$) and the radiant power ($1\,W$; $125\,W/mm^2$) were kept constant, except for a dozen of laser spots fired in zone II of a single, strongly myopic, eye, where the radiant power was lowered to $0.4\,W$ ($50\,W/mm^2$): this was done at the clinician's demand, in view of keeping these laser spots at the limit of the subthreshold regime, as detailed in §4.2.2.

The results are presented in Figure 4.6, which shows the analyzed laser spots independently from the patient's eye pathology. Occurences of retinal burns are shown by triangular marks ($\triangle$) while subthreshold spots are marked with filled dots ($\bullet$).

The same results are presented in Figure 4.7, taking into account the treated eyes' pathologies. Specific symbols are assigned to each pathology. Retinal burns are distinguished from subthresholds laser spots through the use of a filled symbol.

All results do not show a clear correlation between local IR reflectance and propensity to retinal burns. This can also be observed by examining groups of iso-energetic laser spots (which lie along horizontal lines in our scatterplots). Retinal burns appear to be randomly distributed between low reflectance spots (*i.e.* high absorbance) and high reflectance spots (*i.e.* weak absorbance), suggesting that the local normalized reflectance is not an adequate parameter to predict the occurrence of retinal burns.

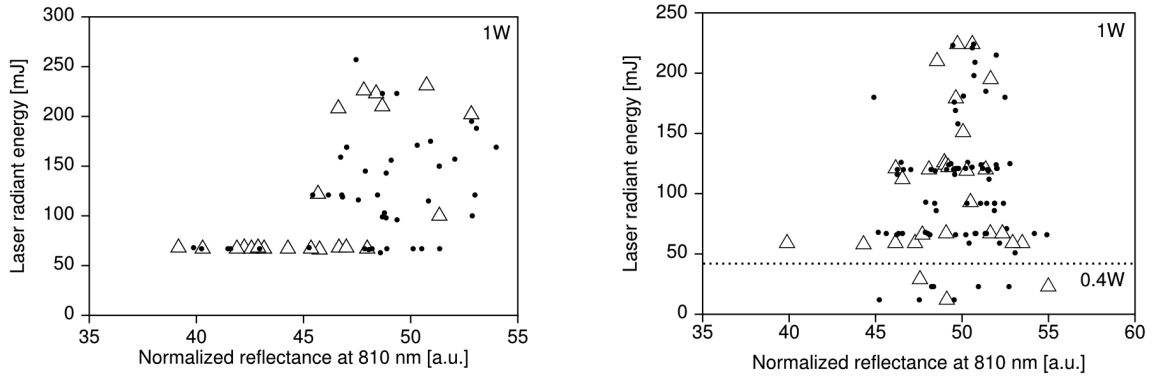

(a) Retinal zone I

(b) Retinal zone II

Figure 4.6: Scatterplots showing the occurrence of retinal burns (△) as a function of the local, normalized IR reflectance and the effective laser energy administered. Subthreshold laser spots are shown as filled dots (●)

Furthermore, by analysing the results according to laser shot radiant energy (*i.e.* along the vertical axis in Fig. 4.6), considerable variations (up to a factor of 5) in the energy of retinal burn-tagged laser spots can be noted. Similarly, in figure 4.7, pathology-specific clustering along the vertical axis is observed: patients affected by retinitis pigmentosa, for example, were found to be grouped in the lower part of the graph. This may be related to a high *absolute value* of their fundus' absorbance, which is not measurable with our setup.

4.4 Discussion

Reflectance imaging is a reference method for analysing the eye fundus. Since the first quantitative studies published in 1950, several hundred investigations of the *in vivo* human eye fundus were done [8]. This growing interest in quantitative measurements paralleled the adoption of new, laser-based diagnostic technologies, such as the scanning laser ophthalmoscope and optical coherence tomography (OCT), now considered as standard opthalmologic instruments [14, 77].

Most of these investigations aimed at assessing the retinal oxygen contents or the macular pigmentation density, in different pathologies [7, 8, 12, 21, 88], while a small number of studies focused on systems or methods to optimize the irradiation parameters in thermal retinal therapies. Thus, in the framework of PRP, the treated spot's quantitative reflectance was monitored to adapt the irradiation time: it was found that the very changes in tissue reflectance, induced by retinal burns, could be used to drive this thermal

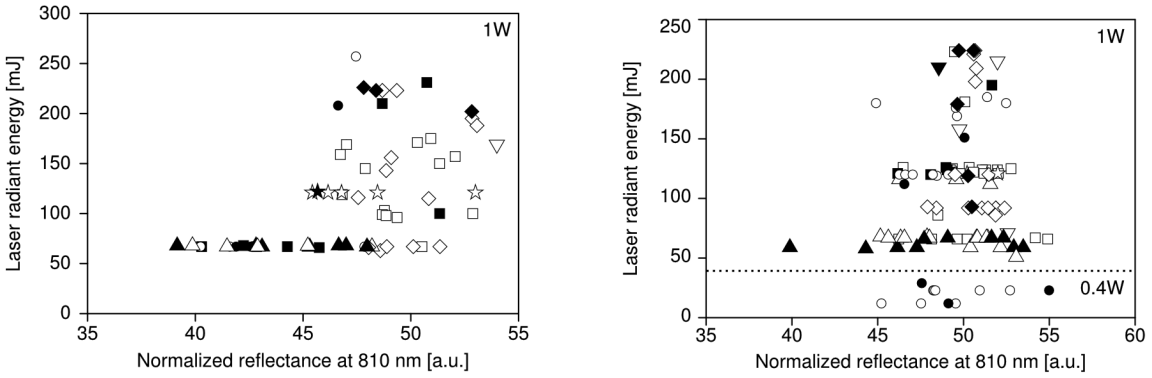

(a) Zone I

(b) Zone II

Figure 4.7: Scatterplots of all treated eyes, according to retinal zone and eye pathology. Empty symbols correspond to subthreshold laser spots. Filled symbols correspond to retinal burns. ☆: Myopic Retinopathy; △: Retinitis pigmentosa; ◇: Atrophic Age Related Macular Degeneration; □: Papillary Atrophy; ▽: Diabetic Retinopaty; ○: Glaucoma.

therapy and control the extent of tissue modifications [6, 10, 11, 66].

To our knowledge, however, no study investigated the local *infrared* reflectance to optimize a thermal, IR laser therapy. The main advantages of near IR radiation reside in (i) their deeper tissue penetration, as compared to shorter wavelengths, and (ii) in their improved transmission through blood and retinal edema [82, 83]. In general, the fraction ($20-30$ % at 810 nm) of diode laser radiation absorbed by the ocular fundus, is much smaller than that of shorter wavelengths ($\approx$ 95% at 532 nm) [3]. This explains why much more IR radiant energy is needed to produce retinal burns ($20\,kJ/cm^2$ at 810 nm as compared to $1\,J/cm^2$ at 532 nm).

More precisely, the light fraction absorbed in the RPE is about $30-35$ % at $810\,nm$, as compared to $\approx$ 70% at $532\,nm$ [3, 30, 46]. Therefore the pigmentation and the amount of hemoglobin within the choroid, which is linked to choroidal thickness, will probably play a significant role in the absorption process. Moreover, in such a situation, where there are no evidently dominating absorbing structures, modeling the thermal process causing the retinal burns is difficult. The most plausible hypothesis is that the IR radiant energy is primarily absorbed by the choroidal melanocytes and by the RPE; the heat generated at these two main absorbing centers, then diffuses to the neuroretinal layers, where it causes the retinal burns [13, 18, 40, 46, 70]. It follows that homogenizing the outcome of IR thermal therapies on the basis of the tissue's absorbance is not trivial, as the absence of correlation

found in our study could be the consequence of several effects.

First of all, it is worth recalling that this therapy relies on a protocol at the upper limit of the "subthreshold" regime, which implies that *all* the laser spots administered were very close to the radiant energy required to generate a retinal burn. We should also note that (i), our absorbance measurements are integrated over all the eye media and fundus layers and (ii), the longitudinal distribution of the absorbing centers was not measured. Therefore, small changes in eye tissues properties or in the administered energy could lead to these apparently heterogeneous results. Hereunder, other parameters that may influence the tissue's response to HRL treatment are analyzed and discussed:

Small, involuntary patient's eye movements during the spot's duration (max. 200 ms) can probably be neglected: this relatively short irradiation time, the almost painless nature of the treatment, the nearly invisible laser beam and the Goldmann contact lens assisted irradiation are all elements that support this assumption [28, 55, 82]. In a recent publication Lund [50] studied the impact of small-scale ocular motion on retinal thermal laser therapies. The *relief factor*[1] depended on the irradiation time; it was calculated to be $\approx 10\%$ for an irradiation of 200 ms. As these evaluations were made in the framework of an He-Ne laser therapy (633 nm), it follows that, for the more spatially diffuse tissue absorption during IR therapy, this relief factor should be further reduced.

Laser spot focus changes, caused by the clinician's aiming errors, are probably also not important. Even though the small numerical aperture of the human eye could induce a notable reduction in irradiance, by a factor of up to 3 when a longitudinal error of $400\,\mu m$ is assumed. Adjusting the laser spot focus when using a standard slit-lamp is easy, and intra-therapy laser spot focus variations are probably minimal. Moreover, weak absorption and strong diffusion in RPE and choroidal tissues further reduce the effect of this parameter.

The choroidal blood flow is known to play an effect in the cooling down process. However, in thermal irradiations, this tissue cooling effect is only significant for long therapies ($> 10\,s$) [22, 37, 51, 54].

Diffusion of the infrared radiation is probably the main cause of the lack of correlation found in our study. It has been shown, [26], that reflectance at 810 nm of dark-pigmented fundi and light-pigmented fundi, did not strongly differ. This suggests that the

[1] the "relief factor" is defined as the ratio between the retinal thermal threshold damage in a moving eye and in a theoretical stationary eye. Therefore, if during the treatment the patient's eye movement are dampen, the "relief factor" will decrease accordingly

reason why such *reflectance* measurements failed to provide us with useful information on the *absorbing* structures in the eye fundus, stems from the inability of such measurements to discriminate between *reflected* light and *scattered* light. Weak absorption and long scattering distances are thus probably responsible for the poor detection of absorbing centers in the choroid. Although large and highly pigmented choroidal structures are easily seen, physiological choroidal pigmentation changes cannot be detected. This hypothesis is supported by many publication where the imaging of the choroid was found to be difficult, even with more sophisticated techniques [14, 26, 33, 77].

Variations in choroidal thickness and in the *spatial distribution of the melanocytes* probably play an important role in retinal burns: if the IR radiation is indeed absorbed by the RPE and the choroid, then the heat deposited in these absorbing centers must diffuse down to the neuronal layer to create a retinal burn; the longitudinal location of the melanocytes may thus exert a significant influence on the tissue reaction [80]. Also, the resulting heating effect may notably change in function of the chorio-retinal thickness and the presence of exudate.

Recent setups, still at the research stage, can produce contrasted images of the choroidal structures [29, 69, 80, 85], with a much better resolution than that of our fundus camera. At a wavelength of 810 nm, the latter had an estimated resolution on the order of $\approx 100\,\mu m$ for structures at the surface of the retina, dropping to maybe $\approx 300\,\mu m$ for structures deeper into the choroidal tissue. Optical coherence tomographic systems, adapted to investigate these choroidal structures, at the longer wavelength of 1100 nm, could also yield more valuable information.

Another interesting approach, relying on the measurement of the longitudinal reflectance profile (*i.e* OCT A-scan) of the laser spot during irradiation, was proposed by Lanzetta and Dorin [45], Lanzetta et al. [47]. It enables the detection of reflectance variations of specific layers within the fundus. This approach could allow, for example, to monitor the reflectance of Bruch's membrane, and use this measurement to modulate the laser irradiation period, to prevent the formation of visible retinal burns [33].

4.5 Acknowledgments

This work was supported by the Swiss National Science Foundation (Grant 205320-116556) and funded in part by the J. Jacobi Trust.

References

[1] J. Albon, P. P. Purslow, W. S. Karwatowski, and D. L. Easty. Age related compliance of the lamina cribrosa in human eyes. *Br J Ophthalmol*, 84(3):318–23, March 2000. ISSN 0007-1161. 35

[2] D. V. Alfaro. *Age-Related Macular Degeneration: A Comprehensive Textbook*. Lippincott Williams & Wilkins, 1 edition, 2005. 33

[3] M. W. Balles, C. A. Puliafito, D. J. D'Amico, J. J. Jacobson, and R. Birngruber. Semiconductor diode laser photocoagulation in retinal vascular disease. *Ophthalmology*, 97(11): 1553–61, November 1990. ISSN 0161-6420. 45

[4] R. K. Banerjee, L. Zhu, P. Gopalakrishnan, and M. J. Kazmierczak. Influence of laser parameters on selective retinal treatment using single-phase heat transfer analyses. *Med Phys*, 34(5):1828–41, May 2007. ISSN 0094-2405. 34

[5] A. S. Banker and W. R. Freeman. Retinal detachment. *Ophthalmol Clin North Am*, 14(4):695–704, December 2001. ISSN 0896-1549. 33

[6] S. F. Barrett, C. H. Wright, E. D. Oberg, B. A. Rockwell, C. Cain, H. G. Rylander, and A. J. Welch. Development of an integrated automated retinal surgical laser system. *Biomed Sci Instrum*, 32:215–24, 1996. ISSN 0067-8856. 45

[7] T. T. J. M. Berendschot and D. van Norren. Objective determination of the macular pigment optical density using fundus reflectance spectroscopy. *Arch Biochem Biophys*, 430(2):149–55, October 2004. ISSN 0003-9861. 44

[8] T. T. J. M. Berendschot, P. J. DeLint, and D. van Norren. Fundus reflectance–historical and present ideas. *Prog Retin Eye Res*, 22(2):171–200, March 2003. ISSN 1350-9462. 44

[9] J. W. Berger. Thermal modelling of micropulsed diode laser retinal photocoagulation. *Lasers Surg Med*, 20(4):409–15, 1997. ISSN 0196-8092. 33

[10] R. Birngruber, V. P. Gabel, and F. Hillenkamp. Fundus reflectometry: a step towards optimization of the retina photocoagulation. *Mod Probl Ophthalmol*, 18:383–90, 1977. ISSN 0077-0078. 45

[11] M. S. Blumenkranz, D. Yellachich, D. E. Andersen, M. W. Wiltberger, D. Mordaunt, G. R. Marcellino, and D. Palanker. Semiautomated patterned scanning laser for retinal photocoagulation. *Retina*, 26(3):370–6, March 2006. ISSN 0275-004X. 45

[12] L. J. Bour, L. Koo, F. C. Delori, P. Apkarian, and A. B. Fulton. Fundus photography for measurement of macular pigment density distribution in children. *Invest Ophthalmol Vis Sci*, 43 (5):1450–5, May 2002. ISSN 0146-0404. 44

[13] R. Brancato, R. Pratesi, G. Leoni, G. Trabucchi, and U. Vanni. Histopathology of diode and argon laser lesions in rabbit retina. a comparative study. *Invest Ophthalmol Vis Sci*, 30(7):1504–10, July 1989. ISSN 0146-0404. 45

[14] E. M. Brezinski. Optical coherence tomography theory. In *Optical Coherence Tomography*, pages 97–145. Academic Press, Burlington, 2006. ISBN 978-0-12-133570-0. doi: DOI:10.1016/B978-012133570-0/50007-X. URL `http://www.sciencedirect.com/science/article/B870N-4P9TW7Y-9/2/7842118e3041ce8762ae450e49e720cd`. 44, 47

[15] R. Brinkmann, G. Hüttmann, J. Rögener, J. Roider, R. Birngruber, and C. P. Lin. Origin of retinal pigment epithelium cell damage by pulsed laser irradiance in the nanosecond to microsecond time regimen. *Lasers Surg Med*, 27(5):451–64, 2000. ISSN 0196-8092. 34

[16] R. Brinkmann, J. Roider, and R. Birngruber. Selective retina therapy (srt): a review on methods, techniques, preclinical and first clinical results. *Bull Soc Belge Ophtalmol*, 302:51–69, 2006. ISSN 0081-0746. 34

[17] H. Y. Cho, Y. T. Kim, and S. W. Kang. Laser photocoagulation as adjuvant therapy to surgery for large macular holes. *Korean J Ophthalmol*, 20(2):93–8, June 2006. ISSN 1011-8942. 33

[18] B. P Connolly, C. D. Regillo, R. C. Eagle, C. L. Shields, J. A. Shields, and H. Moran. The histopathologic effects of transpupillary thermotherapy in human eyes. *Ophthalmology*, 110(2):415–20, February 2003. ISSN 0161-6420. 33, 36, 45

[19] P. W. de Graaf, S. F. Barrett, and C. H. Wright. A method to control irradiation time for laser photocoagulation of the retina–part ii. *Biomed Sci Instrum*, 35:159–63, 1999. ISSN 0067-8856. 36

[20] F. C. Delori and K. P. Pflibsen. Spectral reflectance of the human ocular fundus. *Applied Optics*, 28(6):17, 3 1989. 36

[21] K. R. Denninghoff, D. A. Salyer, S. Basavanthappa, R. I. Park, and R. A. Chipman. Blue-green spectral minimum correlates with oxyhemoglobin saturation in vivo. *J Biomed Opt*, 13(5): 054059, 2008. ISSN 1083-3668. 44

[22] T. J. Desmettre, S. Soulie-Begu, J. M. Devoisselle, and S. R. Mordon. Diode laser-induced thermal damage evaluation on the retina with a liposome dye system. *Lasers Surg Med*, 24 (1):61–8, 1999. ISSN 0196-8092. 46

[23] T. J. Desmettre, C. A. Maurage, and S. Mordon and. Transpupillary thermotherapy (ttt) with short duration laser exposures induce heat shock protein (hsp) hyperexpression on choroidoretinal layers. *Lasers Surg Med*, 33(2):102–7, 2003. ISSN 0196-8092. 34

[24] G. Dorin. Subthreshold and micropulse diode laser photocoagulation. *Semin Ophthalmol*, 18(3):147–53, September 2003. ISSN 0882-0538. 33

[25] G. Dorin. Evolution of retinal laser therapy: minimum intensity photocoagulation (mip). can the laser heal the retina without harming it? *Semin Ophthalmol*, 19(1-2):62–8, 2004. ISSN 0882-0538. 33

REFERENCES

[26] A. E. Elsner, S. A. Burns, J. J. Weiter, and F. C. Delori. Infrared imaging of sub-retinal structures in the human ocular fundus. *Vision Res*, 36(1):191–205, January 1996. ISSN 0042-6989. 46, 47

[27] R. W. Flower. Optimizing treatment of choroidal neovascularization feeder vessels associated with age-related macular degeneration. *Am J Ophthalmol*, 134(2):228–39, August 2002. ISSN 0002-9394. 34

[28] F. Frankhauser and S. Kwasniewska. *Lasers in Opthalmology - Basics, Diagnostics, and Surgical Aspects - A Review*. Not Avail, 2003. 46

[29] T. Fujiwara, Y. Imamura, R. Margolis, J. S. Slakter, and R. F. Spaide. Enhanced depth imaging optical coherence tomography of the choroid in highly myopic eyes. *Am J Ophthalmol*, 148(3):445–50, September 2009. ISSN 1879-1891. 47

[30] V.P. Gabel, R. Birngruber, and F. Hillenkamp. Visible and near infrared light absorption in pigment epithelium and choroid. *Exerpta Med. Int. Congr.*, 14:658–662, 1978. 45

[31] D. G. Gomez, R. P. Manzo, J. D. Fenstermacher, and D. G. Potts. Cerebrospinal fluid absorption in the rabbit. optic pathways. *Graefes Arch Clin Exp Ophthalmol*, 226(1):1–7, 1988. ISSN 0721-832X. 35

[32] C. Gustavsson and E. Agardh. Transpupillary thermotherapy for occult subfoveal choroidal neovascularization: a 1-year, prospective randomized pilot study. *Acta Ophthalmol Scand*, 83(2):148–53, April 2005. ISSN 1395-3907. 34

[33] H Hammer, D Schweitzer, E Thamm, A Kolb, and J Strobel. Scattering properties of the retina and the choroids determined from oct-a-scans. *Int Ophthalmol*, 23(4-6):291–5, 2001. ISSN 0165-5701. 47

[34] S. S. Hayreh. Management of central retinal vein occlusion. *Ophthalmologica*, 217(3):167–88, 2003. ISSN 0030-3755. 33

[35] S. S. Hayreh. Prevalent misconceptions about acute retinal vascular occlusive disorders. *Prog Retin Eye Res*, 24(4):493–519, July 2005. ISSN 1350-9462. 35

[36] Y. J. Hu. Pain relief during panretinal photocoagulation for diabetic retinopathy. *Eye (Lond)*, [Epub ahead of print], March 2010. ISSN 1476-5454. 33

[37] M. S. Ibarra, J. Hsu, N. Mirza, I. H. Wu, G. Ying, M. A. Mainster, and M. J. Tolentino. Retinal temperature increase during transpupillary thermotherapy: effects of pigmentation, subretinal blood, and choroidal blood flow. *Invest Ophthalmol Vis Sci*, 45(10):3678–82, October 2004. ISSN 0146-0404. 46

[38] Y. Ito, K. Mori, H. Takita, T. Sodeyama, K. Anzai, D. Imai, M. Shibuya, D. M. Moshfeghi, S. Yoneya, and G. A. Peyman. Transpupillary thermotherapy: effect of wavelength on normal primate retina. *Retina*, 25(8):1046–53, December 2005. ISSN 0275-004X. 34

[39] M. R. Jerath, D. Kaisig, H. G. Rylander III, and Ashley J. Welch. Calibrated real-time control of lesion size based on reflectance images. *Appl. Opt.*, 32(7):1200–1209, 1993. URL `http://ao.osa.org/abstract.cfm?URI=ao-32-7-1200`. 36

[40] J. G. Journée-de Korver, J. A. Oosterhuis, D. de Wolff-Rouendaal, and H. Kemme. Histopathological findings in human choroidal melanomas after transpupillary thermotherapy. *Br J Ophthalmol*, 81(3):234–9, March 1997. ISSN 0007-1161. 45

[41] R. S. Kaiser, M. G. Maguire, J. E. Grunwald, D. Lieb, B. Jani, A. J. Brucker, A. M. Maguire, A. C. Ho, and S. L. Fine. One-year outcomes of panretinal photocoagulation in proliferative diabetic retinopathy. *Am J Ophthalmol*, 129(2):178–85, February 2000. ISSN 0002-9394. 33

[42] C. N. Keilhauer and F. C. Delori. Near-infrared autofluorescence imaging of the fundus: visualization of ocular melanin. *Invest Ophthalmol Vis Sci*, 47(8):3556–64, August 2006. ISSN 0146-0404. 36

[43] J. M. Kim, K.H. Park, Y. J. Kim, H. J. Park, and D. M. Kim. Thermal injury induces heat shock protein in the optic nerve head in vivo. *Invest Ophthalmol Vis Sci*, 47(11):4888–94, November 2006. ISSN 0146-0404. 34

[44] A. Kotecha, S. Izadi, and G. Jeffery. Age-related changes in the thickness of the human lamina cribrosa. *Br J Ophthalmol*, 90(12):1531–4, December 2006. ISSN 0007-1161. 35

[45] P. Lanzetta and G. Dorin. Method and apparatus for real-time detection, control and recording of sub-clinical therapeutic laser lesions during ocular laser photocoagulation. Technical report, Patent No. 01932680.0-2305-US0113559, 2001. 47

[46] P. Lanzetta, G. Virgili, and U. Menchini. Diode laser photocoagulation of choroidal neovascular membranes. *Int Ophthalmol*, 19(6):347–54, 1996. ISSN 0165-5701. 45

[47] P. Lanzetta, G. Dorin, A. Pirracchio, and F. Bandello. Theoretical bases of non-ophthalmoscopically visible endpoint photocoagulation. *Semin Ophthalmol*, 16(1):8–11, March 2001. ISSN 0882-0538. 33, 47

[48] M. L. Laursen, F. Moeller, B. Sander, and A. K. Sjoelie. Subthreshold micropulse diode laser treatment in diabetic macular oedema. *Br J Ophthalmol*, 88(9):1173–9, 9 2004. 33

[49] D. A. Ludwig, S. F. Barrett, and R. F. Kubichek. Laser dosimetry control for retinal surgery. *Biomed Sci Instrum*, 37: 479–84, 2001. ISSN 0067-8856. 36

[50] B. J. Lund. Laser retinal thermal damage threshold: impact of small-scale ocular motion. *J Biomed Opt*, 11(6):064033, 2006. ISSN 1083-3668. 46

[51] M. A. Mainster. Decreasing retinal photocoagulation damage: principles and techniques. *Semin Ophthalmol*, 14(4):200–9, December 1999. ISSN 0882-0538. 33, 46

[52] M. A. Mainster and E. Reichel. Transpupillary thermotherapy for age-related macular degeneration: long-pulse photocoagulation, apoptosis, and heat shock proteins. *Ophthalmic Surg Lasers*, 31(5):359–73, 2000. ISSN 1082-3069. 34

[53] M. A. Mainster and E. Reichel. Transpupillary thermotherapy for age-related macular degeneration: principles and techniques. *Semin Ophthalmol*, 16(2):55–9, June 2001. ISSN 0882-0538. 34

[54] M. A. Mainster and D. H. Sliney. Ttt: local light absorption and heat convection versus heat conduction. *Br J Ophthalmol*, 89(11):1545, November 2005. ISSN 0007-1161. 46

[55] M. A. Mainster, J. L. Crossman, P. J. Erickson, and G. L. Heacock. Retinal laser lenses: magnification, spot size, and field of view. *Br J Ophthalmol*, 74(3):177–9, March 1990. ISSN 0007-1161. 35, 46

[56] R. R. Margherio, A. R. Margherio, and M. E. DeSantis. Laser treatments with verteporfin therapy and its potential impact on retinal practices. *Retina*, 20(4):325–30, 2000. ISSN 0275-004X. 34

[57] A. L. McKenzie. Physics of thermal processes in laser-tissue interaction. *Phys Med Biol*, 35(9):1175–209, September 1990. ISSN 0031-9155. 33

[58] G. A. Moo-Young. Lasers in ophthalmology. *West J Med*, 143 (6):745–50, December 1985. ISSN 0093-0415. 33

[59] D. J. Moore, A. A. Hussain, and J. Marshall. Age-related variation in the hydraulic conductivity of bruch's membrane. *Invest Ophthalmol Vis Sci*, 36(7):1290–7, June 1995. ISSN 0146-0404. 35

[60] C. M. Moorman and A. M. Hamilton. Clinical applications of the micropulse diode laser. *Eye (Lond)*, 13 (Pt 2):145–50, April 1999. ISSN 0950-222X. 33

[61] E. Naess, T. Molvik, D. A. Ludwig, S. F. Barrett, S. Legowski, C. Wright, and P. de Graaf. Computer-assisted laser photocoagulation of the retina–a hybrid tracking approach. *J Biomed Opt*, 7(2):179–89, April 2002. ISSN 1083-3668. 36

[62] R. S. Newsom, J. C. McAlister, M. Saeed, and J. D. McHugh. Transpupillary thermotherapy (ttt) for the treatment of choroidal neovascularisation. *Br J Ophthalmol*, 85(2): 173–8, February 2001. ISSN 0007-1161. 34

[63] M. B. Parodi, G. Virgili, and J. R. Evans. Laser treatment of drusen to prevent progression to advanced age-related macular degeneration. *Cochrane Database Syst Rev*, 1(3):CD006537, 2009. ISSN 1469-493X. 33, 34

[64] R. Parrozzani, B. Boccassini, V. De Belvis, P. P. Radin, and E. Midena. Long-term outcome of transpupillary thermotherapy as primary treatment of selected choroidal melanoma. *Acta Ophthalmol*, [Epub ahead of print], September 2008. ISSN 1755-3768. 33, 34

[65] Y. M. Paulus, A. Jain, R. F. Gariano, B. V. Stanzel, M. Marmor, M. S. Blumenkranz, and D. Palanker. Healing of retinal photocoagulation lesions. *Invest Ophthalmol Vis Sci*, 49(12): 5540–5, December 2008. ISSN 1552-5783. 33

[66] K. P. Pflibsen, F. C. Delori, O. Pomerantzeff, and M. Pankratov. Fundus reflectometry for photocoagulation dosimetry. *Applied Optics*, 28(6):1084–1096, 3 1989. 45

[67] F. Piffaretti, J. P. Ballini, E. Vezzola, M. Sickenberg, D. Vezzola, D. Vezzola, R. Perotti, C. Magni, and G. Wagnières. Hydrodynamic rebalancing laser therapy to treat age related macular degeneration: Developpement of an instrumental setup to monitor this treatment using the retina reflectance at 810 nm, November 2006. URL `http://www.oculista-vezzola.it`. Poster. 34, 35

[68] J. S. Pollack, J. E. Kim, J. S. Pulido, and J. M. Burke. Tissue effects of subclinical diode laser treatment of the retina. *Arch Ophthalmol*, 116(12):1633–9, December 1998. ISSN 0003-9950. 33

[69] B. Povazay, B. Hermann, B. Hofer, V. Kajić, E. Simpson, T. Bridgford, and W. Drexler. Wide-field optical coherence tomography of the choroid in vivo. *Invest Ophthalmol Vis Sci*, 50(4):1856–63, April 2009. ISSN 1552-5783. 47

[70] E. M. Procaccini, G. Riccio, M. Bellocci, C. Di Martino, and G. Monfrecola. The effects of a diode laser (810 nm) on pigmented guinea-pig skin. *Lasers Med Sci*, 16(3):171–5, 2001. ISSN 0268-8921. 45

[71] F. Ricci, F. Missiroli, F. Regine, M. Grossi, and G. Dorin. Indocyanine green enhanced subthreshold diode-laser micropulse photocoagulation treatment of chronic central serous chorioretinopathy. *Graefes Arch Clin Exp Ophthalmol*, 247(5):597–607, May 2009. ISSN 1435-702X. 33

[72] J. Roider. Laser treatment of retinal diseases by subthreshold laser effects. *Semin Ophthalmol*, 14(1):19–26, March 1999. ISSN 0882-0538. 33

[73] P. Rol, F. Fankhauser, H. Giger, U. Dürr, and S. Kwasniewska. Transpupillar laser phototherapy for retinal and choroidal tumors: a rational approach. *Graefes Arch Clin Exp Ophthalmol*, 238(3):249–72, March 2000. ISSN 0721-832X. 34

[74] J. Sandeau, J. Kandulla, H. Elsner, R. Brinkmann, G. Apiou-Sbirlea, and R. Birngruber. Numerical modelling of conductive and convective heat transfers in retinal laser applications. *J Biophotonics*, 1(1):43–52, March 2008. ISSN 1864-0648. 36

[75] S. H. Sarks, J. J. Arnold, J. P. Sarks, M. C. Gilles, and C. J. Walter. Prophylactic perifoveal laser treatment of soft drusen. *Aust N Z J Ophthalmol*, 24(1):15–26, February 1996. ISSN 0814-9763. 33

[76] M. Sculpher. A preliminary economic evaluation of the diode laser in ophthalmology. *Lasers in Medical Science*, 8(3):163–169, 1993. doi: http://dx.doi.org/10.1007/BF02547872. 33

[77] P F Sharp and A Manivannan. The scanning laser ophthalmoscope. *Phys Med Biol*, 42(5):951–66, May 1997. ISSN 0031-9155. 44, 47

[78] M Sickenberg. Verteporfin therapy for subfoveal choroidal neovascularization in age-related macular degeneration: from clinical trials to clinical practice. *Semin Ophthalmol*, 16(4): 207–12, December 2001. ISSN 0882-0538. 33

[79] M. Sickenberg, E. Vezzola, G. Villani, C. Magni, J. P. Ballini, and H. van den Bergh. Incidence and fluorescence pharmacokinetic study of a temporal disc leak in wet age-related macular degeneration. In preparation, 2005. 34, 35

[80] R. F. Spaide, H. Koizumi, and M. C. Pozzoni. Enhanced depth imaging spectral-domain optical coherence tomography. *Am J Ophthalmol*, 146(4):496–500, October 2008. ISSN 1879-1891. 47

[81] P. Thévenaz, U. E. Ruttimann, and M. Unser. A pyramid approach to subpixel registration based on intensity. *IEEE Transactions on Image Processing*, 7(1):27–41, 1998. 41

[82] M. W. Ulbig, D. A. McHugh, and A. M. Hamilton. Photocoagulation of choroidal neovascular membranes with a diode laser. *Br J Ophthalmol*, 77(4):218–21, April 1993. ISSN 0007-1161. 45, 46

[83] T. J. van den Berg and H. Spekreijse. Near infrared light absorption in the human eye media. *Vision Res*, 37(2):249–53, January 1997. ISSN 0042-6989. 45

[84] H. van den Bergh, J. P. Ballini, and M. Sickenberg. On the selectivity of photodynamic therapy of choroidal neovascularization associated with age-related macular degeneration. *J Fr Ophtalmol*, 27(1):75–8, January 2004. ISSN 0181-5512. 33

REFERENCES

[85] D. van Norren and J. van de Kraats. Imaging retinal densitometry with a confocal scanning laser ophthalmoscope. *Vision Res*, 29(12):1825–30, 1989. ISSN 0042-6989. 47

[86] C. J. Walter. Disc leak in the pathogenesis of posterior retinal degenerations. *Aust J Ophthalmol*, 8(3):235–9, August 1980. ISSN 0310-1177. 35

[87] B. C. Wilson and M. S. Patterson. The physics, biophysics and technology of photodynamic therapy. *Phys Med Biol*, 53 (9):R61–109, May 2008. ISSN 0031-9155. 33

[88] S. Yoneya, T. Saito, Y. Nishiyama, T. Deguchi, M. Takasu, T. Gil, and E. Horn. Retinal oxygen saturation levels in patients with central retinal vein occlusion. *Ophthalmology*, 109 (8):1521–6, August 2002. ISSN 0161-6420. 44

[89] M. F. Zuluaga, C. Mailhos, G. Robinson, D. T. Shima, R. Gurny, and N. Lange. Synergies of vegf inhibition and photodynamic therapy in the treatment of age-related macular degeneration. *Invest Ophthalmol Vis Sci*, 48(4):1767–72, April 2007. ISSN 0146-0404. 34

Part II

In Vivo Measurements of the Delayed Fluorescence Lifetime Issued from the pO_2-Sensitive Protoporphyrin IX to Individualize the Light Dose during Photodynamic Therapy

5

Introduction

5.1 A Brief Overview on Tissular Oxygen

Molecular oxygen is one of the most important gas in our environment since it is found as either a reactant or a product in a vast number of chemical and biochemical reactions. Thus, the determination of oxygen is important in various fields of chemical and clinical analysis, as well as for environmental monitoring [8]. The amount of oxygen is one of the most important variables in many physiological, pathological and therapeutic processes. We can express the amount of oxygen as a concentration $[O_2]$ or partial pressure of oxygen pO_2; these are related by $[O_2] = pO_2/k_H$, where k_H is the Henry's constant $[atm \times L/mol]$. In the present document we will use the pO_2 [%].

There is an increasing recognition that it would be very useful to directly measure the pO_2 in tissues with sufficient sensitivity, accuracy and ease. This would enhance the basic understanding of many types of physiological and pathophysiological phenomena at both macroscopically and microscopically levels. Such measurements could enable clinicians to improve the diagnosis and the treatment of many diseases, such as cancer and peripheral vascular insufficiency [29, 31].

Additionally, the response of tumors to ionizing radiation highly depends on pO_2 [31]. Therefore, different approaches were developed in radio-oncology to measure the tissular oxygen *in vivo*. The critical value was found to be about $5\,mmHg$; tissues with a lower pO_2 were shown to be significantly more resistant to ionizing radiation [28, 31]. In a series of experimental and clinical studies, different studies demonstrated that clinical measurements of the pO_2 provided useful inforamtions to predict the tumors response to radiation therapy [6, 19, 28, 32]. Despite the limited precision and the invasiveness of the technology used for these measurements, it is

interesting to note that their results were already significant.

Currently available techniques to measure the pO_2 can be broadly classified in two categories: (i) direct methods (invasive and noninvasive) that measure the $[O_2]$ or pO_2, (ii) indirect methods that measure a parameter related to the presence of oxygen, such as the saturation of hemoglobin [13].

The existing methods for directly measuring the pO_2 in cells and tissues include the Clark electrode [11, 25, 26], fluorescence quenching [22, 23], O_2 binding to myoglobin [10], chemiluminescence [7], phosphorescence quenching [1, 30] and spin label oximetry [4, 12, 20]. Indirect methods include the "comet assay" [2, 21] and drugs that selectively localize in hypoxic tissues. All these techniques, however, have some significant limitations, especially regarding their ability to make repeated measurements, their degree of invasiveness, and/or their sensitivity/accuracy. Considerable efforts are still ongoing in order to solve these problems [9, 18]. Luminescence lifetime measurements of the oxygen-dependent phosphorescence quenching to evaluate intravascular pO_2 is another common approach used *in vivo* [3, 16, 33, 34]. Shonat et al. [24] was the first to apply phosphorescence quenching imaging *in vivo* in retinal vessels by measuring the lifetime of a palladium porphyrin. An advantage of lifetime measurements is their independence to the concentration of the luminophore, making quantitative measurements possible *in vivo*. Most of the measurements of the tissular oxygen using the phosphorescence quenching technique have been based, up to now, on the use of porphyrin derivatives which are not approved for clinical use yet [5, 24, 27]. This situation explains why indirect methods are used to assess the oxygenation of tissues in humans.

The need for oxygen measurements at the cellular level, combined with the increasing concern for the understanding of the basic mechanisms responsible for the tissue destruction during PDT [15], strongly stress the interest of developing new approaches to assess the level of oxygen in different compartments of biological tissues. One promising approach, realistically applicable in the clinics, consists to determine the oxygen concentration via measurements of the delayed fluorescence of approved photosensitizers [14, 17, 18]. This approach would be intrinsically minimal invasive and will virtually measure the cellular pO_2 in the near proximity of the activated photosensitizer molecules within the PDT target zone. This last characteristic is of high interest; such a measurement would enable the measure of the O_2 consumption exactly in the same place were the reactive oxygen species (ROS) are produced.

5.2 Objectives of this Work

The first objective of this study was to demonstrate the feasibility of monitoring the tissular pO_2 *in vivo* by time-resolved measurements of the PpIX's delayed fluorescence (see Part I §2.4). To reach this goal, a new fiber based time-resolved spectrofluorometer was designed. The delayed fluorescence signal of the PpIX was then measured on the chick chorioallontoic membrane (CAM) *in vivo* model following topical administration of ALA.

As described in §5.1 the tissular pO_2 is depleted during PDT due to various photochemically initiated reactions between the PS and the oxygen. Therefore, the second objective was to verify the existing correlation between the tissular pO_2 depletion and the PDT irradiation dose administered to the CAM. Finally, we also wanted to verify whether monitoring tissular pO_2 consumption during PDT would predict the CAM's induced vascular damages.

Therefore, in Chapter 6, we will characterize the designed time-resolved spectrofluorometer and present the first preliminary pO_2 *in vivo* measurements.

In Chapter 7, we will present the correlation between the tissular oxygen depletion and the PDT light dose, as well as the correlation between the PDT induced vascular damages and the tissular pO_2 depletion.

References

[1] S V Apreleva, D F. Wilson, and S A Vinogradov. Tomographic imaging of oxygen by phosphorescence lifetime. *Appl Opt*, 45 (33):8547–59, November 2006. ISSN 0003-6935. 56

[2] C Aquino-Parsons, C Luo, C M Vikse, and P L Olive. Comparison between the comet assay and the oxygen microelectrode for measurement of tumor hypoxia. *Radiother Oncol*, 51(2): 179–85, May 1999. ISSN 0167-8140. 56

[3] P Babilas, G Liebsch, V Schacht, I Klimant, O S Wolfbeis, R M Szeimies, and C Abels. In vivo phosphorescence imaging of po2 using planar oxygen sensors. *Microcirculation*, 12(6): 477–87, September 2005. ISSN 1073-9688. 56

[4] J E Baker, W Froncisz, J Joseph, and B Kalyanaraman. Spin label oximetry to assess extracellular oxygen during myocardial ischemia. *Free Radic Biol Med*, 22(1-2):109–15, 1997. ISSN 0891-5849. 56

[5] S Blumenröder, A J Augustin, and F H Koch. The influence of intraocular pressure and systemic oxygen tension on the intravascular po2 of the pig retina as measured with phosphorescence imaging. *Surv Ophthalmol*, 42 Suppl 1:S118–26, November 1997. ISSN 0039-6257. 56

[6] J M Brown. Tumor hypoxia in cancer therapy. In Helmut Sies and Bernhard Brï£¡ne, editors, *Oxygen Biology and Hypoxia*, volume 435 of *Methods in Enzymology*, pages 295, 297–321. Academic Press, 2007. doi: DOI:10.1016/S0076-6879(07)35015-5. URL `http://www.sciencedirect.com/science/article/B7CV2-4R41NW6-H/2/413b3e95eee88aa8073143256e9d6ccf`. 55

[7] C Dodeigne, L Thunus, and R Lejeune. Chemiluminescence as diagnostic tool. a review. *Talanta*, 51(3):415–439, 2000. ISSN 0039-9140. doi: DOI:10.1016/S0039-9140(99)00294-5. URL `http://www.sciencedirect.com/science/article/B6THP-3YJYG1H-1/2/13c0e1eb4cc51b2432f869a0af22b18a`. 56

[8] J F Fernández-Sánchez, T Roth, R Cannas, Md K Nazeeruddin, S Spichiger, M Graetzel, and U E Spichiger-Keller. Novel oxygen sensitive complexes for optical oxygen sensing. *Talanta*, 71(1):242–50, 1 2007. doi: 10.1016/j.talanta.2006.03.043. 55

[9] Megan C. Frost, Steven M. Rudich, Huiping Zhang, Martín A. Maraschio, and Mark E. Meyerhoff. In vivo biocompatibility and analytical performance of intravascular amperometric oxygen sensors prepared with improved nitric oxide-releasing silicone rubber coating. *Analytical Chemistry*, 74(23):5942–5947, 2002. doi: 10.1021/ac025944g. URL `http://pubs.acs.org/doi/abs/10.1021/ac025944g`. 56

[10] C R Honig, T E Gayeski, W Federspiel, A Clark, and P Clark. Muscle o2 gradients from hemoglobin to cytochrome: new concepts, new complexities. *Adv Exp Med Biol*, 169:23–38, 1984. ISSN 0065-2598. 56

[11] A Y Isa, T H Ward, C M L West, N J Slevin, and J J Homer. Hypoxia in head and neck cancer. *Br J Radiol*, 79(946):791–8, October 2006. ISSN 1748-880X. 56

[12] H Jiang, N Beghei, R B Clarkson, H M Swartz, and B Galle. Microencapsulation of carbon particles used as oxygen sensors in epr oximetry to stabilize their responsiveness to oxygen in vitro and in vivo. *Phys Med Biol*, 46(12):3323–9, December 2001. ISSN 0031-9155. 56

[13] N Khan, B B Williams, H Hou, H Li, and H M Swartz. Repetitive tissue po2 measurements by electron paramagnetic resonance oximetry: current status and future potential for experimental and clinical studies. *Antioxid Redox Signal*, 9(8): 1169–82, August 2007. ISSN 1523-0864. 56

[14] I Lukomsky, V Gottfried, and S Kimel. Delayed fluorescence of porphyrins in different media. *Journal of Fluorescence*, 4(1): 49–51, 1994. 56

[15] B W McIlroy, A Curnow, G Buonaccorsi, M A Scott, S G Bown, and A J MacRobert. Spatial measurement of oxygen levels during photodynamic therapy using time-resolved optical spectroscopy. *J Photochem Photobiol B*, 43(1):47–55, April 1998. ISSN 1011-1344. 56

[16] E G Mik, C Donkersloot, N J H Raat, and C Ince. Excitation pulse deconvolution in luminescence lifetime analysis for oxygen measurements in vivo. *Photochemistry and Photobiology*, 76(1):12–21, 7 2002. 56

[17] E G Mik, J Stap, M Sinaasappel, J F Beek, J A Aten, T G van Leeuwen, and C Ince. Mitochondrial po2 measured by delayed fluorescence of endogenous protoporphyrin ix. *Nature Methods*, 3(11):939–45, 11 2006. doi: 10.1038/nmeth940. 56

[18] E G Mik, T Johannes, C J Zuurbier, A Heinen, J H P M Houben-Weerts, G M Balestra, J Stap, J F Beek, and C Ince. In vivo mitochondrial oxygen tension measured by a delayed fluorescence lifetime technique. *Biophysical Journal*, 95(8): 3977–90, 10 2008. doi: 10.1529/biophysj.107.126094. 56

[19] H Minn, T J Grönroos, G Komar, O Eskola, K Lehtiö, J Tuomela, M Seppänen, and O Solin. Imaging of tumor hypoxia to predict treatment sensitivity. *Curr Pharm Des*, 14 (28):2932–42, 2008. ISSN 1873-4286. 55

[20] J A O'Hara, N Khan, H Hou, C M Wilmo, E Demidenko, J F Dunn, and H M Swartz. Comparison of epr oximetry and eppendorf polarographic electrode assessments of rat brain pto2. *Physiol Meas*, 25(6):1413–23, December 2004. ISSN 0967-3334. 56

[21] P L Olive, R E Durand, S M Jackson, J C Le Riche, C Luo, R Ma, D B McLaren, C Aquino-Parsons, T A Thomson, and T Trotter. The comet assay in clinical practice. *Acta Oncol*, 38(7):839–44, 1999. ISSN 0284-186X. 56

[22] N Opitz and D W Lübbers. Theory and development of fluorescence-based optochemical oxygen sensors: oxygen optodes. *Int Anesthesiol Clin*, 25(3):177–97, 1987. ISSN 0020-5907. 56

[23] A D Shaw, Z Li, Z Thomas, and C W Stevens. Assessment of tissue oxygen tension: comparison of dynamic fluorescence quenching and polarographic electrode technique. *Crit Care*, 6(1):76–80, February 2002. ISSN 1364-8535. 56

REFERENCES

[24] R D Shonat, D F Wilson, C E Riva, and M Pawlowski. Oxygen distribution in the retinal and choroidal vessels of the cat as measured by a new phosphorescence imaging method. *Appl. Opt.*, 31(19):3711–3718, 1992. URL http://ao.osa.org/abstract.cfm?URI=ao-31-19-3711. 56

[25] I A Silver. Microelectrodes in medicine. *Philos Trans R Soc Lond B Biol Sci*, 316(1176):161–7, August 1987. ISSN 0962-8436. 56

[26] I A Silver. Polarography and its biological applications. *Phys Med Biol*, 12(3):285–99, July 1967. ISSN 0031-9155. 56

[27] T K Stepinac, S R Chamot, E Rungger-Brändle, Pierre Ferrez, J L Munoz, Hubert van den Bergh, C E Riva, C J Pournaras, and G A Wagnières. Light-induced retinal vascular damage by pd-porphyrin luminescent oxygen probes. *Invest Ophthalmol Vis Sci*, 46(3):956–66, March 2005. ISSN 0146-0404. 56

[28] H B Stone, J. Martin Brown, T L Phillips, and R M Sutherland. Oxygen in human tumors: correlations between methods of measurement and response to therapy. summary of a workshop held november 19-20, 1992, at the national cancer institute, bethesda, maryland. *Radiat Res*, 136(3):422–34, December 1993. ISSN 0033-7587. 55

[29] H M Swartz and R B Clarkson. The measurement of oxygen in vivo using epr techniques. *Physics in Medicine and Biology*, 43(7):1957–1975, 1998. URL http://stacks.iop.org/0031-9155/43/1957. 55

[30] J M Vanderkooi, G Maniara, T J Green, and D F Wilson. An optical method for measurement of dioxygen concentration based upon quenching of phosphorescence. *The Journal of Biological Chemistry*, 262(12):5476–82, 4 1987. URL http://www.jbc.org/cgi/pmidlookup?view=long\&pmid=3571219. 56

[31] Vaupel, A Mayer, S Briest, and M Höckel. Hypoxia in breast cancer: Role of blood flow, oxygen diffusion distances, and anemia in the development of oxygen depletion. *Advances in Experimental Medicine and Biology*, 566:333–42, 2005. doi: 10.1007/0-387-26206-7_44. URL http://dx.doi.org/10.1007/0-387-26206-7_44. 55

[32] B Vileno. *Oxidative stress on biomaterials*. PhD thesis, EPFL, Lausanne, 2006. URL http://library.epfl.ch/theses/?nr=3501. 55

[33] D F Wilson. Measuring oxygen using oxygen dependent quenching of phosphorescence: a status report. *Adv Exp Med Biol*, 333:225–32, 1993. ISSN 0065-2598. 56

[34] D F. Wilson, S A Vinogradov, P Grosul, N Sund, M N Vacarezza, and J Bennett. Imaging oxygen pressure in the rodent retina by phosphorescence lifetime. *Adv Exp Med Biol*, 578:119–24, 2006. ISSN 0065-2598. 56

6

Delayed Fluorescence Setup (Submitted Paper)

An Optical Fiber-based Setup for *in vivo* Measurement of the Delayed Fluorescence Lifetime of Oxygen Sensors

Filippo Piffaretti, Santhakumar Kanappan, Eddy N. Forte, Hubert E. van den Bergh, Georges Wagnières

Federal Institute of Technology Lausanne (EPFL)
Lausanne, Switerland

Keywords: Tissular, Oxygen, *In vivo*, Lifetime, PpIX, Luminescence, Delayed fluorescence

Abbreviation: (PDT) Photodynamic therapy, (ALA) 5-amino-levulinic acid, (PpIX) Protoporphyrin IX, (CAM) Chick chorio-allantoic membrane, (AMD) Age-related Macular Degeneration,(PS) Photosensitizer, (DF) Delayed fluorescence, (ISC) Intersystem crossing, (PF) Prompt fluorescence, (PMT) Photomultiplier tube, (DSO) Digital storage oscilloscope

Abstract

A new optical-fiber-based spectrofluorometer for *in vivo* or *in vitro* detection of delayed fluorescence is presented and characterized. This compact setup is designed so that it can be readily adapted for future clinical use. Optical excitation is done with a nitrogen laser-pumped, tunable dye laser, emitting in the UV-Vis part of the spectrum. Excitation and luminescence signals are carried to and from the biological tissues under investigation, located *out* of the setup enclosure, by a single optical fiber. These measurements, as well as measurements performed without a fiber on *in vitro* samples in a thermostatable quartz cell, in a controlled-atmosphere enclosure, are possible due to the efficient collection of the laser induced luminescence light which is collected and focused on the detector with a high aperture parabolic mirror. The detection is based on a gated photomultiplier which allows for time-resolved measurements of the delayed fluorescence intensity. Thus, relevant luminescence lifetimes, in the microsecond-to-millisecond range can be measured, with near total rejection of the sample's prompt fluorescence. The instrument's spectral and temporal resolution, as well as its sensitivity, are characterized and measurement examples are presented. The primary application foreseen for this setup is the monitoring and adjustment of the light dose delivered during photodynamic therapy.

6.1 Introduction

Photodynamic therapy (PDT) is a well established method for the treatment of Age-related Macular Degeneration (AMD) and various kinds of light-accessible tumors [23, 46]. It relies on the use of light, a light-sensitive dye molecule and molecular oxygen present in the tissue [5, 10, 22, 28, 33, 41, 49, 51, 53, 66, 69, 76]. The mechanisms responsible for tissue destruction by PDT involve highly reactive singlet oxygen [$^1O_2(^1\Delta_g)$], or oxygen radical species generated by the photoexcited dye molecule also called the photosensitizer (PS). These oxygen species oxidize the biological substrate thus inducing photodamage which can lead to direct cell death and/or blood vessel occlusion [43, 51, 77]. The efficiency of this process depends among others on the concentration of tissular oxygen. Excitation of the PS to the lowest excited singlet state, which can, in some molecules, undergo intersystem crossing to the PS's triplet state, may be followed by phosphorescence of this triplet state. This phosphorescence may, in turn, be quenched by the tissue oxygen, allowing for an indirect measurement of the dissolved molecular oxygen concentration using the Stern-Volmer equation 6.1. The latter relates this tissular oxygen concentration [O_2] to the photosensitizer's triplet state phosphorescence intensity I and its lifetime τ as follows:

$$I_0/I = \tau_0/\tau = 1 + k_q\tau_0[O_2] \tag{6.1}$$

where I_0 and I are the phosphorescence intensities in the absence, respectively the presence of an oxygen concentration [O_2], τ_0 and τ are the corresponding phosphorescence lifetimes and k_q is the bimolecular quenching constant.

Measuring the oxygen concentration [O_2], usually expressed as its partial pressure pO_2, at the actual location where the PS is applied for PDT, can help to determine and optimize the therapeutic light dose, if knowledge is available on several other PDT parameters [76]. Indeed, differences in the oxygen consumption rate as well as differences between the initial oxygen concentration in normal and neoplastic tissues are likely to be responsible for over - or under - treatment of the targeted tissues. In any case, the oxygen concentration in the tissue and its diffusion towards the PDT-treated zone will influence the therapeutic efficacy. Furthermore, it is known that certain regions of larger tumors can become hypoxic, which may negatively affect the efficacy of PDT or radiotherapy [6, 11, 32, 52, 65, 75]. More generally, measurement of the pO_2 can in principle provide valuable information for the early diagnosis of various diseases. Among others, this may be the case for exsudative AMD,

as well as vascular occlusive diseases, diabetic retinopathy and possibly even glaucoma [12, 54, 61]. Such diseases are very likely associated with changes of the micro-vasculature due to decreased cellular oxygen concentrations [1, 26, 74].

Various kinds of oxygen-sensitive phosphorescent molecules have been proposed to monitor the pO_2 [56, 60, 73]. However only a few among them can be exploited as PSs and none of these oxygen sensing molecules have been approved for use in humans. Unfortunately, most PSs - including PpIX, which is commonly used for PDT treatment of oncologic conditions - do not present a phosphorescence that is easily detectable *in vivo*, either because the phosphorescence quantum yield is too low and/or because this luminescence takes place at wavelengths too long to be easily detected [4, 56, 60]. PpIX's triplet state de-excitation has been measured at low temperature ($77° K$) in a solid octane matrix [68], showing a phosphorescence peak at around 792 nm, a quantum yield of 6×10^{-3} and a lifetime of 11 msec, with a non-radiative T1-S0 decay probability about twice as large as the radiative one. More recently, phosphorescence lifetimes of HpD and PpIX were measured at room temperature at 894 nm - but in lipophilic milieux [45]. In a biological milieu at about $37° C$, the non-radiative decay pathways are even more favoured than at low temperature in non-polar matrixes. Thus, measuring PpIX's phosphorescence under experimental conditions compatible with a clinical environment would be very difficult indeed [44, 63]. This difficulty can be overcome by measuring the *delayed fluorescence* lifetime *instead of* the PS's *phosphorescence* lifetime [25, 38, 41]. This idea underlies the work described in the present paper. The "delayed fluorescence" (DF) phenomenon is schematically represented in the Jablonski diagram of Figure 6.1.

The electronic ground state of the PS is a singlet state (S_0). Upon light absorption (1) the PS is excited to a short-lived, vibrationally excited, first excited singlet state which rapidly vibrationally relaxes to its ground state S_1 . The overall lifetime of S_1 in cuvette conditions is about $15\,ns$ for PpIX in acqueous solution [34], and $\approx 7\,ns$ *in-vivo* [31, 57]). The PS can return to the S_0 state by fluorescing (2) or by internal conversion (3). Alternatively, S_1 can undergo "spin-forbidden" *intersystem crossing* (ISC) to the triplet state T_1, (4). This fairly long-lived T_1 state, whose lifetime is in the μs-to-ms range for PpIX, may return directly to the ground state by *phosphorescence* (5) or through a non-radiative path (6). Some molecules in the T_1 state may, however, have sufficient thermal energy to undergo reverse ISC, from a vibrationnally excited level of T_1 to the S_1 singlet state (7), after which they may return to the ground state, through what

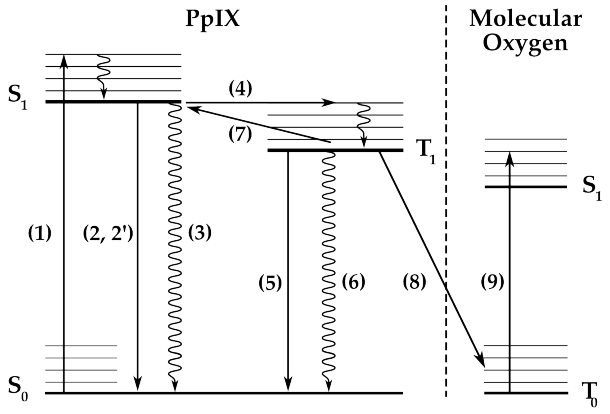

Figure 6.1: Jablonski diagram of the PpIX photosensitizer and its interaction with molecular oxygen. See text for details.

is now *delayed fluorescence* (2'): *i.e.* the PS returns to the ground state by emitting photons of essentially the same spectral distribution as normal "prompt" fluorescence. However, this "delayed fluorescence" (DF) generally has a much weaker intensity than the prompt fluorescence and its lifetime is similar to that of phosphorescence. This is why delayed fluorescence might sometimes be taken for phosphorescence [48]. In the presence of molecular oxygen, near-resonant collisional energy transfer (8) between the T_1 state of PpIX and the T_0 ground state ($^3\Sigma$) of molecular O_2 takes place, leading to (9) the excitation of O_2 ($^3\Sigma$) to its S_1 singlet excited state $O_2(^1\Delta_1)$ [30, 58] and simultaneously the return of PpIX to its ground S_0 state.

One advantage of using this approach for the *in-vivo* measurement of tissular pO_2 is that no exogenous molecular probe needs to be administered. In the case of PpIX, an additional benefit arises from the fact that it becomes possible, through the PS's quenched phosphorescence, to measure the pO_2 at the very locations where the PS is acting (see §6.3.2).

In this paper, we report on the design, characterization (in terms of excitation source, spectral and temporal resolution and sensitivity), and calibration, of a sensitive, time-resolved, optical-fiber-based spectrofluorometer, which can be used for both *in vitro* and *in vivo* detection of delayed fluorescence. The setup must be able to detect the very weak DF signals emitted by most PS's, and allow (in the case of *in vivo* PDT), for using an optical fiber to probe tissues which would be difficult to access otherwise, for instance in the hollow organs.

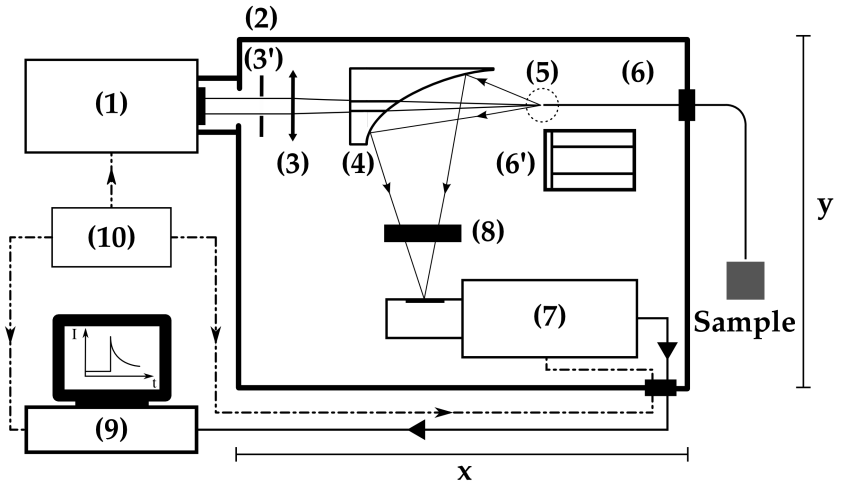

Figure 6.2: Optical design and overall geometry of the spectrofluorometer. (1) dye laser; (2) metal-and-wood experimental enclosure, x = 430 mm, y = 230 mm, height = 250 mm; (3') diaphragm; (3) lens, F = 150 mm; (4) parabolic mirror with cylindrical hole; (5) irradiation location; (6) optical fiber; (6') Thermostatable cell holder; (7) Gatable photomultiplier; (8) rotatable optical filters holder; digotal storage oscilloscope and PC; (10) signal delay generator.

6.2 Design of the Spectrofluorometer

One specific problem of this oxygen measurement approach is that prompt (normal) fluorescence (PF) and DF have essentially the same spectroscopies. In addition, the system must be usable for *in vivo* measurements. An optimal and practical design of the measurement setup must therefore address three main problems: (i) The weak intensity of the DF signal, as compared to the much stronger normal fluorescence, requires a high light gathering and transmission capacity. (ii) Because DF and PF differ only by their lifetimes, we need a system to discriminate between these two signals: basically, the detector must be blinded during the emission of the strong PF to enable the detection of the much weaker DF. (iii) The system should allow both to measure *in vitro* samples and to monitor living tissues.

The first and third concerns are dealt with and discussed under section 6.2.1 hereunder, while section 6.2.2 deals with the second problem. We also discuss the mathematical processing of the acquired data in section 6.2.3. Validation of the sensitivity of the measurements, and their calibration, including the setup's spectral and temporal resolution, are dealt with in sections 6.2.4 and 6.2.5, respectively.

6.2.1 General design and Optics

A schematic representation of the apparatus is shown in Figure 6.2. The excitation light pulses at 405 nm are provided by a dye laser (1) (LTB® model UDL-200), pumped by a pulsed N_2 laser (not shown, LTB® model MSG 803-TD). The laser beam enters the main, light-tight, blackened experimental enclosure (2) through a small hole and then passes through an iris diaphragm (3') which blocks most of the spontaneous emission of the dye cell. The beam passes through a small channel drilled in the parabolic mirror (4) (Edmund Optics® NT47-103, 90°off-axis, aluminium coated, EFL = 50.8 mm), while being focused with a low luminescence plano-convex lens (3) (Edmund Optics® NT47-276, ∅ 20 mm, EFL = 150 mm) onto the tip (5) of a multimode optical fiber (6) (Laser Components® HCG-M0550T, core diameter = 550 μm, NA = 0.22). For *in-vitro* experiments, a quartz cuvette (Hellma®, 174-QS) is held inside the apparatus at the irradiation location (5), using a thermostatable cuvette holder (6'), see figure 6.3. The plano-convex lens (3) is mounted on a 5-degrees-of-freedom holder, allowing for easy focusing of the laser beam on a pre-defined point, (5). The luminescence emitted from the irradiated sample is collected by the far-end of the optical fiber (6) and returned to the enclosure, where a large fraction (probably more than 80 %) of this light falls on the parabolic metal mirror (4) and is reflected and focused by it on a gatable photomultiplier (PMT) (7) (Hamamatsu® R955). The reflected laser light and unwanted optical background noise are filtered out by a band-pass filter (Chroma® HQ645/75) in the filter wheel (8). The PpIX DF signal is recorded with a digital storage oscilloscope (DSO) (Lecroy® LT342), connected to a PC (9). Note that a signal delay generator (10) (Stanford Research Systems®, DG535) is used to synchronize the gating of the PMT with the laser pulses and to trigger the DSO with the DF signals.

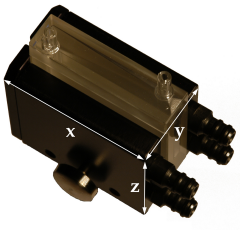

Figure 6.3: Thermostatable quartz cell holder with dual, water-heated side-blocks. Cast aluminium, $x = 55\,mm$, $y = 32\,mm$, $z = 45\,mm$.

The present optical design, based on the use of a parabolic mirror, presents some advantages as compared to standard configurations for optical-fiber-based spectrometers. These include: (i) the abscence of spectral distortions due to the fact that no refraction - but only reflections - take place in this part of the optical setup; (ii) no autoluminescence

is induced in this optical element which, due to its metallic nature, does not interact with the excitation pulse; (iii) the solid angle of acceptance of the parabolic mirror (≈ 0.6 sr) is larger than the entrance solid angle of the optical fiber ($\approx$ 0.15 sr), which leads to a high light recovery fraction; (iv) the mirror's parabolic shape eliminates the need of an additional lens to focus the luminescence emitted by the fiber tip (or the quartz cuvette) on the detector. This is because the detector's window is conveniently located at the imaging point of this mirror. Note: the setup is designed for a 1:1 magnification.

The fiber-based measurement mode is well suited for in vivo studies, where the light must be delivered to tissue, outside of the setup's light-tight enclosure. When measuring a sample in the thermostatable quartz cell (6'), placed at the focal point of the laser beam (5), again a sizable fraction of the luminescence from the liquid sample falls on the parabolic mirror. The measurements in that case are thus completed inside the light-tight enclosure (2). This leads to a higher sensitivity and less noise. In addition, it is possible, if desired, to control the temperature the humidity and gas composition in the enclosure.

6.2.2 Delayed and Prompt Fluorescence Discrimination

As the whole setup is constructed in a light-tight enclosure, undesired light is eliminated. The time-resolved detection of the weak DF signal nevertheless requires gating to avoid saturation of the detector by the much stronger PF signal. To achieve this, the photomultiplier tube can be electrically switched on, about $3\,\mu s$ *after* the laser pulse. During this time, the intensity of any PF decreases to the noise level. Because the intensity of the PF is at least 2 orders of magnitude *stronger* than that of the DF, and because the photons of the PF hit the inactive photocathode during the $\approx 3\,\mu s$ offset-time, fast recovery of the high gain as well as proper correction for PMT artefacts are required. For these reasons, we used an R955 Hamamatsu PMT with a broad wavelength response ($185 - 900\,nm$), low noise and high gain.

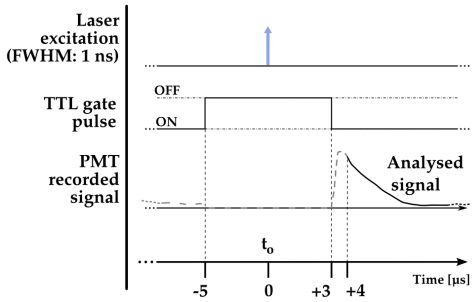

Figure 6.4: Chronogram of the PMT gating and signal acquisition process.

A gated D-Type socket assembly (Hamamatsu® C1392-57) was used together with this PMT. The PMT is "gated" by holding the photocathode at a potential of about +10 V with respect to the first dynode. The

gate function is driven by an external user-triggered TTL pulse. In this way, the PMT is blinded during the laser excitation and prompt fluorescence emission. The signal delay generator (10, Figure 6.2) thus turns the PMT off, about $5\,\mu s$ before triggering the laser pulse, for about $8\,\mu s$. The rise time for the gating is typically $400\,ns$ (see Figure 6.4).

6.2.3 Data Acquisition and Analysis

The DF signal is transformed by the PMT into an analog electrical signal which is supplied to the DSO for averaging. The analog signal from about 30 transients is digitized[1] and transferred to the PC for further analysis. The parameters describing the luminescence decay are obtained by fitting the time-dependent digitized signal $f(t)$ with a sum of exponential functions:

$$f(t) = \sum_{i=1}^{n} A_i \, exp^{(t/\tau_i)} \qquad (6.2)$$

The set of exponential lifetimes (τ_i) characterizes the PS molecule and its physical environment. Each pre-exponential factors A_i is proportional to the intensity of the i^{th} component to the total luminescence intensity.

The Levenberg-Marquardt (L-M) method is used for non-linear least-squares fit of the measured data [37, 39, 47, 55, 62]. We wrote and used an Octave® [GNU GPL] L-M algorithm implementation. The calculated mathematical fits were graphically checked by plotting the residuals of each fit and the autocorrelation of the residuals [7, 19], as shown, *e.g.*, in Figure 6.5.

6.2.4 Setup calibration and system sensitivity

We have validated and calibrated the setup through luminescence measurements on well-characterized molecules. The luminescence lifetime of reference samples depends on the fluorochrome's environment, on small changes in the molecular structure, on the presence of quenchers and on temperature. For these reasons, we have chosen two different cristalline lanthanide(III) complexes whose properties and behaviours were known to be stable in the chosen environments.

The first reference compound was a powdered samarium complex: [Sm^{III} -(hfa)$_3$(4-cypNO)]$_2$ [18] [2]. This sample was used to verify the validity of our measurements close to the temporal resolution limit of our system ($\approx 0.7\,\mu s$, see §6.2.5). When the luminescence of this powder was measured with our setup, we observed a signal with a mono-exponential lifetime of $(1.27 \pm 0.09\,\mu s)$. This compares well with the litterature value

[1] as a 24 bits floating point number (IEEE 745) corresponding to a decimal precision of $log_{10}(2^{24}) \approx 7$ decimal digits

[2] hfa$^-$ = hexafluoroacetylacetonate; 4-cpyNO = 4-cyanopyridine N-oxide

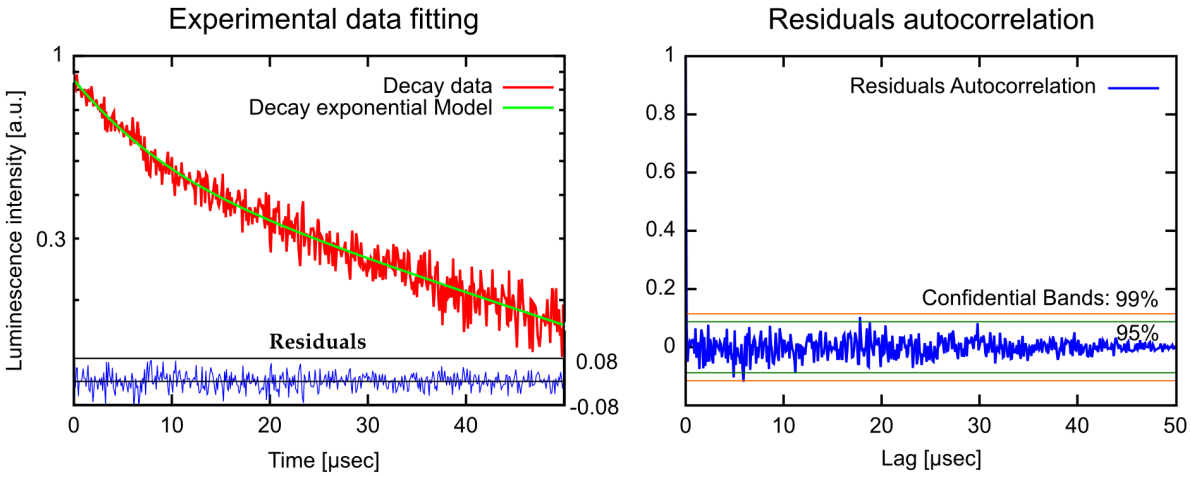

Figure 6.5: Analysis of the fitting results: the semi-logarithmic scale used to plot the experimental data and the fitting results help to visualize a bad fit. Random dispersions, around zero, of the residuals and their autocorrelation, confirm the quality of the fit.

of $(1.13 \pm 0.05\,\mu s)$ [15]. The second reference compound was a *2:3* stoichiometric solution of an europium complex [Eu^{III}-:H_2L^{C2}] in water/glycerol (9/1, v/v)[1] whose lifetime is expected to be in the milliseconds range. With a fiber-to-quartz-cell distance of $100\,\mu m$, we measured a mono exponential decay with a lifetime of $(2275 \pm 127)\,\mu s$, as compared to the published value of $(2200 \pm 100)\,\mu s$ [15]. The small differences of $< 10\%$ resp. $< 5\%$ observed between our measurements and those made by Chauvin *et al* are compatible with the stated error limits. They might be explained by small differences in (i) the sample excitation wavelengths: 355 nm *vs* 405 nm, and (ii) the actual physical environments of the lanthanide complexes.

The sensitivity of the system was determined by measuring the time-resolved luminescence decay of solutions of PpIX in dimethyl sulfoxide (DMSO) and of Pd-meso-tetra(4-carboxyphenyl)-porphyrin (PdTCPP) in phosphate buffered saline (PBS). PpIX is a frequently used photosensitizer and presents a delayed fluorescence [13, 14, 40], while PdTCPP is a commonly used oxygen sensor for in vivo measurements [4, 56, 60, 62, 70]. Luminescence decays were thus measured at decreasing concentrations ranging between 10^{-4} and $10^{-7}\,M$, within 1 hour of sample preparation. The sensitivity limit was then determined for the lowest photosensitizer concentration, still yielding measurements with a signal to noise ratio (SNR) allowing for the retrieval of accurate lifetimes. The latter is defined here as the

[1] H_2L^{C2}: homoditopic ligand 6,6' - for very long luminescence lifetimes

(a) SNR of the time-resolved luminescence decay of PpIX (MW= 606 g/mol) in DMSO solution at different concentrations, at standard environmental oxygen concentration ($pO_2 \approx 150$ mm Hg)

Concentration $[M]$	SNR
5×10^{-5}	64.45
1×10^{-5}	36.46
8.2×10^{-6}	32.97
1.6×10^{-6}	5.64
8.2×10^{-7}	2.89

(b) SNR of the time-resolved luminescence decay of PdTCPP (MW=895 g/mol) in PBS solution at different concentrations

Concentration $[M]$	SNR
5×10^{-5}	28.1
1×10^{-5}	26.3
5×10^{-6}	23.0
1×10^{-6}	10.2
5×10^{-7}	6.4

Table 6.1: Setup sensitivity assessment

standard deviation on the measured lifetime being $< 10\%$. The SNR was expressed as the ratio of the signal to the RMS noise level. Tables 6.1(a) and 6.1(b) show the calculated SNR at the different concentrations. The sensitivity of the system is therefore sufficient to measure the weak delayed fluorescence of PpIX in typical *in vivo* conditions where its concentration might be on the order of $1 \times 10^{-5}\, M$.

After these preliminary validating results, we compared the radiant DF energy of PpIX, which is proportional to the area under the recorded signal - and therefore to the totality of detected DF photons - to its *total* luminescence. The ratio of these energies yields an estimate of the DF's detectability. The DF signal was recorded and measured as already described. The signal of the total luminescence (proportional to the sum of all molecule's emissive desexcitation) was measured by (i) adding neutral density (OD 3.9) filters between the parabolic mirror and the PMT, and (ii) recording the luminescence emitted by the PpIX sample from the beginning of the laser excitation pulse. The ratio of the total PpIX's luminescence to its DF was found to be 145:1 for *in vitro* measurements performed on a DMSO solution at pH=7.2, and 300:1 for *in-vivo* measurements performed on a CAM membrane topically treated with ALA, a precursor of PpIX (see § 3.2 for details). The values obtained are in reasonable agreement with the estimates given in the litterature [27]

6.2.5 Setup temporal resolution

The two devices that limit the temporal resolution of the setup are the PMT and the current-to-voltage converter circuit connected in series between the PMT and the DSO. The loss of temporal resolution due to the PMT can be approximated by the sum

of the anode pulse rise time and the electron Transit Time Spread (TTS) $\approx 2.2\,ns + 1.2\,ns$, for a total of $\approx 3.5\,ns$, which is negligible with respect to the contribution made by the current-to-voltage circuit. The latter is characterized by an RC response time. A load resistance value of $R_{load} = 500\ \Omega$ was chosen in order to have a comfortable signal intensity during *in vivo* measurements. With the help of a very short light pulse (the nearly *delta* excitation laser pulse: $\approx 300 - 400\,ps$) and with two different load resistances, the parasite capacitance of the circuit was measured to be $145\,pF$. The characteristic temporal response of the setup is therefore set to be $R_{load} \times C = 72\,ns$, which is the setup's temporal resolution. This response time of $\approx 72\,ns$ is negligible if the measured signals have typical lifetimes larger then $10\,\mu s$, as is the case for the delayed-fluorescence lifetime of PpIX.

6.2.6 Background Optical Noise

To generate a well defined maximum optical background noise, we placed a non-fluorescing white reflecting coated plate (SphereOptics®, White Reflecting Coating, reflection $>$ 98% of incident light) perpendicular to and in contact with the end of the optical fiber, and recorded the signal generated by this diffusely reflected light. The aim was to evaluate if this maximum optical background noise could still be considered as negligible when compared to the weak DF signal expected from an *in vivo* measurement of the PpIX's DF. The back-scattered signal was recorded after a delay of $3\,\mu s$ from the excitation and averaged over 30 sweeps.

An appreciable optical background signal, probably due to both the parasitic luminescence of the optical fiber itself and the SphereOptics plate, plus the luminescence of the band-pass filter located in front of the PMT, was observed. The intensity of this background noise was in the worst case one order of magnitude smaller than the expected experimental signal. The background noise created by the reflection of the laser excitation on the sample can therefore be neglected.

6.3 Results and Discussion

6.3.1 Examples of *In Vitro* Lifetime Measurements

The luminescence lifetime of two porphyrins, PdTCPP and PpIX, in aqueous (PBS) and DMSO solutions respectively, were carefully characterized *in vitro* to confirm that the sensitivity of the setup would allow to observe luminescence lifetime changes due to variations in O_2 quencher concentration. By bubbling during $30\,min$ different, well defined, oxygen-nitrogen gas mixtures[1], the O_2 dissolved in

[1] Oxygen solubility at $1\,atm$, 25°, is $2.2 \pm 0.09\,mM$ in DMSO [2] and $2.5\,mM$ in water.

pO_2 $[mmHg]$	$[O_2]$ [%]	Measured lifetime $[\mu s]$	Literature $[\mu s]$
0	0	358 ± 15	$340 - 360$
7.4	1	61.2 ± 1.5	
37	5	12.2 ± 0.5	
74	10	6.2 ± 0.3	
155	21	3.11 ± 0.2	

Table 6.2: PdTCPP phosphorescence quenching by oxygen: Lifetime measurements of an $83\,\mu M$ solution of PdTCCP in PBS at room temperature, pH 7.4, at different pO_2 values.

the porphyrin solutions was changed. All measurements were carried out at room temperature (22°) and the solutions were freshly prepared (within 1 h from the measurement) and stored in quartz cuvettes.

As a validation measurement, the lifetimes of a PdTCPP solution in PBS ($83\,\mu M$, pH = 7.4) were measured, by the analysis of the averaged luminescence decay signal over 30 sweeps at 5 different pO_2. An excellent linear Stern-Vollmer relationship was verified and good agreement was found between our measurement at $pO_2 = 0$ and the values reported in the literature for oxygen-free PdTCPP solutions (see Figure 6.6). No attempt was made to compare lifetimes at other O_2 concentrations as the strong dependency of Henry's coefficients on temperature and exact solvent nature cannot be easily corrected for, see Table 6.2) [67, 71, 72].

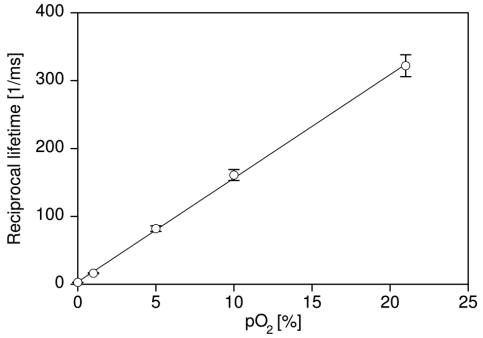

Figure 6.6: Verification of the Stern-Volmer equation ($\tau_0 = 0.358\,ms$, $k_q = 2.04\,(mmHg \quad ms)^{-1}$) for a solution of PdtCPP in PBS ($83\,\mu M$, pH = 7.4)

As mentionned in §6.1, there are few *in vitro* PpIX's delayed fluorescence lifetime measurements in the literature and they are not directly comparable, due to the sensitivity of PpIX's DF lifetime to pH, temperature, concentration of the solution and quencher concentration [8, 14, 35, 42, 59]. Therefore a directly comparative study could not be performed for this molecule. A PpIX solution in DMSO ($1.6\,\mu M$, pH=7.2) was prepared and stored in a quartz cuvette as described before.

The measurements reported in Table 6.3 allow us to confirm the possibility (*in vitro)* of measuring *changes* in PpIX's lifetime ascribable to changes in the O_2 concentration. Our measurement at $pO_2 = 0$ is here compared with the one published by Mik et al. [40] and found to be in reasonable agreement with it.

The same PpIX solution was measured (after 3h of pure N_2 bubbling) with a commercial (Perkin Elmer LS 50B) time resolved spectrofluorometer to compare the spectrum of the measured luminescence with that of the prompt fluorescence. This allowed to confirm that the luminescence measured was really the delayed fluorescence as it exhibited the same spectroscopy as that of the *prompt* fluorescence, but displayed lifetimes characteristic of the triplet state (see Figure 6.7).

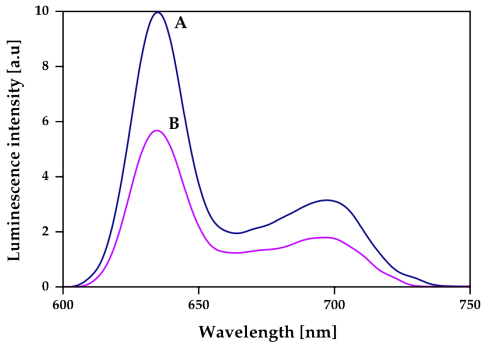

Figure 6.7: PpIX's luminescence spectrum. Measurements performed with a Perkin-Elmer LS 50B spectrofluorometer. (A): Prompt fluorescence; (B): Delayed fluorescence measured 1.3 ms after the excitation. The gain difference is *ca.* a factor of 100.

6.3.2 Examples of *In Vivo* Measurements

When using PpIX as a PS, the usual approach consists in administering to the patient *a precursor* of the drug. The most commonly used precursor molecules are 5-aminolevulinic acid (ALA) or certain of its esterified derivatives [9, 17, 50]. The biosynthetic pathway involves the combination of two ALA molecules to form a pyrrole unit, and four of these finally are combined to form one PpIX moiety, which itself is a part of haemoglobin [20, 29]. Because of the enzymatic activity in diseased or cancerous tissues, the production of PpIX is locally and selectively strongly enhanced, as compared to the surrounding normal tissue [3, 16, 21].

Our setup must allow, in this case, to measure through the PpIX's delayed fluorescence, the pO_2 at any location where the PS is being formed. In this section, we report three examples of *in vivo* delayed fluorescence measurements, performed on the chick chorio-allantoic membrane (CAM) model.

Fifteen fertilized eggs underwent routine handling in order to obtain healthy developing CAMs until day 10 [24, 36, 64]. Four hours before the measurements and after removal of the upper part of the shell, as described by Lange et al. [36], the chick embryos where topically administered a droplet of ALA solution[1]. As described in §6.1, the

[1]droplet volume $20\,\mu l$, $152\,mM$ ALA-H_2O solution, adjusted to pH 6.0, corresponding to $\approx 40\,mg/kg$.

pO_2 $[mmHg]$	$[O_2]$ [%]	Measured lifetime $[\mu s]$	Literature $[\mu s]$
0	0	1630 ± 120	1200 ± 100
7.4	1	56 ± 4	270 ± 20
22.2	3	14 ± 0.4	90 ± 7

Table 6.3: Influence of variations in pO_2 on PpIX's DF lifetime: Luminescence lifetime measurements of an $1.6\,\mu M$ solution of PpIX in DMSO at room temperature, pH=7.2, at different pO_2 values.

DF lifetime is related to the concentration of molecular O_2 which acts as quencher in this case.

It should be noted that the oxygen concentration in the CAM is also influenced by molecular O_2 diffusing from the atmosphere. In order to reduce this O_2 inflow significantly and make the CAM's tissular $[O_2]$ decrease measurable, just before start of irradiation, we placed an impermeable barrier on the CAM: the region to be measured was covered by a round microscope cover glass ($\varnothing\ 20\,mm$, $0.15-0.19\,mm$ thick, Schott D263M). The optical fiber probe was made to point towards the middle of the cover glass ($\approx 100\,\mu m$ from the surface, probed surface diameter $\approx \varnothing\ 500\,\mu m$).

The probing laser ($405\,nm$) excites the PpIX molecules produced during the $4\,h$ of incubation and the resulting luminescence was collected by the fiber tip and analyzed as described earlier. It was demonstrated that the probing laser pulses did not photodynamically or otherwise damage the CAM and did not significantly affect the tissular oxygen concentration if the total number of consecutive pulses was limited to 30. Therefore, for the following *in-vivo* measurements, only 20 shots were averaged.

The first *in vivo* experiment presented demonstrates the phenomenon of tissular oxygen consumption during laser irradiation, as monitored by measuring the PpIX's DF lifetime. Measurement of oxygen consumption was performed using the following experimental protocol: four series of 400 probing laser shots (at a pulse frequency of $10\,Hz$) were fired at the CAM sample, with a break of $1\,min$ of darkness between each series. The DF measurements of the firsts 20 and the lasts 20 probing shots of each series were averaged, recorded and compared. Using this experimental protocol, we observed an appreciable shift (towards longer values) in the PS's DF lifetime, between the first and the last group of 20 laser shots of any given series (400 shots in $40\,s$). The $60\,s$ break between two

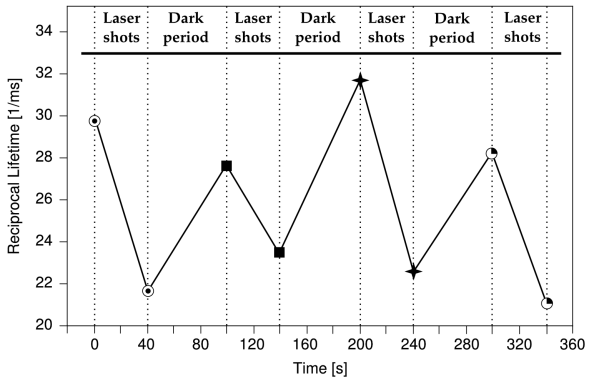

Figure 6.8: PpIX's delayed fluorescence reciprocal lifetime change, as measured in CAM, showing PDT-induced tissular oxygen consumption and its regeneration during the treatment breaks. Results from 4 sequential series of 400 laser shots each ($3.4\,mJ/cm^2$ per pulse, spot diameter $\varnothing 500\,\mu m$), separated by 1 min breaks. To demonstrate oxygen consumption, the initial and final oxygen levels are deduced from the DF recovered from the firsts 20 and the lasts 20 laser shots of each series. Their respective, averaged, reciprocal DF lifetimes are shown. The 4 different symbols in the graph corresponds to the 4 consecutive laser shots series.

consecutive series allows for (predominantly vascular) oxygen to re-diffuse to the region of the probed spot, thereby restoring - at least partially - the tissular oxygen concentration, as confirmed by a shortening of the observed DF lifetime (see figure 6.8).

The second *in vivo* example illustrates the relation between the PS's DF lifetime and the concentration of oxygen in the atmosphere surrounding the CAM sample: A small gas chamber (see figure 6.9(a)) was built for easily regulating the oxygen content in the atmosphere surrounding the sample. A small hole (A) in the top part of the chamber allowed for positioning the fiber tip at the CAM's surface, while two lateral inlets-outlets (B and C) allowed to flush it continuously with known N_2/O_2 gas mixtures. We used it to measure the DF lifetime of PpIX (endogenously produced by the CAM, following the ALA administration protocol described above) under different O_2 atmosphere conditions. The CAM was introduced in the chamber and left for 3 minutes, in view of an approximate equilibration of O_2 in the CAM itself, immersed in a homogeneous atmosphere of known, stable composition. The linear relation obtained with 12 different samples (see figure 6.9(b)) satisfies the Stern-Volmer equation (see equation 6.1), confirming and validating these *in vivo* measurements. These results show noticeable dispersion, increasing with the applied oxygen concentration, leading to the increasing error bars at 5, 10, 15 and 21 % O2

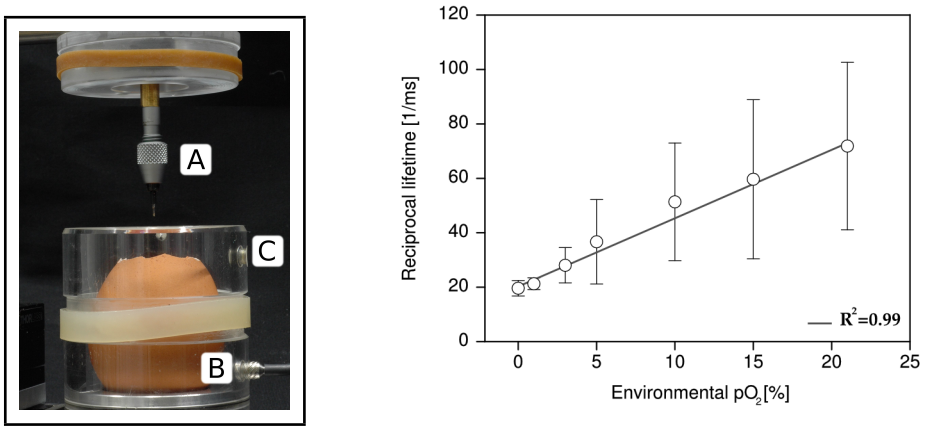

(a) Gas chamber to control the O_2 concentration on the atmosphere surrounding the egg

(b) The DF lifetime in function of the ammont of oxygen in the chamber's atmosphere

Figure 6.9: (b): Relation between PpIX's DF reciprocal lifetime, measured on the CAM's surface, as a function of oxygen concentration in the controlled atmosphere gas chamber (a).

content, linked to intra-sample and/or inter-sample variations, such as the actual vascular and micro-vascular density in the probed area.

The third *in vivo* experiment was designed to evaluate the scale/importance of any intra sample dispersion, when locally measuring the pO_2. This experiment was conducted in the same way as the previous one, but the oxygen concentration was measured in 8 different points of the same egg's CAM (see Figure 6.10(b)). The results showed sizable differences, increasing with the applied oxygen concentration, to be ascribed directly to local, intra sample, fluctuations (i.e. location-specific attributes which influence the measured pO_2 value, such as the actual vascular density in the probed area), as shown by the large error bars at 15% and 21% O_2 content, Figure 6.10(b). As in the previous experiment, this dispersion increases in parallel to that of the pO_2. It may originates in (i) the increasing measurement errors when the lifetimes become shorter (at high pO_2) and (ii) in the fact that the amplitude of any pO_2 variation, linked to the density of the vasculature, is directly proportional to the pO_2 itself.

6.4 Conclusion

We have designed, developed and characterized a time-resolved optical fiber-based spectrofluorometer for the *in vivo* detection of the delayed fluorescence of photosensitizers with simultaneous spectral and temporal resolu-

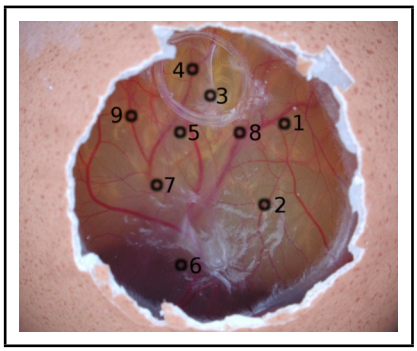

(a) Measurement spots on the CAM

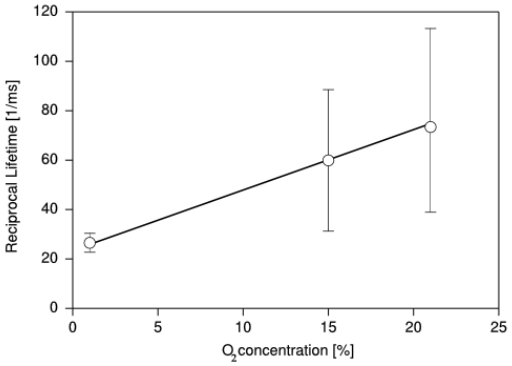

(b) The DF lifetime in function of the ammont of oxygen in the chamber's atmosphere in 8 different location of the same egg

Figure 6.10: Intra sample fluctuations, measured by exciting the CAM of the same egg in 8 different locations with different environmental oxygen concentration.

tion. Our setup is designed in such a way that: (i) *In vivo* and *in vitro* lifetime measurements can be easily performed through the use of a $\varnothing 500\,\mu m$ optical fiber, allowing for the measurement of poorly luminescent, endogenously produced, small photosensitizer concentrations ($C = 1 \times 10^{-5}\,M$) with a lifetime ranging from a few hundreds of nanoseconds to a few milliseconds. (ii) *In vitro* solutions can be easily measured at different temperatures (15°- 60°) and with different gas concentrations by bubbling the appropriate gas mixture in the measuring cuvette. (ii) *In vivo* CAM samples can be easily measured under controled conditions of temperature and moisture and with controled gas concentrations in the surrounding atmosphere, by using a simple gas chamber. (iii) *In vivo* and future clinical measurements on hollow organs can easily be performed, thanks to the simple fiber-based excitation/sensing design. (iv) Liquid and solid state (powders, crystals and deposited thin films) samples can be analyzed. (v) The excitation wavelength can be adjusted (400 to 850 nm) by simply changing the dye of the laser or through the use of a grating. Moreover, if an increased sensitivity is needed (one order of magnitude) it is possible to place the sample directly inside the light-tight enclosure (see figure 6.2) and/or modifying the delay or the acquisition time.

The described setup offers the following advantages as compared to other commercial setups (e.g., Perkin-Elmer LS 50B):

(a) its high sensitivity over a large spectral range (185-900 nm) coupled to the ability of measuring much shorter events (on the or-

der of 100 ns) and a better dynamic range both in the time and intensity dimensions. Indeed, the temporal dynamic range can be easily adapted to measure nano seconds up to steady state events and the intensity dynamic range start at several Watts down to $\approx 2.5 \times 10^{-10}\,W$ (*i.e. approx.* 1000 photoelectrons whithin $30\,\mu s$)

(b) the possibility to excite the sample with a short ($\approx 300\,ps$) and spectrally defined laser excitation pulse, which allows to excite selectively the molecules of interest and, consequently, to obtain measurable signals from low concentrations samples. The use of a very tightly focused laser beam (rather than the much larger image of a traditional lamp) results in the coupling of essentially *all* the available excitation energy into an optical fiber, enabling to probe small ($\varnothing \approx 100\ \mu m$) samples.

(c) the compactness of the instrumentation (≈ 25 litres) and the use of a fiber-based probe for both sample excitation and luminescence collection meet all the requirements needed for laboratory and clinical settings.

Measuring the oxygen partial pressure ($p\mathrm{O}_2$) can provide valuable information for the early diagnosis and characterization of numerous diseases related to changes of the tissues metabolism in hollow organs, as discussed in §1. Because delivery of O_2 takes place primarily in the micro-circulation, it is of high relevance to develop $p\mathrm{O}_2$ measuring techniques that have a sufficient spatial resolution to be applicable in the capillaries, arterioles and venules *in vivo*. Therefore, an evolution of the system presented here toward an imaging delayed-fluorescence time-resolved spectrometer, that can be adapted to an eye fundus camera for example, would be particularly valuable in this context. Since Visudyne® also presents a $p\mathrm{O}_2$-dependent delayed fluorescence lifetime (data not shown), such an approach would enable us to individualize the light dose for the treatment of AMD by PDT.

More generally, the technique presented in this report will help to understand the impact of oxygen on tissue sensitization. This is why, following this study, several well accepted photosensitizers used in the clinic, exhibiting delayed fluorescence, are currently being investigated with our CAM model. Oxygen concentration measurements performed before, during and after PDT are conducted on this model to demonstrate the feasibility of this approach and to optimize the treatment conditions.

6.5 Acknowledgments

This work was supported by the Swiss National Science Foundation (Grant 205320-116556) and funded in part by the J. Jacobi Trust.

References

[1] O Arjamaa and M Nikinmaa. Oxygen-dependent diseases in the retina: role of hypoxia-inducible factors. *Exp Eye Res*, 83 (3):473–83, September 2006. ISSN 0014-4835. 64

[2] R. L. Arudi, A. O. Allen, and B. H.J. Bielski. Some observations on the chemistry of ko2—dmso solutions. *FEBS Letters*, 135(2):265–267, 1981. ISSN 0014-5793. doi: DOI:10.1016/0014-5793(81)80797-1. URL `http://www.sciencedirect.com/science/article/B6T36-448HVF4-Y8/2/31359a1e9340f61449dc748781e759de`. 72

[3] A M Batlle. Porphyrins, porphyrias, cancer and photodynamic therapy–a model for carcinogenesis. *J Photochem Photobiol B*, 20(1):5–22, September 1993. ISSN 1011-1344. 74

[4] S Blumenröder, A J Augustin, and F H Koch. The influence of intraocular pressure and systemic oxygen tension on the intravascular po2 of the pig retina as measured with phosphorescence imaging. *Surv Ophthalmol*, 42 Suppl 1:S118–26, November 1997. ISSN 0039-6257. 64, 70

[5] R Bonnett. Photodynamic therapy in historical perspective. *Reviews in Contemporary Pharmacotherapy*, 10:1–18, 1999. 63

[6] F Borle, A Radu, P Monnier, H van den Bergh, and G Wagnières. Evaluation of the photosensitizer tookad for photodynamic therapy on the syrian golden hamster cheek pouch model: light dose, drug dose and drug-light interval effects. *Photochem Photobiol*, 78(4):377–83, October 2003. ISSN 0031-8655. 63

[7] G E P Box, G M Jenkins, and G C Reinsel. *Time series analysis. Forecasting and control. 4th ed.* Hoboken, NJ: John Wiley & Sons. xxiv, 746 p. , 2008. 69

[8] M Reyes Calvo, Jens Ulrik Andersen, Preben Hvelplund, Steen Brøndsted Nielsen, Ulrik V Pedersen, Jimmy Rangama, Shigeo Tomita, and James S Forster. Photophysics of protoporphyrin ions in vacuo: Triplet-state lifetimes and quantum yields. *The Journal of Chemical Physics*, 120(11):5067–72, 3 2004. doi: 10.1063/1.1647056. 73

[9] A Casas, H Fukuda, G Di Venosa, and Alcira Batlle. Photosensitization and mechanism of cytotoxicity induced by the use of ala derivatives in photodynamic therapy. *Br J Cancer*, 85(2):279–84, July 2001. ISSN 0007-0920. 74

[10] A P Castano, T N Demidova, and M R Hamblin. Mechanisms in photodynamic therapy: Part one photosensitizers, photochemistry and cellular localization. *Photodiagnosis and Photodynamic Therapy*, 1(4):279–293, 2004. 63

[11] K Cengel, E Glatstein, and S Hahn. *Intraperitoneal Photodynamic Therapy*, volume Part 6. Springer, 2007. doi: http://dx.doi.org/10.1007/978-0-387-48993-3_34. 63

[12] S R Chamot, S D Cranstoun, B L Petrig, C J Pournaras, and C E Riva. Blood po2 and blood flow at the optic disc. *J Biomed Opt*, 8(1):63–9, January 2003. ISSN 1083-3668. 64

[13] S J Chantrell. Excited states of protoporphyrin ix dimethyl esterreaction of the triplet with carotenoids. *J. Chem. Soc.*, 76:417–425, 1980. doi: 10.1039/F19807600417. 70

[14] S J Chantrell, C McAuliffe, A. R Munn, and A W C Pratt. Luminescence from protoporphyrin ix dimethyl ester. *Journal Chemical Society*, Com 320, 1975. 70, 73

[15] A S Chauvin, S Comby, B Song, C D B Vandevyver, and J C G Bünzli. A versatile ditopic ligand system for sensitizing the luminescence of bimetallic lanthanide bio-imaging probes. *Chemistry*, 14(6):1726–39, 2008. ISSN 0947-6539. 70

[16] S Collaud, A Juzeniene, J Moan, and N Lange. On the selectivity of 5-aminolevulinic acid-induced protoporphyrin ix formation. *Curr Med Chem Anticancer Agents*, 4(3):301–16, May 2004. ISSN 1568-0118. 74

[17] R F Donnelly, P A McCarron, and A D Woolfson. Derivatives of 5-aminolevulinic acid for photodynamic therapy. *Perspect Medicin Chem*, 1:49–63, 2008. ISSN 1177-391X. 74

[18] S V. Eliseeva, M Ryazanov, F Gumy, S I Troyanov, L S Lepnev, J C G Bünzli, and N P Kuzmina. Dimeric complexes of lanthanide(iii) hexafluoroacetylacetonates with4-cyanopyridine *N*-oxide: Synthesis, crystal structure, magnetic and photoluminescent properties. *European Journal of Inorganic Chemistry*, 2006(23):4809–4820, 2006. doi: 10.1002/ejic.200600673. URL `http://dx.doi.org/10.1002/ejic.200600673`. 69

[19] A Fassò. Residual autocorrelation distribution in the validation data set. *J. Time Ser. Anal.*, 21(2):143–153, 2000. doi: 10.1111/1467-9892.00178. 69

[20] N Fotinos, M A Campo, F Popowycz, R Gurny, and N Lange. 5-aminolevulinic acid derivatives in photomedicine: Characteristics, application and perspectives. *Journal of Photochemistry and Photobiology*, 82(4):994–1015, 2006. ISSN 0031-8655. 74

[21] H Fukuda, A Casas, and A Batlle. Aminolevulinic acid: from its unique biological function to its star role in photodynamic therapy. *The International Journal of Biochemistry & Cell Biology*, 37(2):272–6, 2 2005. doi: 10.1016/j.biocel.2004.04.018. 74

[22] M Geissbuehler, T Spielmann, A Formey, I Märki, M Leutenegger, B Hinz, K Johnsson, D Van De Ville, and T Lasser. Triplet imaging of oxygen consumption during the contraction of a single smooth muscle cell (a7r5). *Biophys J*, 98(2):339–49, January 2010. ISSN 1542-0086. 63

[23] P Grosjean, G Wagnieres, C Fontolliet, H van den Bergh, and P Monnier. Clinical photodynamic therapy for superficial cancer in the oesophagus and the bronchi: 514 nm compared with 630 nm light irradiation after sensitization with photofrin ii. *Br J Cancer*, 77(11):1989–95, June 1998. ISSN 0007-0920. 63

REFERENCES

[24] R Hornung, M J Hammer-Wilson, S Kimel, L H Liaw, Y Tadir, and M W Berns. Systemic application of photosensitizers in the chick chorioallantoic membrane (cam) model: Photodynamic response of cam vessels and 5-aminolevulinic acid uptake kinetics by transplantable tumors. *Journal of Photochemistry and Photobiology*, 49(1):41–9, 3 1999. doi: 10.1016/S1011-1344(99)00014-7. 74

[25] C Ince and E G Mik. Device and method for determining the concentration of a substance, January 10 2007. EP Patent 1,742,038. 64

[26] M Ito, K Murayama, T Deguchi, M Takasu, T Gil, M Araie, G Peyman, and S Yoneya. Oxygen saturation levels in the juxta-papillary retina in eyes with glaucoma. *Exp Eye Res*, 86 (3):512–8, March 2008. ISSN 0014-4835. 64

[27] D. Mauzerall J. Fitelson. Reactions of triplet states of a porphyrin measured by delayed fluorescence. *J. Phys. Chem.*, 86 (9):1623–1628, April 1982. doi: 10.1021/j100206a029. 71

[28] P K Kaiser. Combination therapy with verteporfin and anti-vegf agents in neovascular age-related macular degeneration: where do we stand? *Br J Ophthalmol*, 94(2):143–5, February 2010. ISSN 1468-2079. 63

[29] J C Kennedy and R H Pottier. Endogenous protoporphyrin ix, a clinically useful photosensitizer for photodynamic therapy. *J Photochem Photobiol B*, 14(4):275–92, July 1992. ISSN 1011-1344. 74

[30] A A Krasnovsky. Primary mechanisms of photoactivation of molecular oxygen. history of development and the modern status of research. *Biochemistry (Mosc)*, 72(10):1065–80, October 2007. ISSN 0006-2979. 65

[31] M Kress, T Meier, R Steiner, F Dolp, R Erdmann, U Ortmann, and A Rück. Time-resolved microspectrofluorometry and fluorescence lifetime imaging of photosensitizers using picosecond pulsed diode lasers in laser scanning microscopes. *J Biomed Opt*, 8(1):26–32, January 2003. ISSN 1083-3668. 64

[32] F Krummenauer, M Braun, and H B Dick. Clinical outcome and subjective quality of life after photodynamic therapy in patients with age-related macular degeneration. *Eur J Ophthalmol*, 15(1):74–80, 2005. ISSN 1120-6721. 63

[33] G R Kürzinger, B Stender, G K Lang, and G E Lang. Photodynamic therapy witverteporfin in occult choroidal neovascularization in age-related macular degeneration. *Klin Monbl Augenheilkd*, 131(5):541–60, May 2010. ISSN 1439-3999. 63

[34] S Kuszaj, P Kaszycki, and Z Wasylewski. A fluorescence quenching study on protoporphyrin ix in a model membrane system. *Chemistry and Physics of Lipids*, 83(2):153–160, 1996. ISSN 0009-3084. doi: DOI:10.1016/0009-3084(96)02605-9. URL `http://www.sciencedirect.com/science/article/B6T2N-497C77H-1G/2/fd42d53526ac018fa47c16ed1061d3e0`. 64

[35] J Lafferty and T G Truscott. Triplet state of protoporphyrin ix. *J. Chem. Soc.*, Com. 989:51–52, 1978. doi: 10.1039/C39780000051. 73

[36] N Lange, J-P Ballini, G Wagnieres, and Hubert van den Bergh. A new drug-screening procedure for photosensitizing agents used in photodynamic therapy for cnv. *Investigative Ophthalmology & Visual Science*, 42(1):38–46, January 2001. ISSN 0146-0404. 74

[37] D W Marquardt. An algorithm for least-squares estimation of nonlinear parameters. *Journal of the Society for Industrial and Applied Mathematics*, 11(2):431–441, 1963. doi: 10.2307/2098941. URL `http://dx.doi.org/10.2307/2098941`. 69

[38] W Melhuish. Nomenclature, symbols, units and their usage in spectrochemical analysis—vi molecular luminescence spectroscopy. *Spectrochimica Acta*, 37(3):259–272, 1982. 64

[39] E G Mik, C Donkersloot, N J H Raat, and C Ince. Excitation pulse deconvolution in luminescence lifetime analysis for oxygen measurements in vivo. *Photochemistry and Photobiology*, 76(1):12–21, 7 2002. 69

[40] E G Mik, J Stap, M Sinaasappel, J F Beek, J A Aten, T G van Leeuwen, and C Ince. Mitochondrial po2 measured by delayed fluorescence of endogenous protoporphyrin ix. *Nature Methods*, 3(11):939–45, 11 2006. doi: 10.1038/nmeth940. 70, 74

[41] E G Mik, T Johannes, C J Zuurbier, A Heinen, J H P M Houben-Weerts, G M Balestra, J Stap, J F Beek, and C Ince. In vivo mitochondrial oxygen tension measured by a delayed fluorescence lifetime technique. *Biophysical Journal*, 95(8):3977–90, 10 2008. doi: 10.1529/biophysj.107.126094. 63, 64

[42] J Moan. The photochemical yield of singlet oxygen from porphyrins in different states of aggregation. *Photochemistry and Photobiology*, 4:445–449, 1984. doi: 10.1111/j.1751-1097.1984.tb03873.x. Norsk Hydro's Institute for Cancer Research, Montebello, Oslo 3, Norway. 73

[43] J Moan and P Juzenas. Singlet oxygen in photosensitization. *Journal of Environmental Pathology, Toxicology and Oncology : Official Organ of the International Society for Environmental Toxicology and Cancer*, 25(1-2):29–50, 2006. URL `http://www.begellhouse.com/journals/0ff459a57a4c08d0,5d84548f012e18bf,59bbacd00ecbd94a.html`. 63

[44] A Molnar, R Dedic, A Svoboda, and J Hala. Singlet oxygen production by lipophilic photosensitizers in liposomes studied by time and spectral resolved phosphorescence. *Journal of Molecular Structure*, 834-836:488–491, May 2007. doi: 10.1016/j.molstruc.2006.12.019. 64

[45] A. Molnàr, R Dedic, A Svoboda, and J Hála. Spectroscopic study of singlet oxygen photogeneration by lipophilic photosensitiser in liposomes. *Journal of Luminescence*, 128(5-6):783–785, 2008. ISSN 0022-2313. doi: DOI:10.1016/j.jlumin.2007.12.009. URL `http://www.sciencedirect.com/science/article/B6TJH-4R9GH1F-8/2/25f8c416617ed14119c71e34dd4fcf93`. Proceedings of the 16th International Conference on Dynamical Processes in Excited States of Solids, 16th International Conference on Dynamical Processes in Excited States of Solids. 64

[46] Y Monnier, P Pasche, P Monnier, and S Andrejevic-Blant. Second primary squamous cell carcinoma arising in cutaneous flap reconstructions of two head and neck cancer patients. *Eur Arch Otorhinolaryngol*, 265(7):831–5, July 2008. ISSN 0937-4477. 63

[47] Jorge Moré. The levenberg-marquardt algorithm: Implementation and theory. *Numerical Analysis*, 630:105–116, 1978. doi: http://dx.doi.org/10.1007/BFb0067700. Without Abstract. 69

[48] C A Parker. *Photoluminescence of Solutions*. Elsevier Amsterdam, 1968. 65

[49] Q Peng, T Warloe, K Berg, J Moan, M Kongshaug, K E Giercksky, and J M Nesland. 5-aminolevulinic acid-based photodynamic therapy. clinical research and future challenges. *Cancer*, 79(12):2282–308, 6 1997. 63

[50] C Perotti, H Fukuda, G DiVenosa, A J MacRobert, Alcira Batlle, and A Casas. Porphyrin synthesis from ala derivatives for photodynamic therapy. in vitro and in vivo studies. *Br J Cancer*, 90(8):1660–5, April 2004. ISSN 0007-0920. 74

[51] S Pervaiz and M Olivo. Art and science of photodynamic therapy. *Clinical and Experimental Pharmacology and Physiology*, 33:551–6, 2006. doi: 10.1111/j.1440-1681.2006.04406.x. URL http://www3.interscience.wiley.com/resolve/openurl?genre=article\&sid=nlm:pubmed\&issn=0305-1870\&date=2006\&volume=33\&issue=5-6\&spage=551. 63

[52] S Piermarocchi, M Sartore, G Lo Giudice, G Monterosso, E Pilotto, and T Segato. Is there any relationship between photodynamic therapy for exudative age-related macular degeneration and choroidal neovascolarization recurrence? a rationale for combined treatments. *Eur J Ophthalmol*, 16(5):686–94, 2006. ISSN 1120-6721. 63

[53] K Plaetzer, B Krammer, J Berlanda, F Berr, and T Kiesslich. Photophysics and photochemistry of photodynamic therapy: fundamental aspects. *Lasers in Medical Science*, 24(2):259–68, March 2009. ISSN 0268-8921. 63

[54] C E Riva. Noninvasive measurement of oxygen tension in the optic nerve head. *Curr Opin Ophthalmol*, 9(2):56–60, April 1998. ISSN 1040-8738. 64

[55] T Roth. *Ruthenium(II) diimine complexes for luminescence-based oxygen sensors and Impedance spectroscopy of nitrogen dioxide- sensitive polymeric membranes*. PhD thesis, Swiss Federal Institute of Technology, Zurich, 1972. Diss. ETH No. 14001. 69

[56] W L Rumsey, J M Vanderkooi, and D F Wilson. Imaging of phosphorescence: a novel method for measuring oxygen distribution in perfused tissue. *Science*, 241(4873):1649–51, September 1988. ISSN 0036-8075. 64, 70

[57] J A Russell, K R Diamond, T J Collins, H F Tiedje, J E Hayward, and T J Farrell. Characterization of fluorescence lifetime of photofrin and delta-aminolevulinic acid induced protoporphyrin ix in living cells using single- and two-photon excitation. *IEEE Journal of Selected Topics in Quantum Electronics*, 14(1):158–166, 2008. ISSN 1077-260X. 64

[58] R Schmidt. Photosensitized generation of singlet oxygen. *Journal of Photochemistry and Photobiology*, 82(5):1161–1177, 2007. doi: 10.1562/2006-03-03-lR-833. 65

[59] L M Scolaro, M Castriciano, A Romeo, S Patane, E Cefal, and M Allegrini. Aggregation behavior of protoporphyrin ix in aqueous solutions: Clear evidence of vesicle formation. *Journal of Physical Chemistry. B, Condensed Matter, Materials, Surfaces, Interfaces, & Biophysical Chemistry*, 106(10):2453–2459, 2002. 73

[60] R D Shonat, D F Wilson, C E Riva, and M Pawlowski. Oxygen distribution in the retinal and choroidal vessels of the cat as measured by a new phosphorescence imaging method. *Appl. Opt.*, 31(19):3711–3718, 1992. URL http://ao.osa.org/abstract.cfm?URI=ao-31-19-3711. 64, 70

[61] E Stefánsson, R Machemer, E de Juan, B W McCuen, and J Peterson. Retinal oxygenation and laser treatment in patients with diabetic retinopathy. *Am J Ophthalmol*, 113(1):36–8, January 1992. ISSN 0002-9394. 64

[62] T K Stepinac, S R Chamot, E Rungger-Brändle, Pierre Ferrez, J L Munoz, Hubert van den Bergh, C E Riva, C J Pournaras, and G A Wagnières. Light-induced retinal vascular damage by pd-porphyrin luminescent oxygen probes. *Invest Ophthalmol Vis Sci*, 46(3):956–66, March 2005. ISSN 0146-0404. 69, 70

[63] H J Sterenborg, De Wolf J. W., M. Koning, B. Kruijt, A. Van Den Heuvel, and D. J. Robinson. Phosphorescence-fluorescence ratio imaging for monitoring the oxygen status during photodynamic therapy. *Optics Express*, 12(9):1873, 2004. 64

[64] D M Strick, R L Waycaster, J P Montani, W J Gay, and T H Adair. Morphometric measurements of chorioallantoic membrane vascularity: effects of hypoxia and hyperoxia. *American Journal of Physiology*, 260(4 Pt 2):1385–9, April 1991. ISSN 0002-9513. 74

[65] S M Szabo, M J Potter, and T T Ho. Incidence of Recurrence of Choroidal Neovascular Membranes at 18 Months After Photodynamic Therapy in Patients With Age-Related Macular Degeneration. *Invest. Ophthalmol. Vis. Sci.*, 46(5):300–, 2005. URL http://abstracts.iovs.org/cgi/content/abstract/46/5/300. 63

[66] M Triesscheijn, P Baas, J H M Schellens, and F A Stewart. Photodynamic therapy in oncology. *The Oncologist*, 11(9):1034–44, 10 2006. doi: 10.1634/theoncologist.11-9-1034. URL http://theoncologist.alphamedpress.org/cgi/pmidlookup?view=long\&pmid=17030646. 63

[67] K Tsukada, S Sakai, K Hase, and H Minamitani. Development of catheter-type optical oxygen sensor and applications to bioinstrumentation. *Biosens Bioelectron*, 18(12):1439–45, October 2003. ISSN 0956-5663. 73

[68] M P Tsvirko, K N Solovev, A T Gradyzshko, and S S Dvornikov. Phosphorescence of porphyrin free base and their complexes with light metals. *Optika i Spektroskopiya*, 38:705–713, 1975. 64

[69] H Van den Bergh and J. P. Ballini. *Photodynamic therapy: basic principles and mechanisms*, pages 1–23. Basic Principles and Mechanisms, in Lasers in Ophthalmology Surgical and Diagnostic Aspects. Kugler, The Hague, Nederlands, 2002. 63

[70] J M Vanderkooi, G Maniara, T J Green, and D F Wilson. An optical method for measurement of dioxygen concentration based upon quenching of phosphorescence. *The Journal of Biological Chemistry*, 262(12):5476–82, 4 1987. URL http://www.jbc.org/cgi/pmidlookup?view=long\&pmid=3571219. 70

[71] S A Vinogradov and D F Wilson. Phosphorescence lifetime analysis with a quadratic programming algorithm for determining quencher distributions in heterogeneous systems. *Biophys J*, 67(5):2048–59, November 1994. ISSN 0006-3495. 73

[72] S A Vinogradov and D F Wilson. Metallotetrabenzoporphyrins. new phosphorescent probes for oxygen measurements. *J. Chem. Soc., Perkin Trans. 2*, 2:103–111, 1995. doi: 10.1039/P29950000103. 73

[73] S A Vinogradov, L W Lo, W T Jenkins, S M Evans, C Koch, and D F Wilson. Noninvasive imaging of the distribution in oxygen in tissue in vivo using near-infrared phosphors. *Biophys J*, 70(4):1609–17, April 1996. ISSN 0006-3495. 64

REFERENCES

[74] Norbert D Wangsa-Wirawan and Robert A Linsenmeier. Retinal oxygen: fundamental and clinical aspects. *Arch Ophthalmol*, 121(4):547–57, April 2003. ISSN 0003-9950. 64

[75] B C Wilson and M S Patterson. The physics, biophysics and technology of photodynamic therapy. *Physics in Medicine and Biology*, 53(9):R61–109, May 2008. ISSN 0031-9155. 63

[76] B C Wilson, M S Patterson, and L Lilge. Implicit and explicit dosimetry in photodynamic therapy: a new paradigm. *Lasers in Medical Science*, 12(3):182–199, June 1997. doi: 10.1007/BF02765099. 63

[77] L Zhao, K P Nielsen, A Juzeniene, P Juzenas, V Lani, L W Ma, K Stamnes, J J Stamnes, and J Moan. Spectroscopic measurements of photoinduced processes in human skin after topical application of the hexyl ester of 5-aminolevulinic acid. *Journal of Environmental Pathology, Toxicology and Oncology : Official Organ of the International Society for Environmental Toxicology and Cancer*, 25 (2):307–20, 2006. URL `http://www.begellhouse.com/journals/0ff459a57a4c08d0,5d84548f012e18bf,46a7c27267b3ab34.html`. 63

7

PDT Induced Oxygen Depletion (Submitted Paper)

In vivo Measurement of PpIX's Delayed Fluorescence Lifetime to Monitor Tissular Oxygen Depletion during Photodynamic Therapy

Filippo Piffaretti, Anna Maria Novello, Rajendran Senthil Kumar, Eddy N. Forte, Hubert van den Bergh, Georges Wagnières

Federal Institute of Technology Lausanne (EPFL)
Lausanne, Switerland

Keywords: PDT, *In vivo*, CAM, ALA, PpIX, Delayed Fluorescence, Tissular, Oxygen, Tissular vascular effect

Abbreviation: (PDT) Photodynamic therapy, (ALA) 5-amino-levulinic acid, (PpIX) Protoporphyrin IX, (CAM) Chick chorio-allantoic membrane, (EDD) Embryo development day, (AMD) Age-related Macular Degeneration, (EPP) Erythropoietic protoporphyria, (PS) Photosensitizer, (DF) Delayed fluorescence, (FITC) Fluorescein isothiocyanate-dextran

Abstract

Tissular molecular oxygen is monitored *during* photodynamic therapy. The oxygen concentration in living tissue, expressed hereafter as the tissular $p\mathrm{O}_2$ in %, is evaluated by measuring the photosensitizer's delayed fluorescence lifetime. This enables the collection of real time data reflecting the local availability of oxygen in a small region around the excited photosensitizer (PS) molecules. In this study 5-amino-levulinic acid (ALA), a precursor of the photosensitizer protoporphyrin IX (PpIX), was administered topically ($20\,\mu l$; $20\,mg/ml$) *in vivo*, over a selected area at the surface of the chick egg chorioallantoic membrane (CAM). After a drug-light interval of $4\,h$, the eggs were irradiated with a CW laser with different light doses ($\lambda_{PDT} = 405\,nm$, $0.4 - 2.25\,J/cm^2$) and the diminishing $p\mathrm{O}_2$ was then monitored during photodynamic therapy (PDT), using our optical fiber-based spectrofluorometer which measures the delayed fluorescence lifetime of PpIX as a proxi for the local $p\mathrm{O}_2$. The $p\mathrm{O}_2$ reduction (due to various photochemically initiated reactions between the PS and oxygen, leading to the formation of cytotoxic reactive species) was recorded and correlated with the observed vascular damage (basically, the efficacy of blood vessel closure, on an arbitrary scale), measured with an epifluorescence microscope in the irradiated region of the CAM, $18 - 20$ hours after the treatment.

The PpIX delayed fluorescence lifetime was found to be in the range from $\approx 15\,\mu s$ to $60\,\mu s$ in normal physiological, respectively hypoxic, conditions. These delayed fluorescence signals were only $\approx 1/300$ of the prompt (*i.e.* normal) fluorescence of PpIX, but could still be easily detected with the present simple and clinically compatible device.

The results show a strong correlation between PDT-induced vascular damage and tissular oxygen consumption. Furthermore, PDT efficacy was found to be strongly reduced at low $p\mathrm{O}_2$. This real-time knowledge about tissular $p\mathrm{O}_2$, gained through the measurement of the PS's delayed fluorescence, may be used to adjust the light dose applied, thus reducing intra- an inter- patient fluctuations and stabilizing the clinical outcome of PDT.

7.1 Introduction

Photodynamic therapy (PDT) is an attractive treatment modality, especially for local, superficial early stages cancers in the hollow organs and other regions of the body easily accessible to light application. Thanks to its partial selectivity and to the minimally invasive procedures involved, PDT has established itself as the treatment of choice in, among others, dermatology and also certain ophthalmologic conditions, such as polypoidal choroidal vasculopathy (PCV) and wet age-related macular degeneration (AMD). To obtain the desired cytotoxic and healing effects, PDT relies on the presence in the target tissue of a photosensitizer (PS) and molecular oxygen ($O_2(^3\Sigma_g)$ noted $^3O_2$ for short or simply O_2 if unambiguous), and the administration of light at wavelengths matching, at least partially, the absorption spectrum of the PS. The present work focuses on the use of protoporphyrin IX (PpIX) as the PS[1]. In general, this entails the topical or systemic administration of 5-amino-levulinic acid (ALA, a biochemical precursor of PpIX), followed by a drug- to light-application time interval, necessary for the biosynthesis and accumulation of PpIX in the cells of the target tissue. PpIX is the last intermediate in the heme biosynthetic pathway [14, 57] before the enzyme ferrochelatase inserts an Fe(II) ion in the macrocycle to make heme. PpIX, in contrast to heme, is a photoactive substance with a relatively high singlet oxygen yield ($\approx 56\%$ in specific *in vitro* conditions [46]), and with a high fluorescence quantum yield. ALA-based PDT as well as PDT based on the use of chemical derivatives of ALA, are now approved for certain medical purposes and in common clinical use for the treatment of premalignant and malignant conditions in dermatology.

In most cases, ALA-based PDT relies on cell apoptosis rather than on tissue necrosis, leading to good cosmetic results as most of the connective tissue is not destroyed. For that reason and thanks to its limited side-effects and the minimal invasiveness of the clinical procedure, it is in many cases prefered to alternative treatments [20], like surgery, cryotherapy or the application of 5-fluorouracil. However, despite the encouraging results, clinicians are sometimes dissuaded from using this therapy due to the fluctuations in intra- and inter patient therapeutic outcome. These fluctuations, frequentely linked to the uneven tissular distribution of the PS and/or oxygen, might in

[1] Although there is still some controversy about exactly which molecule is responsible for the observed, post-ALA administration, fluorescence and therapeutic effects, PpIX is the commonly accepted candidate. PpIX also does play a role in the erythropoietic protoporphyria (EPP) condition, where lack of ferrochelatase induces its accumulation in the cells, causing skin photosensitivity and liver disfunction [50].

some cases, be counterbalanced by performing local, fluorescence-based measurements of the PS concentration, and then adjusting the local light dosimetry [3–5]. Nevertheless, since PDT involves three main interdependent variable elements (light dose, photosensitizer concentration and oxygen partial pressure), optimal treatment dosimetry remain a challenge. Thus the interest in finding efficient ways for monitoring the local PS concentration and pO_2, to optimize and drive the delivery of laser light to the tissue.

Light dose optimization for PDT is the focus of ongoing research in several groups [8, 10, 23, 28, 40, 54]. Different approaches have been proposed to efficiently monitor PDT in view of improving its clinical outcome [64]. One of them is *explicit dosimetry* in which the quantities of light, drug and oxygen are continuously and separately monitored during treatment. Alternatively, *implicit dosimetry* makes use of a surrogate of the biological damages, such as the photodegradation (bleaching) of the photosensitizer, to predict the clinical outcome [24, 54, 61].

Recent studies tried to correlate the clinical outcome of PDT with the so called *direct dosimetry*, which entails the direct measurement of singlet oxygen ($O_2(^1\Delta_g)$ noted $^1O_2$ for short) during the therapy [26, 40, 62].

Previous studies [12, 34, 42, 43, 52] have provided strong evidence that $^1O_2$ is in fact the major active cytotoxic species interacting with target tissues and inducing cell apoptosis. Therefore, accurate monitoring of $^1O_2$, though quite difficult to do, might lead to a better prediction of the clinical outcome than other monitoring techniques.

A simplistic summary of the photochemically induced reactions (type-II photochemical reaction pathway) can be represented by the following chemical scheme:

$$S_0 + h\nu \rightarrow S_1 \quad \textit{Photon absorption by the PS}$$

$$S_1 \xrightarrow{ISC} T_1 \quad \textit{Intersystem crossing}$$

$$T_1 + {}^3O_2 \rightarrow S_0 + {}^1O_2 \quad \textit{Collisional energy transfer between the PS and molecular } O_2$$

S_0 is the singlet ground state of the PS which is excited (upon absorption of a photon of energy $h\nu$) to the first excited singlet state S_1. The latter undergoes intersystem crossing with a certain quantum yield (up to 90% for certain porphyrins [11] and $\approx$ 60% for PpIX [46], measured in *in vitro* conditions) to the long lived lowest triplet state T_1, which has a lifetime ranging from μs up to ms. This is why the tissular oxygen in the triplet ground state ($^3O_2$) has enough time to undergo a collision with the PS in the T_1 state, to form the highly reactive and cytotoxic singlet molecular oxygen $^1O_2$. Once generated, $^1O_2$ undergoes de-excitation through several pathways among which a low probability radiative decay with emission of an infrared photon at $1270\,nm$. This $^1O_2$ luminescence is

in fact characterized by a very weak signal, making its measurement not easily applicable in the clinical context (the luminescence emission of $^1O_2$ has a probability of 10^{-8} and a charateristic lifetime of $\approx 100\,ns$ under *in-vivo* conditions [38–40]). These fast and weak signals from $^1O_2$ at 1.27 μm are difficult to work with under clinical conditions, where simple, robust setups and real time measurements are preferred. Moreover, detecting a weak infrared luminescence signal *in vivo* is not a simple matter: several biological molecules, when excited, may also emit in this spectral range. The above may substantially increase the complexity and cost of the instrumentation, as well as the duration of the data acquisition process [26]. Finally, such *signal intensity-based* measurements are subject to errors due to source fluctuation, detector drift, geometry changes, and photodecomposition of luminescent species. To overcome these problems, a compromise between *direct* and *explicit dosimetry* would be appropriate.

Hence the idea to measure the production of excited singlet oxygen *via* the consumption of the PpIX's triplet state (T_1 in the above chemical scheme), which is efficiently quenched by the molecular oxygen found in the tissue: according to Redmond and Gamlin [46], a fraction ranging from 55% to 80% of the PpIX T_1 population is quenched by $^3O_2$, depending on the actual *in vitro* conditions. Therefore, measuring the photosensitizer's luminescence lifetime offers an alternative to measuring the radiative decay of $^1O_2$. Furthermore, in contrast to intensity measurement methods, lifetime measurement methods have the advantage of being inherently self-referential and to be less prone to the above mentioned problems [36].

PpIX's phosphorescence signal, from the radiative path connecting T_1 to S_0, may not be easily detected *in vivo* because the phosphorescence quantum yield is too low and/or because this luminescence takes place at wavelengths too long to be easily detected [2, 31, 35, 51, 55, 58]. This difficulty can be overcome by measuring PpIX's *delayed fluorescence* (DF) lifetime as a substitute for its phosphorescence lifetime [21, 29, 32].

Along these lines, Mik et al. [31, 32] reported *in vitro* and *in vivo* experiments using PpIX's DF lifetime signals, to assess the amount of oxygen in tissues. As compared to other oxygen sensing techniques, DF measurements have the advantage to record the oxygen concentration in a close proximity of

[1] Given the diffusivity of molecular oxygen ($^3O_2$) in tissue ($D \approx 1.7 \times 10^{-5}\, cm^2/s$, [16, 33]) and using PpIX's triplet state maximum *in vivo* lifetime ($\tau \approx 60\,\mu s$), the distance reachable by an O_2 molecule to interact with excited PpIX molecules is calculated to be on the order of $\approx 1\,\mu m$ ($\delta = \sqrt{6D\tau}$, [45]). If the same computation is done for singlet oxygen ($^1O_2$), whose lifetime of $\approx 250\,ns$ is much shorter, the reachable radius is less than 40 nm.

the photosensitizer[1], on the order of $1\,\mu m$. The *critical oxygen diffusion distance*, usually defined as the distance between a *hypoxic tissue* (*i.e.* a tissue in a situation of critically low oxygen level) and the *nearest vessel* has been measured by [16] to be on the order of $100\,\mu m$ in a tumoral tissue. It is therefore clear that this DF-based oxygen sensing method is able to spatially discriminate between hypoxic zones and normally oxygenated tissue, provided that a small enough probing laser beam is used.

The chicken egg chorioallantoic membrane (CAM) has proven to be a good *in vivo* model to assess vascular modifications; in particular it is well suited to characterize PDT's vascular effects [6, 9, 19, 25, 47, 48]. In this work, we use this *in vivo* model to examine if any robust correlation exists between oxygen consumption during PDT and the resulting vascular damage.

7.2 Materials and Methods

7.2.1 Delayed Fluorescence Lifetime Measurement

The tissular $p\mathrm{O}_2$ can be determined by measuring the lifetime τ of the PS's triplet state thanks to the well known Stern-Volmer relationship (7.1):

$$I_0/I = \tau_0/\tau = 1 + K_q\tau_0[p\mathrm{O}_2] \qquad (7.1)$$

where I and τ refer to the intensity and lifetime of the PS's phosphorescence for a given tissue $p\mathrm{O}_2$ while I_0 and τ_0 refer to the values measured in the abscence of oxygen, and K_q is the Stern-Volmer constant. In this study, tissular oxygen concentrations are given as values of $p\mathrm{O}_2$ in units of *percent* (%), meaning that the tissue is assumed to be saturated and in equilibrium with an oxygen-containing gaseous mixture (usually air or calibrated nitrogen/oxygen mixtures) at a pressure of 1 atm. The lifetime τ is determined indirectly, by detecting the DF of the PS's excited triplet state, as previously described in the literature [21, 29, 32, 44]. For this purpose, we have constructed and used a fiber-based, time-resolved spectrofluorometer, (7) in Figure 7.1(b), which has been described in detail in Piffaretti et al. [44].

In short, the essential features of the measurement method are as follows (see Figure 7.1): the PpIX molecules synthetized in the CAM, (1), are excited with a nitrogen-laser-pumped dye laser (part of item 7) (LTB® model MSG 803-TD, $405\,nm$) pulsed at a repetition rate of 10 Hz. The dye laser wavelength is set at $405\,nm$ to match the PpIX's peak of absorption. As we are only interested in probing the superficial tissues of the CAM, the $405\,nm$ wavelength is more than adequate from a tissue penetration point of view. The laser light is conveyed to the sample by an

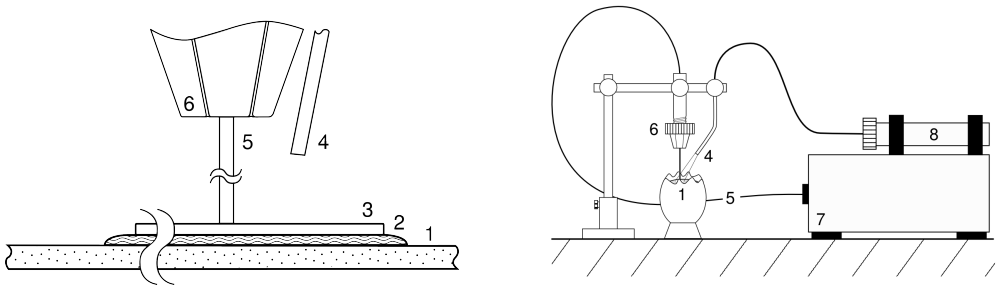

(a) Close-up of the treated CAM zone

(b) General view of the setup

Figure 7.1: Tissular oxygen measurement in the CAM. (a) (1) CAM surface; (2) Protective drop of acqueous serum; (3) 0.19 mm cover-glass; (4) PDT treatment fiber; (5) Excitation/probing fiber; (6) Fiber holder. (b) (1) CAM in the open egg; (8) PDT treatment laser; (4) Fiber used for PDT irradiation; (7) Spectrofluorometer with dye laser excitation source; (5) Excitation and probing fiber; (6) Fiber holder.

optical fiber (5) (Laser Components® HCG-M0550T) which is a multimode optical fiber, with core diameter ∅550 μm, and numerical aperture (NA) of 0.22. The radiant exposure of the laser pulse, at the distal fiber tip was $3.5\,mJ/cm^2$. After each laser pulse, the DF photons emitted by the relaxing PS molecules are collected by the same optical fiber (5) and focalized on a gated photomultiplier tube (PMT, part of item 7). The PMT is blinded (gated to the 'off' state) during the first $3\,\mu s$ after the laser excitation pulse, to avoid saturation by the much stronger normal (prompt) fluorescence signal. This DF decay signal is averaged over 30 consecutive sweeps, bringing the total acquisition time to $3\,s$, and the averaged decay is then digitized and mathematically fitted to a single or multiple exponential function, using the Levenberg-Marquardt non-linear least-squares fit algorithm. In our case, the resulting computation errors on the *in vivo* lifetimes were limited to ±5% [44].

7.2.2 Handling of the Chick Embryo's CAM and ALA Administration

The chick embryo's CAM model has been described previously [9, 15, 25, 56] and was used with minor modifications. Briefly, fertilized chicken eggs were disinfected and transferred (blunt end up) into an automatic turn-incubator, set at 37°C, 60% relative humidity (RH), and in normal atmospheric $p\mathrm{O}_2$ conditions[1], *i.e.* 21% [30, 49]. On embryo development day 3 (EDD 3), a portion of the eggshell was removed at the pointed end of the

[1] Given the geographical location (400 m above see level) of the experimental setup, this corresponds to a partial pressure of approximately $\approx 150\,mmHg$ of O_2.

egg, creating a hole of approximately $\varnothing 3\,mm$ in diameter, which was covered with cling film (Parafilm®) and, at later times, always kept pointing up. This procedure causes the embryo and its enveloping CAM to locally retract from this artificial opening, exposing at its surface a flattened portion of the membrane, and providing an access to observe and treat the CAM's capillary plexus and vasculature. The eggs were then returned to the incubator (blunt end down) and kept in a static position. At EDD 11, the eggs were removed from the incubator for topical ALA administration: a zone of the CAM characterized by homogeneous vascularization was visually selected and a $20\,\mu l$ droplet of a $0.15\,M$ (20 mg/ml) ALA acqueous solution in 0.9% NaCl, adjusted to $pH\,6$ with NaOH, was deposited in the centre of this zone. The eggs were then returned to the incubator and kept static until further use. As a rule, any manipulation of the CAM after ALA application was done in total darkness or under subdued light.

7.2.3 PDT Irradiation and CAM Tissular Oxygen Depletion Measurements

The study design was guided by the following rationale (see Figure 7.2):

Protocol I was used to determine the existence of a robust relationship between PDT duration and $p\mathrm{O}_2$, while using a minimum number of eggs: thus, each egg was submitted to a number of successive, cumulative, irradiations - and measurements.

Protocol II seeked to check the same relationship as protocol I using: (i) a different batch of eggs, (ii) intermediate durations for the incremental PDTs and (iii) a longer total treatment time ($900\,s$), in order to confirm and improve the precision of the relation observed using protocol I, while still keeping the cumulated total measurement time under a certain maximum (6 times $3\,s$). In fact, in protocols I and II, $p\mathrm{O}_2$ measurements were performed once during each $3\,s$ OFF period of the treatment laser, *i.e.* immediately after each *incremental* PDT irradiation period and the difference with the initially determined baseline $p\mathrm{O}_2$ value was computed to be the *tissular oxygen depletion* assignable to the corresponding, cumulated, PDT treatment time.

Protocol III was used to prove that the parasitic effects of the multiple, intermediary, measurements used in protocols I and II were small.

The normal, baseline value of the $p\mathrm{O}_2$ was first determined for each egg before starting any PDT irradiation protocol. The treatment laser was then switched on and off and $p\mathrm{O}_2$ measurements performed according to one of the three experimental protocols described above. In protocol III (described in more detail under §7.3.4), $p\mathrm{O}_2$ measurements were

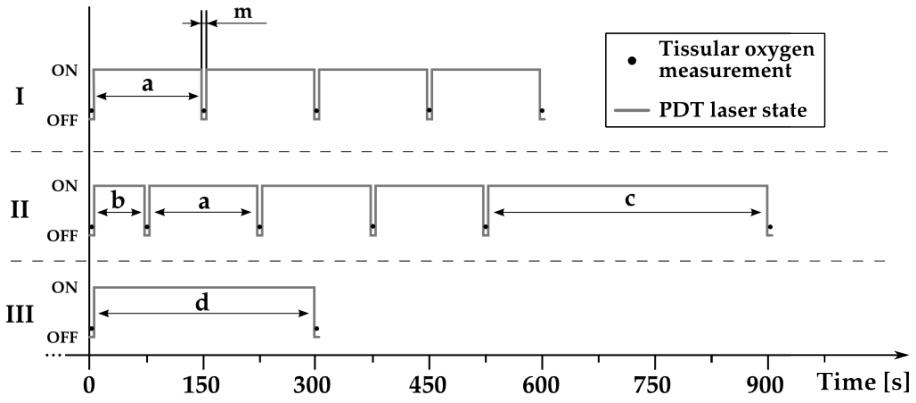

Figure 7.2: Time sequences of the experimental protocols used in experiments 3 and 4. The figure shows the cumulative PDT irradiations, interspersed with O_2 measurements during which the PDT source was suppressed. PDT irradiation durations were: $a = 150\,s$, $b = 75\,s$, $c = 375\,s$, $d = 150 - 900\,s$, while the O_2 measurement duration was: $m = 3\,s$

performed just once before and once after a *continuous, predetermined* irradiation period. The difference between those two pO_2 values was computed to be the *tissular oxygen depletion* assignable to the corresponding, uninterrupted, PDT treatment time.

Details of the PDT irradiation and tissular oxygen measurement procedures were as follows: At EDD 11, $4\,h$ after ALA administration, the egg was taken out of the incubator and placed under the combined PDT-irradiation/DF-measurement setup (Figure 7.1(a)). The drug-light interval of $4\,h$ allowed time for the cells to produce sufficient tissular of PpIX (see §7.3.1). This PpIX biosynthesized *in-situ* serves both as the PS for the PDT and for measuring the pO_2, through its delayed fluorescence lifetime (see §7.2.1).

In order to minimize re-oxygenation of the tissue[1] during PDT by atmospheric oxygen, a round microscope cover-glass (3) (Menzel-Gläser ® $\varnothing 20\,mm$, thickness $0.15\,mm$) was gently floated on the CAM's surface (1) after depositing two drops (2) of human physiologic serum ($\approx 80\,\mu l$ of 0.9% NaCl). This liquid layer, acting as a cushion, was essential to avoid any adherence between the cover-glass and the CAM and possible subsequent injury to the CAM surface.

A PDT treatment zone, featuring blood vessels and capillaries with diameters ranging from 5 to $300\,\mu m$, was visually chosen approximately in the middle of the zone under the cover-glass. The tip of the optical fiber (5) was aimed towards the center of this zone, and held at a distance of $\approx 100\,\mu m$

[1] During PDT or tissular oxygen measurement, oxygen may only diffuse from the CAM vasculature and from the tissues adjacent to the treated zone - not from the shielded surface of the treated zone.

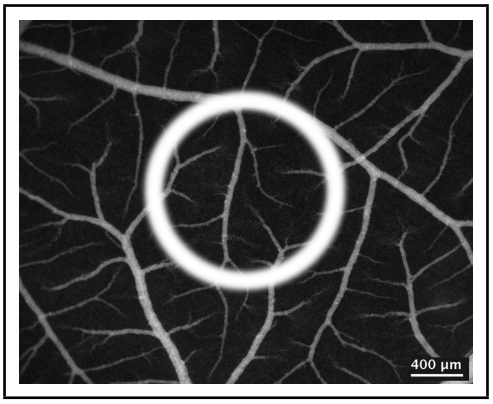

(a) CAM model, objective 4x

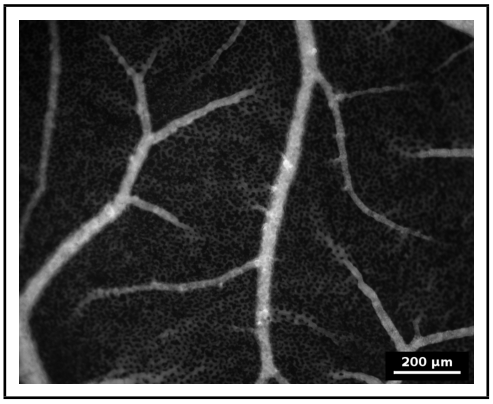

(b) CAM model, objective 10x

Figure 7.3: CAM vascular network after the *i.v.* injection of FITC, no PDT was administered to the egg

above the cover-glass. It was kept in place by a metal fiber holder (6). The PDT light was provided by a CW solid state diode laser (8) (Oxxius®, $405\,nm$, $1.3\,mW$ total power at the distal end of the fiber) and administered through another optical fiber (4) (MedLight® Frontal light distributor, NA = 0.37, core diameter $\varnothing 600\,\mu m$). This treatment fiber was chosen and its distance to the CAM adjusted so as to deliver a homogeneous PDT treatment spot ($\varnothing$ $8\,mm$) on the selected zone of the CAM vasculature. Small irradiances ($\approx 2.5\,mW/cm^2$) were preferred so as to avoid significant photothermal effects. The period during which the eggs were kept out of the incubator was limited to about 15 min.

To keep the DF measurement durations small with respect to PDT exposure times, thus minimizing phototoxic effects and oxygen consumption due to the DF measurements themselves, only 30 consecutive laser sweeps were used and averaged for the oxygen measurements. Thus, as mentioned above, the total acquisition time for one such measurement was $3\,s$, as compared to a minimum PDT exposure time of $75\,s$, and the corresponding total light dose delivered by the probing laser was limited to $\approx 100\,mJ/cm^2$, as compared to a minimum PDT light dose of $\approx 190\,mJ/cm^2$, both at $405\,nm$. A light dose of $100\,mJ/cm^2$ was found to have barely detectable PDT vascular effect. Therefore, we chose to set the minimal PDT light dose to approximately the double of this value.

At the end of the PDT treatment, the cover-glass was carefully removed from the treated zone. Only very small iatrogenic damages were identified after these mechanical operations. In other words, when the cover-glass insertion and removal was per-

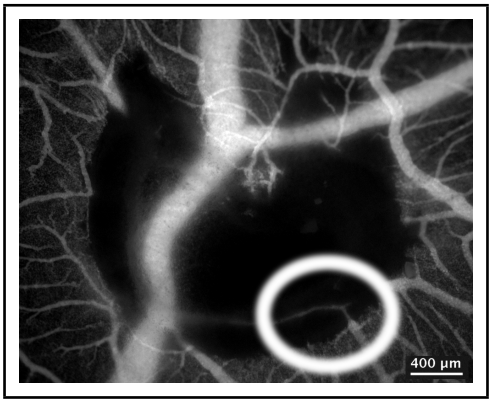

(a) CAM model 4x

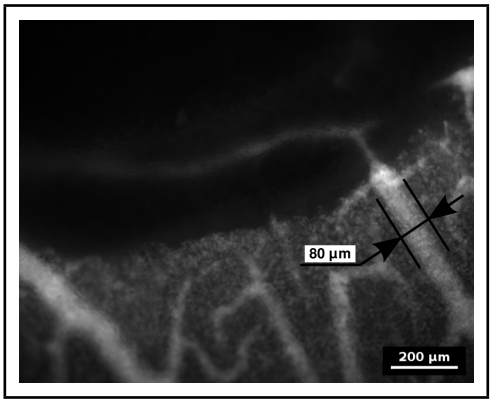

(b) CAM model 10x

Figure 7.4: CAM vascular damage after a PDT total optical dose of $2.25\,J/cm^2$, laser spot $\varnothing 5\,mm$

formed with all needed care, induced injury was imperceptible. The eggs were then returned to the incubator, while waiting for the vascular damage assessment.

7.2.4 Vascular Damage Assessment

The treated eggs were taken out of the incubator $16 - 18\,h$ after termination of the PDT irradiation protocol[1]. An intra-venous (*i.v.*) injection of $20\,\mu l$ of a $150\,\mu M$ solution of fluorescein isothiocyanate-dextran (FITC, $150KDa$, $25\,mg/ml$ in NaCl 0.9%) was administered into one of the large CAM veins, while $1\,ml$ of india ink (Parker®-Quink) was injected *under* the CAM to increase contrast and screen out the continuously changing background fluorescence. Vascular damage due to PDT was then examined and recorded photographically with an epifluorescence microscope (Nikon ® E600FN, excitation wavelength between $450\,nm$ and $490\,nm$, emission wavelength: $> 520\,nm$), see Figure 7.3 and 7.4.

The damage extent was classified on the basis of blood vessel closure: Effectively, the *diameter of the largest blood vessels closed* by the PDT treatment was used as an arbitrarily chosen index of vascular damage (see §7.3.4).

7.3 Results

7.3.1 PpIX Build-up Kinetics after ALA Topical Administration

Limited experimental data have been published about the localization and build-up ki-

[1] This standard time period has been in use in our laboratory for several years, partly for practical reasons, as the measurements are performed overnight. Although it was not methodically optimized, it corresponds to a state of the CAM where PDT damage has had the time to fully develop while the counteracting processes of vessel repair and neo-angiogenesis have not yet interfered significantly with the PDT results.

netics of PpIX in the CAM following topical administration of ALA [17, 27] [18, 19]. In view of optimizing DF signal quality, we performed a first experiment using 10 eggs, whereby each egg was examined after a variable waiting time (ranging from 0 to 6 h) following the topical administration of ALA (see Figure 7.5).

During the several hours of incubation, ALA is absorbed by the vasculature where it circulates, and diffuses out of the vasculature into almost all egg tissues: thus, PpIX is formed and accumulated in most of the tissue volume of the chick embryo. In Figure 7.5(a), the resulting spatial distribution of PpIX in the CAM is shown, 4 hours after ALA administration: The picture reveals a slightly more intense fluorescence (lighter areas) around the center of the administration zone and near the walls of the large vessels, where ALA interacted longer and in higher concentrations. As an illustrative example, the luminescence intensity in the administration zone was, in fact, measured to be $\approx 30\%$ higher than $5\,mm$ away from this zone.

As shown in Figure 7.5(b) and in agreement with the litterature [17–19, 27], the maximum of PpIX accumulation is reached approx. $4\,h$ after ALA administration. Accordingly, a drug-light interval of $4\,h$ was chosen for the PDT and used throughout this study. The zone where ALA was topically administered was then selected to perform DF measurements as this resulted in an adequate signal-to-noise ratio.

7.3.2 *In vivo* Monitoring of Tissular Oxygen Concentration through PpIX's Delayed Fluorescence

In a second experiment, we collected data from 12 eggs exposed to precisely determined oxygen/nitrogen gaseous mixtures, whose oxygen concentration was gradually and successively decreased. The relative concentrations of O_2 were respectively 21%, 15%, 10%, 5%, 3%, 1% and 0%.

Before each measurement, the egg was allowed to stand in the controlled atmosphere of the gas chamber for $10\,min$ to establish an approximate equilibrium between environmental and tissular pO_2. The DF lifetime of PpIX was then determined with our optical fiber-based spectrofluorometer. Figure 7.6(a) confirms the validity of the Stern-Volmer equation in our experimental conditions (see Equation 7.1): PpIX's DF *reciprocal* lifetime appears to be a linear function of the eggs' environmental oxygen concentration. Note the relatively large error bars, corresponding to $\pm$ one standard deviation. These error bars increase with the relative concentrations of O_2, at least partially due to the decreasing accuracy, when determining gradually shorter lifetimes, whose inverse are plotted here.

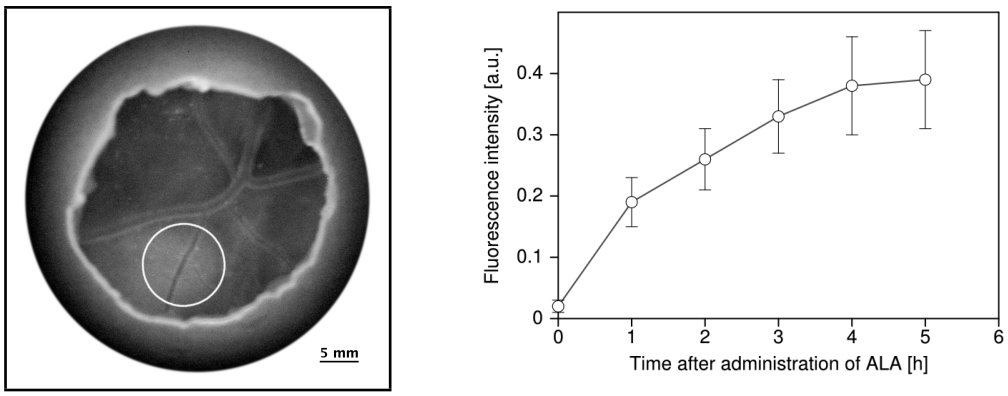

(a) Spatial distribution

(b) Fluorescence pharmacokinetics

Figure 7.5: PpIX fluorescence in the CAM model after topical administration of a droplet ($20\,\mu l$) of $0.15\,M$ ALA solution. (a) Spatial distribution. Fluorescence image recorded 4 h after administration ($\lambda_{Ex} = 405\,nm$, $\lambda_{Em} > 460\,nm$), the white circle shows the location where the ALA droplet was deposed. (b) Fluorescence pharmacokinetics

7.3.3 *In vivo* Measurement of Tissular Oxygen Concentration as a Function of PDT Irradiation Time

In a third type of experiment, we performed DF-based O_2 measurements on a total of 35 eggs, submitted to increasing cumulated PDT illumination times, where each data point is the average of measurements performed on 12 to 20 different eggs.

Figure 7.6(b) shows DF *reciprocal* lifetime measurements acquired after illumination protocols I or II (illustrated in §7.2.3). The vertical scale on the right hand side of Figure 7.6(b) gives an indication of the corresponding residual tissular O_2 concentration based on the results obtained during of the experiments under controlled atmosphere (reported in Figure 7.6(a)). The results show a decreasing oxygen tissular concentration (*i.e.* an increasing oxygen consumption) during the first $500\,s$ of cumulated PDT time, while a limiting asymptotic value is reached at longer treatment times, very near the zero concentration level for tissular O_2. The relatively large error bars ($\pm$ one standard deviation) are probably due, at least in part, to local differences in the aptitude of CAM tissues to renew the consumed O_2, depending on their different metabolic activities, and possibly also to inhomogeneities in the spatial distribution of the photosensitizer.

7.3.4 Tissular Oxygen Depletion as an Index of PDT Efficiency

To establish the expected correlation between tissular oxygen consumption during PDT and the corresponding, observed vascular damage,

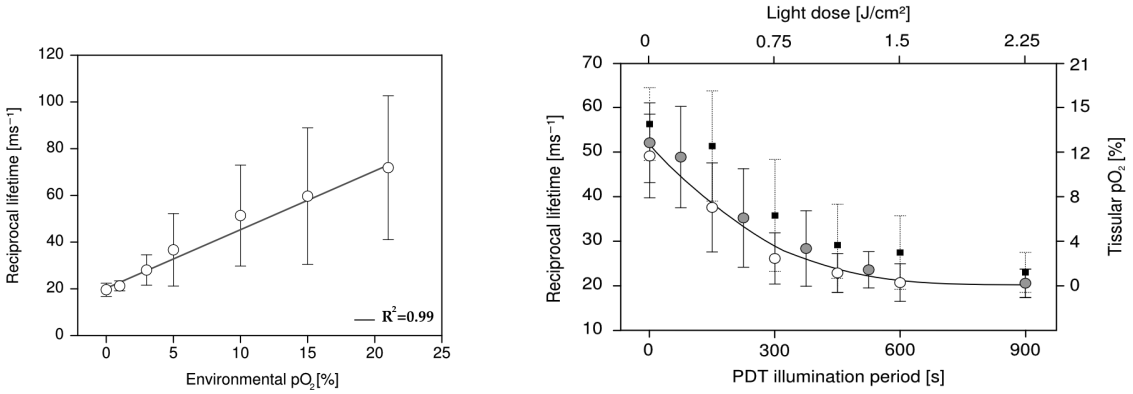

(a) PpIX's reciprocal lifetime under controlled atmosphere

(b) PpIX's reciprocal lifetime as a function of PDT duration

Figure 7.6: Delayed fluorescence reciprocal lifetime of PpIX in the *in vivo* CAM model. (a) PpIX's reciprocal lifetime under controlled atmosphere. (b) PpIX's reciprocal lifetime as a function of PDT duration. Protocol I (○), Protocol II (●), Protocol III (■).

we performed a fourth experiment on five lots of 20 eggs. These eggs were subjected to PDT treatment, using different optical doses as detailed hereunder and following the general scheme of Protocol III (see Figure 7.2). The CAMs were prepared, handled and measured as indicated previously.

Eggs lot	Irradiation period [sec]	Optical dose $[J/cm^2]$
1	150	0.38
2	300	0.75
3	450	1.13
4	600	1.5
5	900	2.25

Table 7.1: PDT light dose administration protocol for eggs lot, see §7.2.3 for details.

The normal, baseline value of tissular pO_2 was first determined for each egg before starting the chosen PDT irradiation protocol. The eggs were then submitted to PDT illumination under a constant irradiance of $2.5\,mW/cm^2$ for durations ranging from 150 to $900\,s$ as indicated in Table 7.1

Immediately after treatment, each egg's tissular O_2 concentration was again measured, through the described PpIX DF reciprocal lifetime determination. Following this, the *difference* between the initial and final values of this DF reciprocal lifetime, *i.e.* the difference between initial and final values of the pO_2 estimator, was taken as the measure of tissular O_2 consumption ascribable to the PDT treatment. Thereafter, the eggs were returned to the incubator and allowed to stand for the usual $16-18\,h$. The eggs were then subjected to the procedure described under

§7.2.4 to determine the extent of vascular damage caused by the PDT, as measured by the selected arbitrary damage index.

In Figure 7.6(b), PpIX's reciprocal DF lifetime and the corresponding residual tissular pO_2 are shown as a function of PDT illumination time (■). The results show the expected *diminishing* pO_2 with increasing light dose. It is wort noting that this pO_2 appears to reach a very low limiting (plateau) value for illumination periods longer than about $500\,sec$ ($\approx 1.3\,J/cm^2$). Figure 7.7 illustrates the correspondingly *increasing oxygen consumption* as computed by the differences in reciprocal lifetimes.

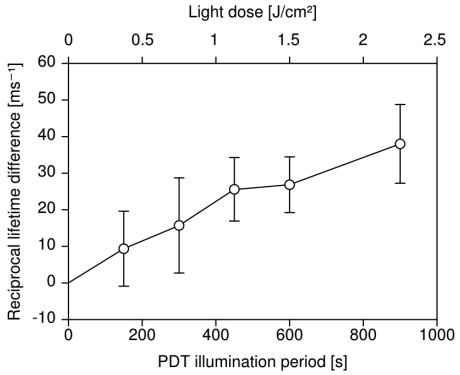

Figure 7.7: Lifetime difference as a function of PDT illumination.

In Figure 7.8(a), the vascular damage index is plotted as a function of the PDT treatment duration. The data shows, despite the substantial error bars, a reasonable correlation between these two parameters. Figure 7.8(b) shows the vascular damage index as a function of *reciprocal lifetime differences*, which are taken as a measure of tissular oxygen consumption during the treatment. Here again a clear correlation between those two parameters is found. It is also of interest to note that despite the fact that (as shown in Figure 7.6(b)) for illumination periods greater than $500\,s$, the residual pO_2 does not decrease significantly anymore, the observed tissular damage continues to increase with increasing light dose, at least until an irradiation time of $900\,s$. This suggests that the PDT mechanism is still operating at these very low oxygen concentrations.

7.4 Discussion

This paper reports the first study aiming at measuring, in vivo and in real time, the level of molecular oxygen contained in tissue, using the DF of a PS, in order to optimize PDT. The results demonstrate a correlation between the PDT-induced vascular damage and the oxygen consumption assessed by the change of DF lifetime. These observations are in agreement with numerous articles reporting the role played by oxygen in the tissue damage induced by PDT [12, 26, 34, 40, 43, 52, 62, 63]. Consequently, adjusting the PDT light dose, based on the monitoring of the tissular pO_2 through the PS's DF, appears feasible.

Thus, our approach appears as a promising way to control the efficacy of PDT, and

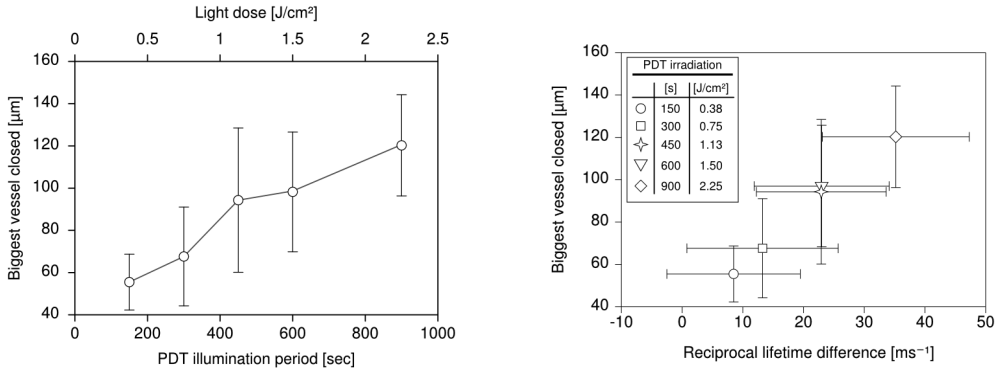

(a) As a function of PDT duration

(b) As a function of tissular oxygen consumption

Figure 7.8: PDT-induced vessel damages in the CAM model. (a) As a function of PDT duration. (b) As a function of tissular oxygen consumption, as measured by the reciprocal PpIX DF lifetimes differences

reduce intra- and inter-patient fluctuations in its clinical outcome. It is an essentially implicit light dosimetry method, because the pO_2 change, a parameter which is proportional to the production of singlet oxygen, is measured close to the PS (about $1\,\mu m$). Therefore, this method is likely to be much more directly related to the tissular effects induced by PDT than the approaches based on an explicit light dosimetry (light dose; PS global concentration; etc.) [22, 24, 54, 61]. In addition, most of these other approaches, for quantifying PDT outcome, suffer from the weakness that the pO_2 is not measured at a subcellular or tissular scale. Furthermore, the method presented here does not require the use of exogenous oxygen sensors since it is based on the DF measurement of the PS itself, which is present in the PDT anyway. This feature is of importance since, besides ALA, several precursors of PpIX are now approved by the medical authorities of a large number of countries.

Since, in our study, both the light used to excite the DF and the light used for PDT have the same wavelength, it cannot be excluded that the DF excitation could induce a reduction in pO_2, as well as PpIX photobleaching and/or vascular damage, thus leading to artifacts. However, as already noted, the DF excitation light dose, for a 30 laser pulse series used to perform a "measurement" (see §7.2.1), is much smaller than the light dose used to induce the smallest detectable PDT effect, as indicated in §7.3.4. In addition, we have demonstrated in a separate study that, in the absence of PDT, the DF excitation light does not induce any detectable vascu-

lar effect, in our applied conditions. Finally, comparing the evolution of the DF lifetime for the three different measurement protocols described in §7.2.3 (see Figure 7.6 (b)), indicates that this DF excitation light does not induce measurable vessel closure.

A drug-light interval of 4 hours was used for the present study. It should be noted that other incubation periods may lead to other values of the DF lifetimes, even if all other conditions are identical, since it is well known that the PpIX buildup, which takes place in specific tissue/cellular compartments, is followed by a diffusion of the PS to other compartments presenting other microenvironments [1]. The changed microenvironments may then lead to changed local $p\mathrm{O}_2$ and hence change in DF lifetime, as well as changed vascular occlusion efficiency. As a consequence, it could be that the results we report in Figures 7.6 and 7.8 may differ if longer or shorter drug-light intervals are used.

The relatively large error bars observed in Figure 7.6(a), which increase with the relative concentrations of O_2, are due, at least partially, to the decreasing accuracy when determining gradually shorter lifetimes, whose inverse are plotted here. Another possible cause may reside in variations of oxygen availability to PpIX molecules, depending on their tissular and/or cellular localization, where different metabolic activities occur. Indeed, the much smaller error bars at very low $p\mathrm{O}_2$ values, *i.e.* below 5 %, support this hypothesis, since death of the eggs when the $p\mathrm{O}_2$ tends to 0 % also implies the end of all these different metabolisms, therefore erasing their previous differences. Similarly, the relatively large error bars affecting the DF lifetimes presented in Figures 7.6(b), 7.7, and 7.8 may well be due to local differences in tissue oxygen renewal during PDT. These local differences could, *e.g.*, be due to spatial and/or temporal differences in the metabolic activity, blood perfusion, inhomogenous distribution of the PS, etc. Therefore, one approach to reduce these fluctuations would consist of probing a larger area (say, $1 - 2\,cm$ in diameter) so that the measurement is averaged over a larger surface. Our observations furthermore suggest that it might be of interest to image the PS's DF lifetime at "high" spatial resolution in the hope of getting information regarding the changes of tissue oxygenation at a tissular and even a cellular level. Recording such images at different times after the beginning of PDT and at different drug-light intervals would certainly help to identify treatment strategies to target specific tissue structures (vessels versus stroma, for instance). Finally, it should be noted that the fluctuations, affecting the DF lifetime measurements, due to the instrumentation and the shot noise are negligible as compared to the other factors mentioned above.

Indeed, repeated measurements performed in identical conditions, at the same location and on the same sample confirm this. Nevertheless, if necessary, the shot noise can be further improved by reducing the time during which the detector is blinded to reject the prompt fluorescence. The resulting increase of DF radiant energy detected will decrease the shot noise, but will also increase the risk to detect: (i) the emission of other endogenous luminophores presenting "long" (between $100\,ns$ and $1\,\mu s$) luminescence lifetimes; (ii) luminescence emitted by the instrumentation (laser spontaneous emission, luminescence from the optics in the setup). This is why we have, in this study, selected a time delay of $3\,\mu s$ for "blinding" the detector, which corresponds to an optimal tradeoff between this delay and the observed signal-to-noise ratio.

The error bars affecting the measurements of the diameter of the largest occluded blood vessels, which are shown in Figure 7.8 are likely to be due to various factors, including: (i) The selection of the area treated by PDT: indeed, somewhat different results may be obtained if the relative density of large and small vessels, or of veins versus arteries, differs from place to place. Although the relative importance of this source of fluctuations is difficult to assess quantitatively, it probably plays a minor role, as described by Lange et al. who used a similar metric to quantify the vascular effects induced by PDT in the CAM model [25]; (ii) the inhomogenous distribution of PpIX, as reported by many authors [59, 60]; (iii) intrinsic errors while measuring the vessels diameter: the fluctuations due to this last reason could be reduced using quantitative image analysis programs to characterize the vascular network, as proposed by Nowak-Sliwinska et al. [41]. One may conclude, considering the above-mentionned factors, which are possibly responsible for the rather large fluctuations affecting measurements of the DF lifetime and blood vessel closure efficacy, that probing of larger well-selected areas, as indicated above, will most likely help to reduce these fluctuations.

The results presented in Figure 7.8(b) indicate that the vascular occlusion effects of PDT and the differences in reciprocal DF lifetime (which can be seen as a metric for the tissular oxygen consumption) are correlated. We have also observed that, for illumination periods longer than $500\,s$ ($1.25\,J/cm^2$), the vascular damage continues to increase for increasing light doses. This is interesting considering that the measured residual $p\mathrm{O}_2$ does not decrease significantly anymore after $500\,s$, as it is already very close to 0% (see Figure 7.6(b)). This observation indicates that some PDT-related mechanism still continues to be effective at very low $p\mathrm{O}_2$. One explanation for this phenomenon is that all the oxygen provided by the blood stream is immedi-

ately consumed during the PDT illumination. This hypothesis is realistic since the blood vessels affected by PDT, depending among others on their size, will close, to a large extent, after the end of the illumination [9], at the applied conditions. Consequently, in such conditions, the PDT effect would be "oxygen supply dependent", as reported by several groups [13, 37, 53]. Although this explanation is the most probable, other phototoxic mechanisms, that do not involve molecular oxygen, as suggested by Plaetzer et al. [45], could cause a PDT effect in the abscence of a significant $p\mathrm{O}_2$. We suggest that experiments, similar to those presented in this paper, but performed at different fluence rates, may help to understand the nature of these effects.

Finally one may note that the approach presented here is of interest, not only for PpIX-based PDT, but also when other PSs with a detectable DF, or a difficult to detect phosphorescence, are used. One may even suggest that the technique presented in this paper be used to monitor the $p\mathrm{O}_2$ during the treatment of age-related macular degeneration with Visudyne®. Indeed, application of the DF measurements to the retina may be helped by the unique optical properties of the eye, and making use of such measurements may help compensate, to some extent, for the inter-patient fluctuations observed during AMD-PDT [7]

In conclusion, the present work has demonstrated *in vivo* that the DF of a photosensitizer can be used to determine the $p\mathrm{O}_2$ in tissues, thus helping to predict the tissular effects induced by PDT. The applications of this approach to other systems are numerous. Thus, the technology developed here may help to get information on the mechanisms involved in the oxygenation and photosensitization of various materials, including biological tissues.

7.5 Acknowledgments

This work was supported by the Swiss National Science Foundation (Grant 205320-116556) and funded in part by the J. Jacobi Trust.

References

[1] M Ascencio, J P Estevez, M Delemer, M O Farine, P Collinet, and S Mordon. Comparison of continuous and fractionated illumination during hexaminolaevulinate-photodynamic therapy. *Photodiagnosis and photodynamic therapy*, 5(3):210–6, September 2008. ISSN 1873-1597. 101

[2] S Blumenröder, A J Augustin, and F H Koch. The influence of intraocular pressure and systemic oxygen tension on the intravascular po2 of the pig retina as measured with phosphorescence imaging. *Surv Ophthalmol*, 42 Suppl 1:S118–26, November 1997. ISSN 0039-6257. 89

[3] F Borle, A Radu, C Fontolliet, H van den Bergh, P Monnier, and G Wagnières. Selectivity of the photosensitiser tookad for photodynamic therapy evaluated in the syrian golden hamster cheek pouch tumour model. *British Journal of Cancer*, 89(12): 2320–6, December 2003. ISSN 0007-0920. 88

[4] D Braichotte, J Savary, T Glanzmann, P Monnier, G Wagnières, and H van den Bergh. Optimizing light dosimetry in photodynamic therapy of the bronchi by fluorescence spectroscopy. *Lasers in Medical Science*, 11(4):247–254, 1996. doi: http://dx.doi.org/10.1007/BF02134915.

[5] T M Busch. Local physiological changes during photodynamic therapy. *Lasers in Surgery and Medicine*, 38(5):494–9, June 2006. ISSN 0196-8092. 88

[6] W Chin, W Lau, S L Lay, K K Wei, and M Olivo. Photodynamic-induced vascular damage of the chick chorioallantoic membrane model using perylenequinones. *Int J Oncol*, 25(4):887–91, October 2004. ISSN 1019-6439. 90

[7] A F Cruess, G Zlateva, A M Pleil, and B Wirostko. Photodynamic therapy with verteporfin in age-related macular degeneration: a systematic review of efficacy, safety, treatment modifications and pharmacoeconomic properties. *Acta Ophthalmologica*, 87(2):118–32, March 2009. ISSN 1755-3768. 103

[8] A Curnow, J C Haller, and S G Bown. Oxygen monitoring during 5-aminolaevulinic acid induced photodynamic therapy in normal rat colon. comparison of continuous and fractionated light regimes. *Journal of Photochemistry and Photobiology*, 58 (2-3):149–55, November 2000. ISSN 1011-1344. 88

[9] E Debefve, B Pegaz, H van den Bergh, G Wagnières, N Lange, and J-P Ballini. Video monitoring of neovessel occlusion induced by photodynamic therapy with verteporfin (visudyne), in the cam model. *Angiogenesis*, 11(3):235–43, 2008. ISSN 1573-7209. 90, 91, 103

[10] J S Dysart and M S Patterson. Photobleaching kinetics, photoproduct formation, and dose estimation during ala induced ppix pdt of mll cells under well oxygenated and hypoxic conditions. *Photochem Photobiol Sci*, 5(1):73–81, January 2006. ISSN 1474-905X. 88

[11] J Feitelson and D Mauzerall. Reaction of triplet states of a porphyrin measured ba delayed fluorescence. *Journal of Physical Chemistry*, 86:1623–1628, 1982. 88

[12] J M Fernandez, M D Bilgin, and L I Grossweiner. Singlet oxygen generation by photodynamic agents. *Journal of Photochemistry and Photobiology B: Biology*, 37 (1-2):131–140, 1997. doi: DOI:10.1016/S1011-1344(96)07349-6. URL `http://www.sciencedirect.com/science/article/B6TH0-3S9DM3B-K/2/10530ae0d094473af3a9d867715591c2`. 88, 99

[13] T H Foster, R S Murant, R G Bryant, R S Knox, S L Gibson, and R Hilf. Oxygen consumption and diffusion effects in photodynamic therapy. *Radiation Research*, 126(3):296–303, June 1991. ISSN 0033-7587. 103

[14] N Fotinos, M A Campo, F Popowycz, R Gurny, and N Lange. 5-aminolevulinic acid derivatives in photomedicine: Characteristics, application and perspectives. *Journal of Photochemistry and Photobiology*, 82(4):994–1015, 2006. ISSN 0031-8655. 87

[15] V Gottfried, E S Lindenbaum, and S Kimel. The chick chorioallantoic membrane (cam) as an in vivo model for photodynamic therapy. *Journal of Photochemistry and Photobiology*, 12(2):204–7, January 1992. ISSN 1011-1344. 91

[16] J Grote, R Süsskind, and P Vaupel. Oxygen diffusivity in tumor tissue (ds-carcinosarcoma) under temperature conditions within the range of 20–40 degrees c. *Pflugers Archiv*, 372(1): 37–42, November 1977. ISSN 0031-6768. 89, 90

[17] M J Hammer-Wilson, D Cao, S Kimel, and M W Berns. Photodynamic parameters in the chick chorioallantoic membrane (cam) bioassay for photosensitizers administered intraperitoneally (ip) into the chick embryo. *Photochemical Photobiological Sciences : Official Journal of the European Photochemistry Association and the European Society for Photobiology*, 1 (9):721–8, 9 2002. 96

[18] C Hoppenheit, D Hüttenberger, H J Foth, W J Spitzer, T E Reichert, and U D A Müller-Richter. Pharmacokinetics of the photosensitizers aminolevulinic acid and aminolevulinic acid hexylester in oro-facial tumors embedded in the chorioallantois membrane of a hen's egg. *Cancer Biotherapy and Radiopharmaceuticals*, 21(6):569–78, December 2006. ISSN 1084-9785. 96

[19] R Hornung, M J Hammer-Wilson, S Kimel, L H Liaw, Y Tadir, and M W Berns. Systemic application of photosensitizers in the chick chorioallantoic membrane (cam) model: Photodynamic response of cam vessels and 5-aminolevulinic acid uptake kinetics by transplantable tumors. *Journal of Photochemistry and Photobiology*, 49(1):41–9, 3 1999. doi: 10.1016/S1011-1344(99)00014-7. 90, 96

[20] Z Huang. A review of progress in clinical photodynamic therapy. *Technology of Cancer Research and Treatement*, 4(3):283–93, June 2005. ISSN 1533-0346. 87

[21] C Ince and E G Mik. Device and method for determining the concentration of a substance, January 10 2007. EP Patent 1,742,038. 89, 90

REFERENCES

[22] M T Jarvi, M J Niedre, M S Patterson, and B C Wilson. Singlet oxygen luminescence dosimetry (sold) for photodynamic therapy: current status, challenges and future prospects. *Journal of Photochemistry and Photobiology*, 82(5):1198–210, 2006. ISSN 0031-8655. 100

[23] B Kruijt, H S de Bruijn, A van der Ploeg-van Den Heuvel, R W F de Bruin, H J C M Sterenborg, A Amelink, and D J Robinson. Monitoring ala-induced ppix photodynamic therapy in the rat esophagus using fluorescence and reflectance spectroscopy. *Journal of Photochemistry and Photobiology*, 84 (6):1515–27, 2008. 88

[24] B Kruijt, Angelique van der Ploeg-van den Heuvel, H S de Bruijn, H J C M Sterenborg, A Amelink, and D J Robinson. Monitoring interstitial m-thpc-pdt in vivo using fluorescence and reflectance spectroscopy. *Lasers in Surgery and Medicine*, 41(9):653–64, November 2009. ISSN 1096-9101. 88, 100

[25] N Lange, J-P Ballini, G Wagnieres, and Hubert van den Bergh. A new drug-screening procedure for photosensitizing agents used in photodynamic therapy for cnv. *Investigative Ophthalmology & Visual Science*, 42(1):38–46, January 2001. ISSN 0146-0404. 90, 91, 102

[26] S Lee, D H Vu, M F Hinds, S J Davis, A Liang, and T Hasan. Pulsed diode laser-based singlet oxygen monitor for photodynamic therapy: in vivo studies of tumor-laden rats. *Journal of Biomedical Optics*, 13(6):064035, 2008. doi: 10.1117/1.3042265. URL http://link.aip.org/link/?jbo/13/064035\&agg=MEDLINE_JBO. 88, 89, 99

[27] E Malik, C Berg, A Meyhöfer-Malik, O Buchweitz, P Moubayed, and K Diedrich. Fluorescence diagnosis of endometriosis using 5-aminolevulinic acid. *Surgical Endoscopy*, 14(5):452–5, May 2000. ISSN 0930-2794. 96

[28] B W McIlroy, A Curnow, G Buonaccorsi, M A Scott, S G Bown, and A J MacRobert. Spatial measurement of oxygen levels during photodynamic therapy using time-resolved optical spectroscopy. *J Photochem Photobiol B*, 43(1):47–55, April 1998. ISSN 1011-1344. 88

[29] W Melhuish. Nomenclature, symbols, units and their usage in spectrochemical analysis—vi molecular luminescence spectroscopy. *Spectrochimica Acta*, 37(3):259–272, 1982. 89, 90

[30] H J Meuer, V Hartmann, and S Jopp. Tissue po2 and growth rate in early chick embryos. *Respiratory Physiology*, 90(2):227–37, November 1992. ISSN 0034-5687. 91

[31] E G Mik, J Stap, M Sinaasappel, J F Beek, J A Aten, T G van Leeuwen, and C Ince. Mitochondrial po2 measured by delayed fluorescence of endogenous protoporphyrin ix. *Nature Methods*, 3(11):939–45, 11 2006. doi: 10.1038/nmeth940. 89

[32] E G Mik, T Johannes, C J Zuurbier, A Heinen, J H P M Houben-Weerts, G M Balestra, J Stap, J F Beek, and C Ince. In vivo mitochondrial oxygen tension measured by a delayed fluorescence lifetime technique. *Biophysical Journal*, 95(8): 3977–90, 10 2008. doi: 10.1529/biophysj.107.126094. 89, 90

[33] J Moan and K Berg. The photodegradation of porphyrins in cells can be used to estimate the lifetime of singlet oxygen. *Journal of Photochemistry and Photobiology*, 53(4):549–53, April 1991. ISSN 0031-8655. 89

[34] J Moan and P Juzenas. Singlet oxygen in photosensitization. *Journal of Environmental Pathology, Toxicology and Oncology : Official Organ of the International Society for Environmental Toxicology and Cancer*, 25(1-2):29–50, 2006. URL http://www.begellhouse.com/journals/0ff459a57a4c08d0,5d84548f012e18bf,59bbacd00ecbd94a.html. 88, 99

[35] A. Molnàr, R Dedic, A Svoboda, and J Hála. Spectroscopic study of singlet oxygen photogeneration by lipophilic photosensitiser in liposomes. *Journal of Luminescence*, 128(5-6):783–785, 2008. ISSN 0022-2313. doi: DOI:10.1016/j.jlumin.2007.12.009. URL http://www.sciencedirect.com/science/article/B6TJH-4R9GH1F-8/2/25f8c416617ed14119c71e34dd4fcf93. Proceedings of the 16th International Conference on Dynamical Processes in Excited States of Solids, 16th International Conference on Dynamical Processes in Excited States of Solids. 89

[36] K J Morris, M S Roach, W Xu, J N Demas, and B A DeGraff. Luminescence lifetime standards for the nanosecond to microsecond range and oxygen quenching of ruthenium(ii) complexes. *Analytical Chemistry*, 79(24):9310–4, 12 2007. doi: 10.1021/ac0712796. URL http://dx.doi.org/10.1021/ac0712796. 89

[37] A T Nathan and M Singer. The oxygen trail: Tissue oxygenation. *British Medical Bulletin*, 55(1):96–108, 1999. URL http://openurl.ingenta.com/content/nlm?genre=article\&issn=0007-1420\&volume=55\&issue=1\&spage=96\&aulast=Nathan. 103

[38] M Niedre, M S Patterson, and B C Wilson. Direct near-infrared luminescence detection of singlet oxygen generated by photodynamic therapy in cells in vitro and tissues in vivo. *Photochemistry and Photobiology*, 75(4):382–91, 4 2002. URL http://www3.interscience.wiley.com/resolve/openurl?genre=article\&sid=nlm:pubmed\&issn=0031-8655\&date=2002\&volume=75\&issue=4\&spage=382. 89

[39] M J Niedre, M S Patterson, A Giles, and B C Wilson. Imaging of photodynamically generated singlet oxygen luminescence in vivo. *Journal of Photochemistry and Photobiology*, 81 (4):941–3, 2005. doi: 10.1562/2005-03-15-TSN-462. URL http://www3.interscience.wiley.com/resolve/openurl?genre=article\&sid=nlm:pubmed\&issn=0031-8655\&date=2005\&volume=81\&issue=4\&spage=941.

[40] M J Niedre, C S Yu, M S Patterson, and B C Wilson. Singlet oxygen luminescence as an in vivo photodynamic therapy dose metric: Validation in normal mouse skin with topical amino-levulinic acid. *British Journal of Cancer*, 92(2): 298–304, 1 2005. doi: 10.1038/sj.bjc.6602331. URL http://dx.doi.org/10.1038/sj.bjc.6602331. 88, 89, 99

[41] P Nowak-Sliwinska, J P Ballini, G Wagnières, and H van den Bergh. Processing of fluorescence angiograms for the quantification of vascular effects induced by anti-angiogenic agents in the cam model. *Microvascular Research*, 79(1):21–8, January 2010. ISSN 1095-9319. 102

[42] M Ochsner. Photophysical and photobiological processes in the photodynamic therapy of tumours. *Journal of Photochemistry and Photobiology. B, Biology*, 39(1):1–18, 5 1997. 88

[43] S Pervaiz and M Olivo. Art and science of photodynamic therapy. *Clinical and Experimental Pharmacology and Physiology*, 33:551–6, 2006. doi: 10.1111/j.1440-1681.2006.04406.x. URL http://www3.interscience.wiley.com/resolve/openurl?genre=article\&sid=nlm:pubmed\&issn=0305-1870\&date=2006\&volume=33\&issue=5-6\&spage=551. 88, 99

[44] F Piffaretti, K Santhakumar, E Forte, H van den Bergh, and G Wagnières. In vivo detection of photosensitizer's delayed fluorescence for photodynamic therapy light dose monitoring and adjustment. *Submitted*, 45(1):1–13, 1 2010. 90, 91

[45] K Plaetzer, B Krammer, J Berlanda, F Berr, and T Kiesslich. Photophysics and photochemistry of photodynamic therapy: fundamental aspects. *Lasers in Medical Science*, 24(2):259–68, March 2009. ISSN 0268-8921. 89, 103

[46] R W Redmond and J N Gamlin. A compilation of singlet oxygen yields from biologically relevant molecules. *Journal of Photochemistry and Photobiology*, 70(4):391–475, October 1999. ISSN 0031-8655. 87, 88, 89

[47] D Ribatti. Chick embryo chorioallantoic membrane as a useful tool to study angiogenesis. *International Review of Cell and Molecular Biology*, 270:181–224, 2008. ISSN 1937-6448. 90

[48] D Ribatti. *The Chick Embryo Chorioallantoic Membrane in the Study of Angiogenesis and Metastasis: The CAM assay in the study of angiogenesis and metastasis*. 1st edition, 2010. ISBN 978-90-481-3843-2. 90

[49] A L Romanoff. *Biochemistry of the Avian Embryo. A Quantitative Analysis of Prenatal Development*. New York: Interscience, 1967. 91

[50] U B Rüfenacht, L Gouya, X Schneider-Yin, H Puy, B W Schäfer, R Aquaron, Y Nordmann, E I Minder, and J C Deybach. Systematic analysis of molecular defects in the ferrochelatase gene from patients with erythropoietic protoporphyria. *Am J Hum Genet*, 62(6):1341–52, June 1998. ISSN 0002-9297. 87

[51] W L Rumsey, J M Vanderkooi, and D F Wilson. Imaging of phosphorescence: a novel method for measuring oxygen distribution in perfused tissue. *Science*, 241(4873):1649–51, September 1988. ISSN 0036-8075. 89

[52] R Schmidt. Photosensitized generation of singlet oxygen. *Journal of Photochemistry and Photobiology*, 82(5):1161–1177, 2007. doi: 10.1562/2006-03-03-lR-833. 88, 99

[53] T Schunck and P Poulet. Oxygen consumption through metabolism and photodynamic reactions in cells cultured on microbeads. *Physics in Medicine and Biology*, 45(1):103–19, January 2000. ISSN 0031-9155. 103

[54] C Sheng, P J Hoopes, T Hasan, and B W Pogue. Photobleaching-based dosimetry predicts deposited dose in ala-ppix pdt of rodent esophagus. *Journal of Photochemistry and Photobiology*, 83(3):738–48, 2007. 88, 100

[55] R D Shonat, D F Wilson, C E Riva, and M Pawlowski. Oxygen distribution in the retinal and choroidal vessels of the cat as measured by a new phosphorescence imaging method. *Appl. Opt.*, 31(19):3711–3718, 1992. URL `http://ao.osa.org/abstract.cfm?URI=ao-31-19-3711`. 89

[56] D M Strick, R L Waycaster, J P Montani, W J Gay, and T H Adair. Morphometric measurements of chorioallantoic membrane vascularity: effects of hypoxia and hyperoxia. *American Journal of Physiology*, 260(4 Pt 2):1385–9, April 1991. ISSN 0002-9513. 91

[57] K Tabata, S I Ogura, and I Okura. Photodynamic efficiency of protoporphyrin ix: Comparison of endogenous protoporphyrin ix induced by 5-aminolevulinic acid and exogenous porphyrin ix. *Photochemistry and Photobiology*, 66(6):842–846, 1997. doi: 10.1111/j.1751-1097.1997.tb03235.x. Department of Bioengineering, Tokyo Institute of Technology, Yokohama, Japan. 87

[58] M P Tsvirko, K N Solovev, A T Gradyzshko, and S S Dvornikov. Phosphorescence of porphyrin free base and their complexes with light metals. *Optika i Spektroskopiya*, 38:705–713, 1975. 89

[59] P Uehlinger, J P Ballini, H van den Bergh, and G Wagnières. On the role of iron and one of its chelating agents in the production of protoporphyrin ix generated by 5-aminolevulinic acid and its hexyl ester derivative tested on an epidermal equivalent of human skin. *Journal of Photochemistry and Photobiology*, 82(4):1069–76, 2006. ISSN 0031-8655. 102

[60] K K H Wang, J D Wilson, M E Kenney, S Mitra, and T H Foster. Irradiation-induced enhancement of pc 4 fluorescence and changes in light scattering are potential dosimeters for pc 4-pdt. *Journal of Photochemistry and Photobiology*, 83(5):1056–62, 2007. ISSN 0031-8655. 102

[61] K K H Wang, W J Cottrell, S Mitra, A R Oseroff, and T H Foster. Simulations of measured photobleaching kinetics in human basal cell carcinomas suggest blood flow reductions during ala-pdt. *Lasers in Surgery and Medicine*, 41(9):686–96, November 2009. ISSN 1096-9101. 88, 100

[62] Y Wei, J Zhou, D Xing, and Q Chen. In vivo monitoring of singlet oxygen using delayed chemiluminescence during photodynamic therapy. *Journal of Biomedical Optics*, 12(1):014002, 2007. doi: 10.1117/1.2437151. URL `http://link.aip.org/link/?jbo/12/014002\&agg=MEDLINE_JBO`. 88, 99

[63] B C Wilson and M S Patterson. The physics, biophysics and technology of photodynamic therapy. *Physics in Medicine and Biology*, 53(9):R61–109, May 2008. ISSN 0031-9155. 99

[64] B C Wilson, M S Patterson, and L Lilge. Implicit and explicit dosimetry in photodynamic therapy: a new paradigm. *Lasers in Medical Science*, 12(3):182–199, June 1997. doi: 10.1007/BF02765099. 88

Part III

Clinical Imaging of the Protoporphyrin IX Steady-State Fluorescence Intensity to Optimize the Treatment of Actinic Keratosis by Photodynamic Therapy

8

Introduction

8.1 A Brief Overview on Actinic Keratosis

Actinic keratosis (AK) is the name of a pathological condition of the skin, where hyperproliferation of the keratinocytes, the cells present in the epidermis (the outermost skin layer), occurs, usually caused or stimulated by daylight. AK is the most common skin condition treated by dermatologists. The skin lesions are clinically identified as rough, scaly, crusted, pink to reddishbrown papules. They are found on sun-exposed skin, especially on the head, neck, forearms, and hands. The patients at greatest risk are middle-aged and elderly men, with fair skin and blue eyes, especially those with occupations involving prolonged exposure to UV, such as farmers, sailors, and construction workers [65].

The account that follows is based on the cited literature, and aims to give a brief overview on the epidemiology, prevalence, and available therapies for treating this condition. The incidence of AK is especially large in populations characterized by skin types I or II, on the Fitzpatrick skin type scale. In a study performed in Australia, Quaedvlieg et al. [45] reported that between 40% and 50% of the population over 40 years, was affected by AK. Similar studies conducted in the UK and in the USA, reported prevalence rates ranging from 20% to 25% of the population over 60 years [11, 47]. Considerable efforts and means are provided for its treatment. Thus it has been estimated that the annual costs (data from 2004) generated by this condition were of the order of $1 billion in the USA [1].

AK is clinically described as a non-severe cutaneous malignancy and, indeed, AK lesions are characterized by substantial spontaneous remission (55% after 1 year and 70% after 5-year follow-up [10]), and a low evolution rate to the more severe and potentially metastatic

squamous cell carcinoma (SCC: 0.60% at 1 year and 2.57% at 4 years [10]). AK is also notable for its slow evolution. Three main reasons justify the treatment of AK. The first - and most important - one resides in the difficulty to distinguish those AK lesions which will eventually evolve into the dangerous SCC, from the ones that will spontaneously disappear. Secondly, AK lesions are treated to provide relief for frequent symptoms, such as tenderness or itching. Finally, treatment may also be desirable for aesthetic, or cosmetic reasons.

Several effective treatments are available to heal AK sufferers, even though, it is worth reminding that, for this conditions, the best treatment is prevention (sun screen, sun hat). Curettage, cryosurgery and topical treatments such as application of 5-fluorouracil and photodynamic therapy (PDT) are the most common treatments [12, 43]. Curettage is effective for almost all clinical types of AK, but this approach has potential complications such as scarring and infection, and local anesthesia is frequently required before the procedure. Cryosurgery is generally well tolerated, presenting, in certain cases, only transitory hypopigmentation. This treatment is, however, limited to patients with only a small number of tiny, localized lesions. The topical application of 5-fluorouracil has a high success rate, but generally not well tolerated . It is also characterized by prolonged erythema in the treated zones. Finally, the topical treatment by PDT is well tolerated and presents excellent cosmetic outcome.

8.2 Treatment of Actinic Keratosis by Photodynamic Therapy

Photodynamic therapy (PDT) is a minimally invasive treatment modality, used in a number of diverse conditions, which allows, in many cases, the selective and highly localized destruction of abnormal cells. The use of PDT for treating AK is relatively recent [43, 44]. Compared to the classical treatment modalities for AK, mentioned previously, PDT offers interesting specific advantages, but also suffers from certain drawbacks, such as a relatively high cost, and the pain experienced during skin irradiation, which needs to be properly managed by the clinician.

A PDT treatment requires the administration of a auxiliary, photoactive product to the patient: the photosensitizer (PS). In dermatology, the PS of choice is Protoporphyrin IX (PpIX) and the PDT procedure relies on the administration of a *precursor* of this PpIX, namely 5-aminolevulinic acid (ALA). The ALA molecule is relatively small and penetrates easily into the skin tissue, where it stimulates the endogenous production of the PpIX (see §2.4.1).

In the case of AK lesions, this topical administration modality is very convenient, as the ALA molecule has just to diffuse and penetrate $\approx 100\,\mu m$ from the skin surface [20] to reach

the hyperplastic and dysplastic cells, where it induces the production of PpIX. Recently, new PpIX precursors, derived from ALA, have been synthesized, such as 5-ALA methyl ester (MAL, Metvix®) and 5-ALA hexyl ester (HAL, Hexvix®), which were developed to improve lesion targetting and reduce the drug-light interval [2, 13, 34, 37, 50].

To further improve the homogeneity of the distribution of the biosynthesized PpIX, it is also of common practice to apply a gentle curettage to carefully scrape out the lesion's scales and crust typical of this condition. The complete treatment is minimally invasive, without the need of any surgical preparation (debunking) prior to PDT illumination. The locally biosynthesized PpIX is activated by illuminating the topically ALA-treated skin with simple, inexpensive and non-coherent lamps like light emitting diodes (LED) arrays. While combining ALA administration with *red* light illumination, allows to treat non-melanoma skin cancers down to a depth of $2\,mm$ [13, 34, 41], in the US, AK lesions are commonly treated with blue light ($405\,nm$), which actually penetrates efficiently only up to $200 - 300\,\mu m$ in the skin. [30, 42, 43, 55, 56].

PDT has proved to be an efficient treatment modality for AK and is also characterized by excellent cosmetic outcome. Several studies reported a clearance rates varying from 68% to 89% after a single treatment, with follow-ups of up to 12 months [17, 27, 36, 41, 42, 55]. Despite these encouraging results, the technique still suffers from lesion recurrences and heterogeneous clinical outcome. This may be due to the fact that the efficacy of PDT depends on a several parameters, including the PS's microscopic and macroscopic distribution at treatment time, the light dose, the tissular oxygen distribution, the irradiance and the tissue's optical properties at the treatment wavelength. Therefore, it turns out to be difficult to ensure that optimal values (of all these measurable parameters) are applied during each individual treatment [46].

Different strategies were developed to study and monitor the dosimetry of PDT [6, 24, 32, 40, 64, 66], but none of them is currently in routine or systematic use. In fact, the parameters involved in the cascade of reactions leading to PDT effect may vary dynamically and interdependently during the treatment. Moreover, sophisticated technologies and challenging measurement modalities are not well accepted in the clinical field, which explains the limited use of these strategies (*e.g.* PDT dose monitoring by measuring the $^1O_2$ luminescence intensity [40]). In the case of AK, the lesions being confined to the epidermis, simple treatment monitoring techniques could be sufficient to enhance the treatment protocol and improve the clinical outcome. Moreover, given the superficial location of these AK lesions, heterogeneous distribution of oxygen in the tissue might not be a crucial problem, as several studies have

shown that oxygen efficiently diffuses in the skin to a depth of $0.4\,mm$ [54]. We can thus assume that, in the epidermis, oxygen is abundantly supplied by the atmosphere and, that, during PDT illumination, its concentration (or equivalently, the pO_2) in these superficial layers of the skin will not be significantly reduced. As a consequence, measuring the oxygen consumption, as we did in Part II of this thesis, would not help to individialize the PDT light dose. In contrast, measuring *the photosensitizer's photobleaching* (*i.e.* the reduction in the fluorescence intensity of PpIX, caused by the PDT irradiation) may be a useful way to evaluate - and adjust - the administration of the PDT light dose [4, 14, 16, 21, 49].

8.3 Objectives of the Actinic Keratosis Clinical Study

The objective of this study, performed in cooperation with the HUG (Hôpitaux universitaires de Genève), was to determine if the PDT clinical outcome, and the pain induced during the treatment of AK, were correlated with the PpIX's fluorescence intensity, as measured before and after irradiation. As a consequence, our study could also provide useful information, to determine if the PDT light dose, used in the treatment of AK, might be individually adjusted, on the basis of a simple, optical monitoring strategy, which could possibly also help to predict the treatment's outcome.

To reach these goals, a new imaging device was designed and adapted, with convenience and ergonomy in mind, to the measurement of the lesion's fluorescence, in a clinical environment. We aimed, during the design phase, to build a system, which could eventually become a standard tool for quantitative measurements of the skin fluorescence and reflectance. Our imaging system was designed for a standard observation of the skin under white light illumination, to enable the comparison of macroscopic aspects, such as skin roughness, pigmentation, and extent of the lesions, with the recorded fluorescence pattern.

9

Materials and Methods

9.1 Study Design

This clinical study was designed in collaboration with the Hôpitaux Universitaires de Genève (HUG) in order to study the PDT treatment of AK lesions. In more detail this study aimed at quantitatively recording and correlating the PS's fluorescence and the PDT induced PS's photobleaching with: patient's age, roughness of the lesion's surface, incubation period, pain experienced during the treatment, and eventually the clinical outcome. In our case the PS was PpIX induced by topical ALA-methylester (MAL) administration.

From September 2009 to January 2010, a total of 25 patients ($\mu_{age} = 72 \pm 11$ *years*, 77 AK lesions) were included in the study and treated by PDT. The treatment outcome was evaluated at three different times, scheduled at 1-2, 6-7, and 12 months after the PDT session. All the patients included in this study were specifically informed about the clinical procedure (including the additional measurements) and gave oral informed consent. During the entire clinical study a single and experienced MD (Dr Behrooz Kasraee, here shortened with BK), was in charge of the patient enrollment and PDT treatment. Therefore, all the gathered measurements were less affected by subjective differences in lesion preparation, in lesions roughness judgment, and differences in the handling of the specific PDT and monitoring devices.

9.2 Patient Management

9.2.1 Lesion Identification

Each AK lesion was identified by BK by feeling the roughness of the lesion surface with the index finger. The lesions were than graded in a scale from 1 to 3, where 1 imply a barely detectable difference with respect to normal skin. Subsequently BK, demarcated the lesion borders by following the roughness threshold grade 1, with a green permanent marker (Steadler® Lumocolor-M). Therefore, the determination of the roughness and the border of each lesion, allowed to study the influence of the latter over the intensity of the PpIX fluorescence measured before PDT illumination.

9.2.2 Lesion Preparation

Prior to MAL administration all the lesions were gently scrapped clean with a curette (Bruns® 17-003-0) in order to efficiently remove the stratum corneum and the hyperkeratotic tissue. This lesion preparation is a standard procedure [11, 22, 37, 43, 62] to facilitate the diffusion of the MAL cream into the lesion, and ensure an efficient PDT illumination. This procedure was not intended to be a therapeutic curettage, and generally no bleeding was observed (see Figure 9.1).

(a) A gentle curettage was performed before MAL administration

(b) No bleeding or very limited bleeding was observed after this procedure

Figure 9.1: To enhance the MAL cream penetration and to remove the scales and crusts that may interfere with the PDT illumination, the *stratum corneum* of the AK lesions was gently removed before MAL administration.

Successively, all AK lesions were precisely indexed in order to localize them even several months after the treatment. Additionally, the fluorescence imaging device's orientation and angle, with respect to the lesion, were precisely defined and kept constant for each fluorescence measurement. These rules of conduct had to be strictly defined since we aimed at comparing fluorescence intensities of the lesions at two different times during the procedure, namely just before and just after the PDT treatment. Due to the limited field of view ($\varnothing 40\,mm$, see §9.3.1) a precise positioning of the monitoring apparatus by the operator was required in order to allow repeatable observation of the lesion.

(a) Lesion bandage to shield the lesion from daylight during PpIX accumulation

(b) Anatomical sketch

Figure 9.2: MAL administration and documentation of all the information gathered during the lesion preparation procedure.

After this preliminary, and important, preparation procedure, a layer of $1\,mm$ of MAL cream , inducing the PpIX precursor, was administered over the entire surface of the lesion. The lesion was then covered with a non-occlusive (gauze plus aluminum foil) bandage to avoid the interaction between the parasitic daylight and the PpIX accumulated within the lesion (see Fiugre 9.2(a)). The tissular PpIX concentration will, in fact, increase during the 3h drug light interval (DLI), *e.g.* PpIX pharmacokinetic in Figure 7.5(b)). The patients were asked to wait for a DLI of $180\,min$ before being illuminated. Nevertheless, in order to study the influence of the drug-light interval on: (i) the clinical outcome, and (ii) the lesion fluorescence measured before the treatment, a subgroup of lesions were treated after only $60\,min$.

All the information gathered during this preparation phase (number of lesions, surface roughness, delimitation and the drug-light interval) were reported and documented on the

patient's anatomical sketch (see Figure 9.2(b)).

9.2.3 PDT Treatment and Pain Assessment

The PDT light dose was delivered with a standard red LED panel delivery device (Aktilite® CL128, $632 \pm 10\,nm$, [39]) providing an irradiance of $67\,mW/cm^2$. The irradiation time ($540\,s$, $36\,J/cm^2$) and the distance between the lesion and the LED panel ($\approx 5\,cm$) were kept constant. Moreover to further homogenize the illumination, each lesion was irradiated perpendicularly. Consequently, for patients presenting multiple lesions, each of them was illuminated separately.

PDT illumination session are frequently associated with a *moderate to severe* pain sensation. Actually, pain is the main adverse effect for this treatment modality. Therefore a painkiller (Méfénacide®, $500\,mg$) was given to each patient 1 *hour* before treatment [48, 58, 62, 63]. Additionally the lesions were sprayed with cold water (T≈5°C), during illumination, to further reduce the burning sensation. Even though the pain sensation was thus well managed, the protocol provided the possibility to interrupt the PDT illumination for breaks of 1-2 *min*, to give the patient time to recover.

The pain experienced by the patient was quantified with the help of a visual analog pain scale as reported by Johnson [29], Langley and Sheppeard [31]. On this scale, the pain feeling is classified from 1 to 10, see Table 9.1. For each lesion, the patients were asked to rank their pain feeling during the illumination between 1 and 10.

9.2.4 Evaluation of the Clinical Outcome

The clinical outcome was assessed by two physicians: Dr Behrooz Kasraee and Dr Denis Salomon. The latter was blinded to the initial diagnostic and to the treatment procedure. The two MDs were asked to rank the lesions' evolution in a scale from 1 to 5 (5 implied the complete clearance of the treated zone). For that purpose they compared the clinical wide field pictures taken before PDT and during the follow-up consultations. Successively the PDT efficacy for each lesion was computed by averaging the two MDs' evaluations.

No pain	0
Mild pain	1-2
Moderate pain	3-4
Severe pain	5-6
Very severe pain	7-8
Worst imaginable pain	9-10

Table 9.1: Visual analogical pain scale

9.3 Clinical Setup and Evaluation

9.3.1 Monitoring Apparatus

The monitoring system was designed to be simple and ergonomic, in order to be accepted in the clinical field. Figure 9.3 depicts the main parts of this monitoring system. A standard clinical photo camera ((1), Nikon®-D90 coupled with the objective Nikon® AF D 50 mm f/1.4) was used as fluorescence imaging sensor. A custom illumination apparatus was developed to excite the inspected lesions with a constant and homogeneous illumination. A stable and spatially homogeneous excitation is in fact important to record quantitative fluorescence images. The custom illumination apparatus was mainly composed of 4 functional components: the emission filter (2), the excitation diodes (3), the excitation homogenizing tube (4), and the fluorescence reference ring (5).

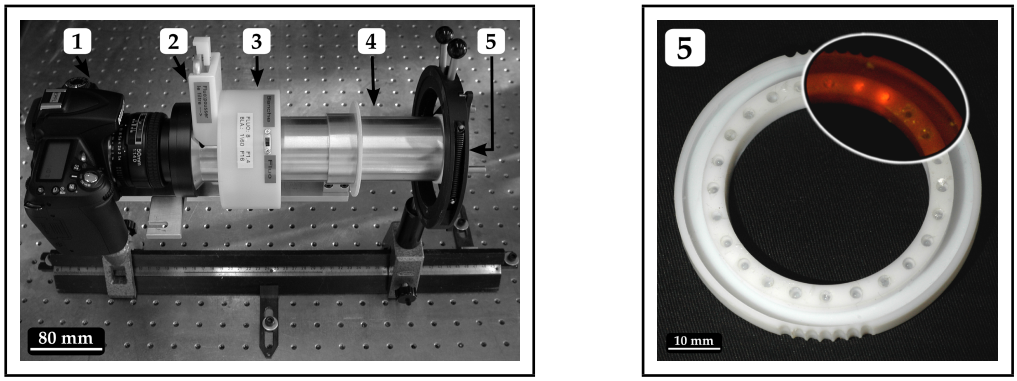

(a) Clinical monitoring apparatus (b) Fluorescence reference ring

Figure 9.3: (a) Fluorescence monitoring apparatus: (1) Standard photo camera Nikon®-D90, (2) Emission filter, (3) Excitation diodes, (4) Excitation homogenizing tube. b) Zoom picture over the reference ring (5): The fluorescence image of the reference spot is showed in the up-right corner of the right image; Ex. 405 nm, filtered by a Kodak® Wratten filter n°9, LP460

The emission filter stage (2) involves simply a long pass filter (Kodak® Wratten filter n° 9, see curve (A) in Figure 9.5) mounted on a sliding support to easily switch from conventional white light reflectance imaging to fluorescence imaging.

The diode excitation stage (3) was designed with two sets of 5 diodes placed radially along the circumference of the excitation tube. The first set emits a broad white light emission (superbrightled® RL5-W6030, 400-660 nm) to record conventional white light reflectance images. The second emits a narrow blue band light (superbrightled® RL5-UV2030, see curve (Ex)

in Figure 9.5) to efficiently excite the PpIX accumulated within the lesion and thus record fluorescence images. This stage was alimented by a commercially available power supply ($24\,V$ DC, $20\,\mu A$). With the help of a switch, it was possible to select between the two illumination modes. An excitation filter (Edmund® NT52-530, see curve (B) in Figure 9.5) had to be placed in front of the blue diodes to reject the parasitic fluorescence of the printed circuit board (PCB) where the diodes where mounted.

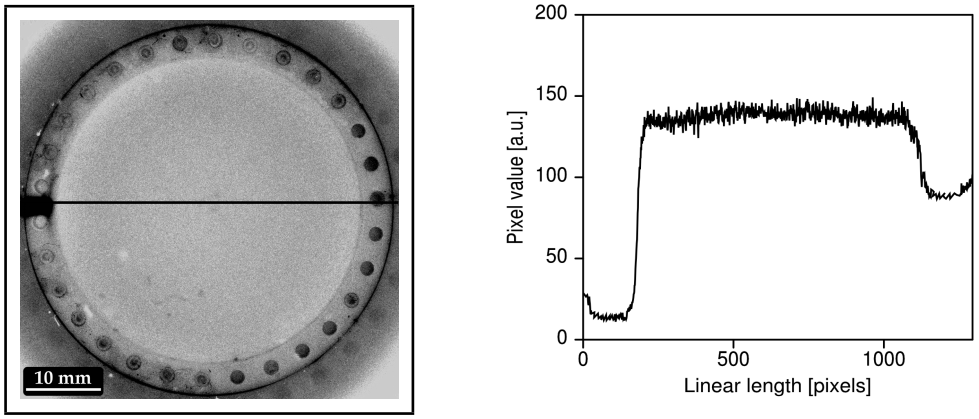

(a) Reflectance image from the white reflecting coating

(b) Reflectance profile

Figure 9.4: Spatial excitation profile measured by recording the reflectance of a white reflecting coating following the excitation with the blue diodes.

The homogenizing tube (4) is an aluminum tube having an highly diffusing coating (Delrin®) on its internal surface. The length was optimized to obtain a compact ($450\,mm$) and light weight (total weight $\approx 1.7\,kg$) system. This system delivers a flat excitation profile over the entire focal plane. Indeed, Figure 9.4 depicts the illumination profile. This non-filtered reflectance image was acquired on a non-fluorescing white reflecting coating (SphereOptics Hoffman® SRM-99H) with blue diode excitation. This measurement illustrate the homogeneity of the excitation profile over the entire field of view.

The fluorescence reference ring (5) was designed to be fastened to the distal end of the homogenizing tube (see Figure 9.3(b)). These stable fluorescent spots localized in the image focal plane allow the normalization of the fluorescence of the inspected lesions. These spots contain stable fluorescing pigments (Lentalux®) embedded in epoxy resin. Their emission spectrum is depicted in Figure 9.5. Pits located around the ring were filled with increasing concentrations of this mixture.

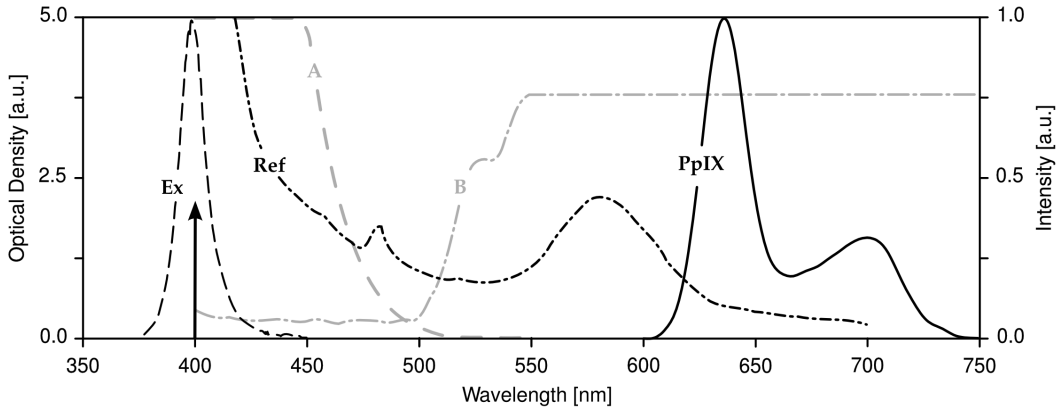

Figure 9.5: Spectral characterization of the optical elements of the fluorescence excitation apparatus. Black lines define the emission spectra normalized to unity, (Ex) is blue diode excitation, (Ref) emission of the fluorescence reference dots, (PpIX) is the emission of the PS. Gray lines indicate the optical densities of the two filters used: (A) emission filter to reject the excitation, (B) Excitation filter to reject the parasitic luminescence of the printed circuit board

9.3.2 Image Processing

The fluorescence images were analyzed with a standard image processing software (ImageJ® version 1.41). Figure 9.6 depict the analysis areas. With the help of simple and basic operations a region of interest (ROI) was selected by following the lesion borders (L). The mean fluorescence intensity of the lesion was computed in the ROI and simultaneously the total lesion surface was evaluated. Similarly, two circular control areas were defined to account for intensity variations. The first area contained the reference fluorescing spot (Ref), and the second contained a lesion free portion of the field (Ctrl). In order, to compare the results coming from different images, the fluorescence intensities of the lesion and the of control zone were first normalized by the mean fluorescence intensity of the reference spot. Eventually the lesion's fluorescence bleaching (B_{PS}) was calculated by subtracting the normalized fluorescence measured after PDT (F_A) from to one measured before PDT (F_B), see Equations 9.1. Note that the tissue autofluorescence (T_{Auto}) was shown to remain constant even after PDT irradiation (data not shown). The PpIX contribution to the recorded fluorescence signal before and after irradiation is symbolized respectively by F_{PS} and F'_{PS} and the stable fluorescence intensity of the reference spot by F_{Ref} (Note that in Equation 9.1 the excitation is considered constant, thus F_{Ref} also remains constant).

$$
\begin{aligned}
F_B &= (F_{PS} + \mathrm{T}_{Auto})/F_{Ref} \\
F_A &= (F'_{PS} + \mathrm{T}_{Auto})/F_{Ref} \\
B_{PS} &= F_B - FA = (F_{PS} - F'_{PS})/F_{Ref}
\end{aligned}
\tag{9.1}
$$

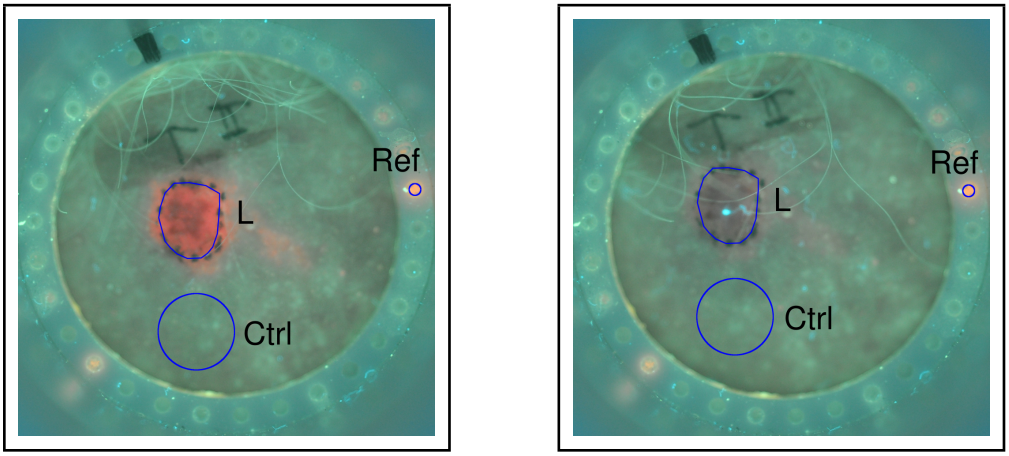

(a) Fluorescence intensity shortly before PDT (b) Fluorescence intensity just after PDT

Figure 9.6: Fluorescence images of the PpIX accumulated within actinic keratosis lesions recorded just before and just after the PDT session (Ex. 400 nm, Em. LP460, see Figure 9.5 for details). MAL was administered 180 min before illumination, (Ctrl) Control zone, (Ref) fluorescence reference spot, (L) Lesion.

10

Results

In the present study, the normalized fluorescence intensity measured before PDT illumination (F_B), the fluorescence photobleaching (B_{PS}), and other clinical parameters were monitored during the PDT of 77 lesions, 26 patients. The lesions were subdivided in three different groups as a function of the drug-light interval: 46 lesions were treated 180 min after MAL application, 20 lesions after a period ranging from 90 to 140 min, and 11 lesions after 60 min. In the original protocol, only two incubation periods (60, 180 min) were foreseen. The third incubation period (90-140 min) was imposed upon us by the management of the timing sequences in the clinical environment. Note that the time precision in the incubation periods is effectively $\approx \pm 15\, min$.

During the first two follow-up consultations, in total, only 13 patients (37 lesions) were controlled. For the last scheduled follow-up consultation (12 months after the treatment), which will fall between September 2010 and January 2011, all the patients have been formally convened. Consequently in that case a much higher participation is expected (see details in §10.2 and §11).

In the following paragraphs we will present the study results by first considering the parameters that may influence or may be influenced by F_B. Successively the PDT treatment outcome is evaluated as a function of F_B and B_{PS}.

10.1 Fluorescence Intensity Related Parameters

10.1.1 Incubation Period

We consider here the fluorescence intensity (F_B) of the lesions treated with an incubation period of 60 *min* (n=11) and 180 *min* (n=46). The fluorescence intensity of the lesions characterized by an incubation period ranging from 90 to 140 *min* are not considered here.

The results show a statistically significant difference of the fluorescence intensity measured 60 *min* and 180 *min* after MAL administration (see Figure 10.1). These differences confirm that the drug-light interval is a crucial parameter regarding the fluorescence build-up in the lesion. In order to asses whether a shorter incubation time (60 *min* vs 180 *min*) would reach the same clinical performance, in section 10.2 we will study the relationship between fluorescence intensity and clinical outcome.

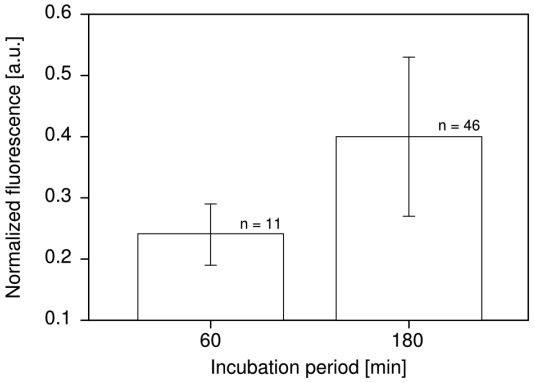

Figure 10.1: Normalized fluorescence intensity measured before PDT illumination (F_B) and after an incubation time of 60 and 180 *min*. (T-test = 6.58, degree of freedom = 40, $p < 0.05$).

10.1.2 Lesion Roughness and Patient Age

To study of the influence of the lesion roughness and of the patient age, on the PpIX fluorescence signal (F_B), we have considered only the lesions administered 180 *min* before PDT (n=46). To emphasize the influence of lesion roughness we subdivided them in the three subgroup depending on their roughness grade, see §9.2.1 for details. In the considered cohort, 16 lesions were characterized by a roughness grade of 1, 16 by a grade of 2, and 14 by a grade of 3. The influence of the patient age was studied by analyzing the fluorescence signal (F_B) as a function of the age of each patient in the running year (2010).

No correlation with the fluorescence intensity was observed (see Figure 10.2) neither for the lesion surface roughness nor for the patient age, suggesting that those two parameters are not relevant for the tissular production of PpIX.

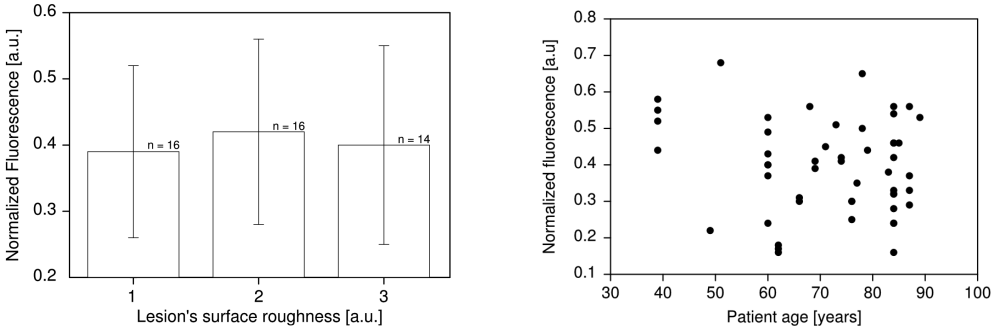

(a) Normalized fluorescence and roughness

(b) Normalized fluorescence and patients' age

Figure 10.2: Normalized fluorescence intensity measured before treatment (F_B) as a function of lesion's surface roughness and patient's age (incubation period 180 *min*).

10.1.3 Pain

To study the relationship between the pain, experienced and evaluated by the patient, and the fluorescence signal F_B all the treated lesions were considered independently from all other clinical parameters (n=77). Figure 10.3(a) shows the pain experienced during the PDT illumination as a function of the fluorescence signal measured just before illumination (F_B). Figure 10.3(b) plots the pain, but this time in function of the fluorescence signal normalized by the lesion surface, see §9.3.2 for more details. Note that the number of lesions characterized by the same pain grade is mentioned, in round brackets, on the right hand part of the plots.

Even though the number of lesions is not sufficient to conclude on this topic the results shows the absence of correlation (see Figure 10.3). This is probably tied to some extent to strong patient subjectivity in pain evaluation and also probably to other uncontrolled parameters, *e.g.* differences in the physiology or lesions innervation. Neveretheless by analysing the distribution of the experienced pain, we confirm that PDT is associated with a moderate to severe pain feeling. In fact, 60% of the treated lesions were graded with a pain feeling on the scale smaller than 5 (mild to moderate pain), and almost all the lesions (85%) were graded below 7 (see Table 9.1).

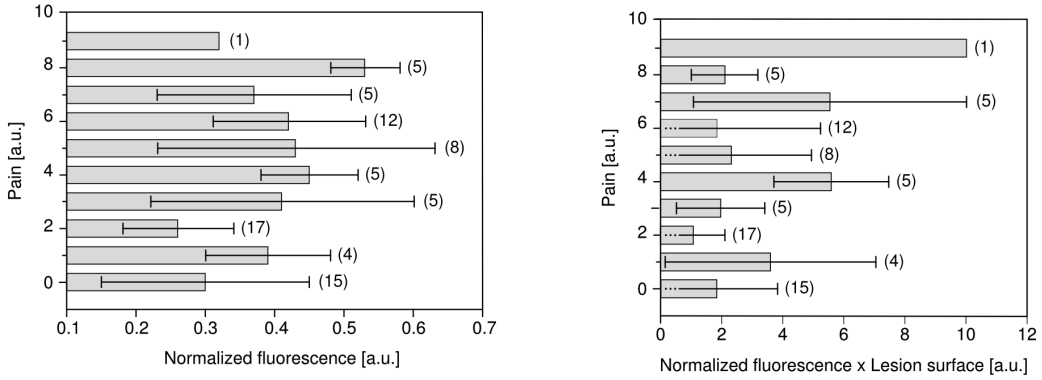

(a) Pain as a function of the normalized fluorescence

(b) Pain as a function of the normalized fluorescence × lesion surface

Figure 10.3: Pain experienced by the patient during PDT irradiation as a function of the fluorescence intensity measured before treatment (F_B)

10.1.4 Fluorescence Photobleaching

The measured normalized fluorescence (F_B) was correlated with the calculated photobleaching (B_{PS}) following PDT (see Equation 9.1). All the treated lesions (n=77), independently of the precursor incubation period and of all other possible parameters, were considered for this analysis. The results shows a strong linear correlation (see Figure 9.5), suggesting that the PpIX's fluorescence measured with our system is independently of the drug light interval and equally photobleached during all the PDT sessions. The PpIX molecules accumulated in the epidermis may indeed interact efficiently with the illumination light and the tissue oxygen which in part diffuses from the atmosphere, so that an efficient fluorescence photobleaching occurs. Nevertheless, by analyzing in more detail as shown in Figure 10.4 we can easily appreciate that the linear regression has roughly a slope of 1, but in the same time we see that the regression line is affected by an offset of ≈ 0.1. This possibly suggests the existence of an unbleachable part of the accumulated PpIX or, alternatively, the presence of unbleachable photoproducts (see §11 for details).

10.2 Clinical Outcome

During the first two follow-up consultations 13 patients (37 lesions) were controlled. Eleven patients (27 lesions) attended the first consultation (1-2 months), and only 8 patients (28

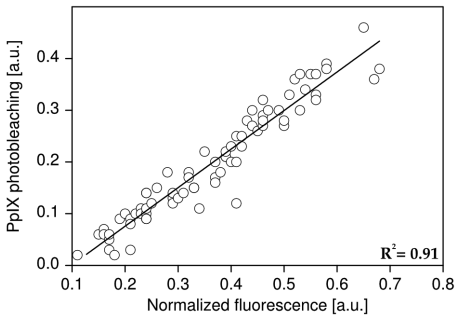

Figure 10.4: PpIX fluorescence photobleaching (B_{PS}) in function of the normalized fluorescence measured before treatment (F_B)

lesions) attend the second consultation 6-7 months after the PDT treatment. Eventually only 6 patients (18 lesions) have complete file record (*i.e.* they attend both follow-up consultations).

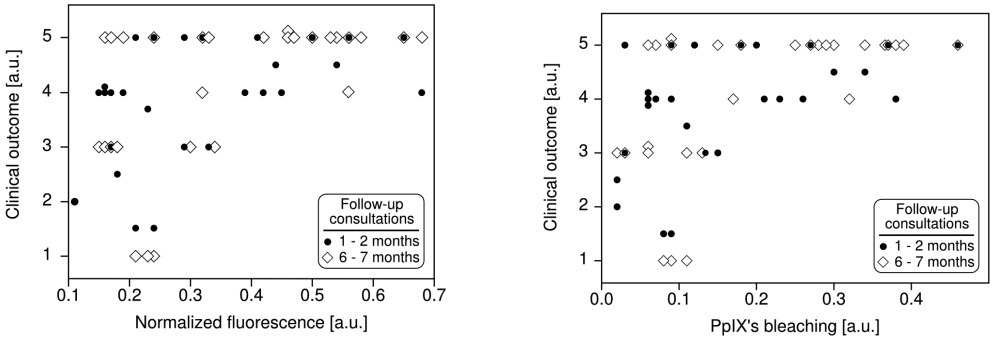

(a) Clinical outcome as a function of the normalized fluorescence measured before illumination (F_B)

(b) Clinical outcome as a function of PpIX's photobleaching (B_{PS})

Figure 10.5: Clinical outcome of AK lesions treated by MAL-PDT and controlled at 1-2 months (•) and at 6-7 months (◇) after the PDT session

In Figure 10.5 the clinical outcome of all the 37 lesions controlled during the first two follow-up consultations are plotted as a function of the PpIX fluorescence measured before treatment (F_B, see Figure 10.5(a)), and respectively in function of the PpIX photobleaching (B_{PS}, see Figure 10.5(b)). The symbols (•) refer to the clinical outcomes assessed during the first consultation (1-2 months), (◇) to the ones evaluated 6-7 months after PDT treatment. Note that if two symbols gave the same clinical outcome a small vertical shift was applied in order to distinguish all the different data points.

For the 18 lesions with a complete file record, we can follow the evolution of the clinical

outcome by looking at the graphs of Figure 10.5 along vertical lines. In fact, if a lesion was controlled during both follow-up consultations the two symbols (•,◇) are aligned along the vertical axis or even superimposed. Nevertheless to simplify the analysis of the clinical outcome evolution from the first (1-2 months) to the second (6-7 months) control consultation the respective clinical outcome is plotted in Figure 10.6.

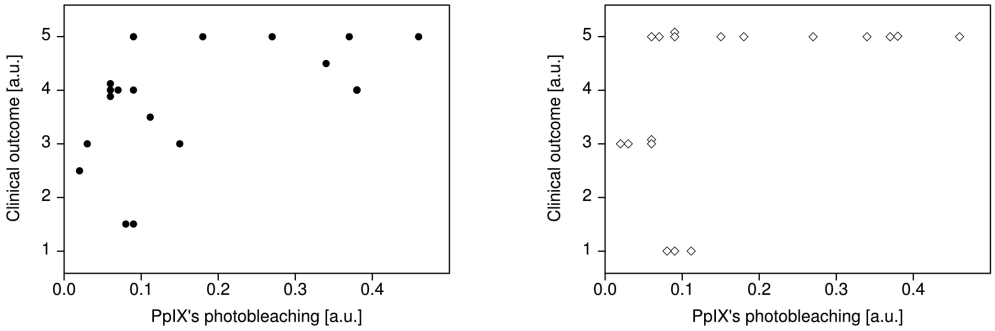

(a) First follow-up consultation after 1-2 months from PDT

(b) Second follow-up consultation after 6-7 months from PDT

Figure 10.6: Clinical outcome evolution, of AK lesions treated by MAL-PDT, from 1-2 months (•) to 6-7 months (◇) after the PDT session

Despite the fact that the final clinical outcome is missing at this point in time (evaluation at 1 year after the PDT treatment), the present results show that the use of either the normalized fluorescence, or the amount of photobleaching are valuable parameters to predict the clinical outcome. In addition by looking at Figure 10.6, the clinical outcome seems to stabilize itself at the higher and hence better clinical outcomes.

11

Discussion

Studying the correlation between the PpIX fluorescence intensity and/or its photobleaching during PDT of AKs with the clinical outcome is an interesting and important topic. Surprisingly, to our knowledge [16, 19], only a very limited number of publications have addressed this issue in detail. Our study demonstrats that this correlation, although not perfect, does exist as long as relatively short follow up times (7 months) are considered. It should be noted that to conclude over the evolution of the clinical outcome the last follow-up consultation needs to be accomplished, thus the final degree of correlation will be determined after the end of this thesis. The PpIX fluorescence intensity was measured before and after PDT with an imaging device developed in our laboratory. Although this device provides, in our conditions, reproducible, background free and linear (data non shown) values of PpIX fluorescence, some of its features can still be improved for a more convenient and routine use in clinic. The irradiance of the excitation light should and will be increased, typically by one order of magnitude, to reduce the time that necessary to record the fluorescence images with an acceptable signal to noise ratio. Such a modification will not significantly increase the PpIX photobleaching since the fluorescence acquisition time will be reduced accordingly.

By analyzing the recorded images and the plots reporting the fluorescence intensity, we show that important intra- and inter- patient variations affect these measurements. These variations are probably due to parameters influencing the PpIX accumulation as reported by Dögnitz et al. [13], such as the precursor diffusion rate, the lesion's temperature, temporal and spatial variations of the metabolic activity, and differences in the density of active cells. Moreover, as was speculated by Wiegell et al. [62], the tissular PpIX content may be influenced by anatomical and regional differences in the skin's aptitudes to accumulate PpIX. Unfortunately, the limited

number of patients involved in the present study does not enable us to subdivide the treated lesions according to their anatomical subgroups.

The precursor's (Metvix®) incubation period, or the drug-light interval necessary to allow the biosynthesis of the photosensitizer (PpIX), is a parameter of major interest especially in the clinical field where optimal time management is becoming more and more important. Statistical relevant differences were observed between the fluorescence intensities measured after 60 *min* or 180 *min* of the precursor incubation time. This results is supported by several publications reporting the fluorescence pharmacokinetics of PpIX in various tissues including the skin [8, 26, 35, 57, 59]. In addition, similar results were observed by several groups active in the development of PDT based therapy to treat AK [17, 18]. This is consistent with the fact that the PpIX concentration within the lesions is directly related to the treatment efficacy [2, 13, 18, 52]. Therefore, to reach a sufficient accumulation of PpIX in the lesions, the AK treatment guidelines recommend a precursor's incubation period of at least 180 *min* or, alternatively, an incubation period of 180 *min* or shorter, but under occlusive bandage [38, 41, 42]. These guidelines are actually supported by our preliminary clinical results suggesting that a non occlusive incubation of only 60 *min* is not sufficient to reach satisfactory accumulation of PpIX and, consequently, to have good clinical results.

However, it should be noted that, although the results presented in Figure 10.1 are statistically relevant to support this statement regarding the PpIX fluorescence, more patients should be treated with an incubation time of 60 *min* to corroborate this statement.

We also studied the influence of the patient's age and of the AK lesion's roughness on the PpIX fluorescence intensity. As reported in the literature, we observed that the patient age is not a parameter that significantly influences the biosynthesis of PpIX [2, 33]. This conclusion is somewhat surprising since we were expecting an impact of the skin aging on the precursor penetration and on the metabolic activities that play a role in the PpIX build-up. Similarly, no correlation was observed between the roughness of the lesion surface and the PpIX fluorescence intensity. To our knowledge no one tried to look for a correlation with these two parameters. However the work of Wiegell et al. [61] demonstrated a positive correlation between the measured AK-PpIX fluorescence and the lesion's redness and inflammation. Even though the rational that brought Wiegell et al. [61] to study this correlation is somewhat similar to ours, the results can not compared. Indeed the concepts of redness and inflammation are not or very poorly correlated with the concept of "roughness", as far as AK's are concerned. Similarly,

Smits et al. [51] reported that there was a positive correlation between the PpIX fluorescence intensity and the "severity" of AK's. According to the classification proposed by Anwar et al. [3], Cockerell and Wharton [7], Yantsos et al. [65], the grade of AKs is closely related to the proliferation of atypical keratinocytes involving different percentages of the epidermis (*i.e.* the grading is tightly related to the amount of dysplastic and hyperplastic cells within the lesion). As a consequence, the absence of correlation we have observed between the PpIX fluorescence and the lesion roughness indicates that this features is also not correlated with the "severity" grading.

In the present study we also failed to demonstrate a correlation between the pain experienced by the patient during the PDT and the normalized fluorescence intensity. Although several groups have extensively studied the pain sensation during the PDT illumination, no clear agreement has been found up to now regarding this correlation. Some studies demonstrated a statistically significant correlation [9, 62, 63], whereas others, as it is our case, did not observed a clear correlation [25, 61]. This discrepancy is probably due, at least in part, to the difficulty of measuring and documenting the sensation of pain. Pain is a difficult parameter to study because it is subject to large intra- and inter- patient variations. In fact, pain assessment is strongly affected by subjective and emotional aspects that depend on the patient's earlier experiences of pain, and on the degree of anxiety of the patient during treatment [25, 28, 29, 60]. It should be noted that the heterogeneity of the AK lesions is very likely to be the most important factor playing a role in this discrepancy. In fact, in general, the PpIX fluorescence and the pain seems to be correlated in normal tissue and early AKs, whereas this correlation no longer exist for more advanced lesions [5, 63]. Therefore, even this correlation would exist in all tissue types, the fluctuation associated with the AK lesions heterogeneity may be to important to reveal to reveal with the limited number of cases studied at present. As already mentioned, the lesions could not be adequately subdivided in different anatomical zones in the present study due to the small cohort considered. This may also degrade the correlation between the PpIX fluorescence and the pain since it has been reported that anatomical innervation differences may play an important role [23, 48].

Nevertheless, Wiegell et al. [62] claimed that no pain difference was observed between different anatomical zones after correction by the fluorescence intensity measured in these zones. This study concluded that differences in pain score found between different parts of the

body are probably due to varying ability of the skin to accumulate PpIX, more than differences in innervation of the skin.

The strong linear correlation presented in Figure 10.4 between the PpIX's photobleaching and the normalized fluorescence before PDT is an expected, but interesting result. The correlation, with a slope of 1, is in agreement with several studies reporting that, in well oxygenated conditions, the PpIX and the PpIX's photoproducts can be efficiently and completely bleached during the illumination [14, 15, 46, 49, 53]. In fact, in our situation the oxygen depletion induced by the PDT illumination is probably not so large as to limit the PDT effect and the PpIX photobleaching. It is also worth while to note that this correlation is observed for all the treated lesions, independently of the anatomical place and independently of all other possible tissue parameters. In addition, the limited deviation from the regression line ($R^2 = 0.91$) further supports the possibility to use the fluorescence intensity, measured before treatment, as a surrogate of the PpIX photobleaching following PDT. Finally it should be noted that the intercept of this regression line with the Y axis appears to be not exactely at $(0, 0)$, but near $(0.1, 0)$. Since all backgrounds and offsets have been corrected for, as described in §9.3.2, this suggest that a "non-photobleachable" fraction of the fluorochrome might be present in the skin. This interesting conclusion deserved further studies to clearly determine if this effect is due to the localization of PpIX in different tissue compartments and/or to the luminescence of different fluorochromes.

Finally, when the clinical outcome is evaluated 1-2 months and 6-7 months following PDT, an high levels of fluorescence intensity, or PpIX photobleaching, corresponded to a more potent therapeutic effect. These encouraging results are supported by other publications that report on correlations between the photobleaching and clinical outcome [4, 16, 19, 49]. However it should be noted that most of these studies reported that the fluorescence photobleaching and not the fluorescence intensity, is well correlated with the clinical outcome. This discrepancy could be explained by the fact that these groups used either "point" measurements, instead of imaging measurements and/or because they measured the fluorescence qualitatively instead of using a scientific camera presenting a linear response, as was the case in our study. With this imaging system, it appears that a PpIX fluorescence intensity of 0.4, and a PpIX fluorescence photobleaching above 0.3, will lead to a positive clinical outcome for both the 1-2 months and 6-7 months follow-ups. Moreover by looking the results presented in Figure 10.1 they suggests that a Metvix® incubation time of 60 *min* is not sufficient to successfully treat AK by PDT.

Actually, it is worth while noting that only 13 patients, out of 25 treated, attended the follow-up consultations. The scanty participation was tied to an organizational problem and also to the fact that the studied cohort was composed by an elderly population ($\mu_{age} = 72 \pm 11$ *years*). Therefore several patients refused to attend the scheduled follow-up visit, probably considering that it was not necessary. Moreover, 3 among the treated patients died in the period between the PDT treatment and follow-up visits.

In conclusion, we can claim that, in the case of AK treated with Metvix®, the fluorescence measured before PDT and the PpIX fluorescence photobleaching are both well and linearly correlated with clinical outcome. In addition a statistically relevant difference of the fluorescence intensity is observed when the incubation time varies from 60 to 180 *min*. Finally these preliminary clinical results support that a satisfactory clinical outcome can only be reached if the PpIX fluorescence intensity or the PpIX fluorescence photobleaching are above a certain threshold. However, surprisingly no correlation was observed in the present study between the pain and the PpIX fluorescence measured before treatment, as well as between this last parameter and the lesion roughness and the patient's age.

References

[1] A B Ackerman and J M Mones. Solar (actinic) keratosis is squamous cell carcinoma. *Br J Dermatol*, 155(1):9–22, July 2006. ISSN 0007-0963. 111

[2] E Angell-Petersen, R Sørensen, T Warloe, A M Soler, J Moan, Q Peng, and K E Giercksky. Porphyrin formation in actinic keratosis and basal cell carcinoma after topical application of methyl 5-aminolevulinate. *J Invest Dermatol*, 126(2):265–71, February 2006. ISSN 0022-202X. 113, 130

[3] J Anwar, D A Wrone, A Kimyai-Asadi, and M Alam. The development of actinic keratosis into invasive squamous cell carcinoma: evidence and evolving classification schemes. *Clin Dermatol*, 22(3):189–96, 2004. ISSN 0738-081X. 131

[4] M Ascencio, P Collinet, M O Farine, and S Mordon. Protoporphyrin ix fluorescence photobleaching is a useful tool to predict the response of rat ovarian cancer following hexaminolevulinate photodynamic therapy. *Lasers Surg Med*, 40(5): 332–41, July 2008. ISSN 0196-8092. 114, 132

[5] J Barge, T Glanzmann, H van den Bergh, and G Wagnières. Correlation between ppix fluorescence and both tissular effects and pain induced by pdt on normal skin using fluorescence imaging. *IPA*, 2007. Abstract. 131

[6] D R Braichotte, J F Savary, P Monnier, and H E van den Bergh. Optimizing light dosimetry in photodynamic therapy of early stage carcinomas of the esophagus using fluorescence spectroscopy. *Lasers Surg Med*, 19(3):340–6, 1996. ISSN 0196-8092. 113

[7] C J Cockerell and J R Wharton. New histopathological classification of actinic keratosis (incipient intraepidermal squamous cell carcinoma). *J Drugs Dermatol*, 4(4):462–7, 2005. ISSN 1545-9616. 131

[8] I Cosserat-Gerardin, L Bezdetnaya, D Notter, C Vigneron, and F Guillemin. Biosynthesis and photodynamic efficacy of protoporphyrin ix (ppix) generated by 5-aminolevulinic acid (ala) or its hexylester (hala) in rat bladder carcinoma cells. *J Photochem Photobiol B*, 59(1-3):72–9, December 2000. ISSN 1011-1344. 130

[9] W J Cottrell, A D Paquette, K R Keymel, T H Foster, and A R Oseroff. Irradiance-dependent photobleaching and pain in delta-aminolevulinic acid-photodynamic therapy of superficial basal cell carcinomas. *Clinical Cancer Research : an Official Journal of the American Association for Cancer Research*, 14 (14):4475–83, 7 2008. doi: 10.1158/1078-0432.CCR-07-5199. 131

[10] V D Criscione, M A Weinstock, M F Naylor, C Luque, M J Eide, and S F Bingham and. Actinic keratoses: Natural history and risk of malignant transformation in the veterans affairs topical tretinoin chemoprevention trial. *Cancer*, 115(11): 2523–30, June 2009. ISSN 0008-543X. 111, 112

[11] D de Berker, J M McGregor, and B R Hughes and. Guidelines for the management of actinic keratoses. *Br J Dermatol*, 156 (2):222–30, February 2007. ISSN 0007-0963. 111, 116

[12] S M Dinehart. The treatment of actinic keratoses. *J Am Acad Dermatol*, 42(1 Pt 2):s25–s28, January 2000. ISSN 0190-9622. 112

[13] N Dögnitz, D Salomon, M Zellweger, J P Ballini, T Gabrecht, N Lange, H van den Bergh, and G Wagnières. Comparison of ala- and ala hexyl-ester-induced ppix depth distribution in human skin carcinoma. *J Photochem Photobiol B*, 93(3):140–8, December 2008. ISSN 1011-1344. 113, 129, 130

[14] J S Dysart and M S Patterson. Photobleaching kinetics, photoproduct formation, and dose estimation during ala induced ppix pdt of mll cells under well oxygenated and hypoxic conditions. *Photochem Photobiol Sci*, 5(1):73–81, January 2006. ISSN 1474-905X. 114, 132

[15] M B Ericson, S Grapengiesser, F Gudmundson, A-M Wennberg, O Larkö, J Moan, and A Rosén. A spectroscopic study of the photobleaching of protoporphyrin ix in solution. *Lasers Med Sci*, 18(1):56–62, 2003. ISSN 0268-8921. 132

[16] M B Ericson, C Sandberg, B Stenquist, F Gudmundson, M Karlsson, A-M Ros, A Rosén, O Larkö, A-M Wennberg, and I Rosdahl. Photodynamic therapy of actinic keratosis at varying fluence rates: assessment of photobleaching, pain and primary clinical outcome. *Br J Dermatol*, 151(6):1204–12, December 2004. ISSN 0007-0963. 114, 129, 132

[17] M B Ericson, A M Wennberg, and O Larkö. Review of photodynamic therapy in actinic keratosis and basal cell carcinoma. *Ther Clin Risk Manag*, 4(1):1–9, February 2008. ISSN 1176-6336. 113, 130

[18] J D Fauteck, G Ackermann, M Birkel, M Breuer, A C E Moor, A Ebeling, and C Ortland. Fluorescence characteristics and pharmacokinetic properties of a novel self-adhesive 5-ala patch for photodynamic therapy of actinic keratoses. *Arch Dermatol Res*, 300(2):53–60, February 2008. ISSN 1432-069X. 130

[19] M Fernández-Guarino, A Harto, M Sánchez-Ronco, B Pérez-García, A Marquet, and P Jaén. [retrospective, descriptive, observational study of treatment of multiple actinic keratoses with topical methyl aminolevulinate and red light: results in clinical practice and correlation with fluorescence imaging]. *Actas Dermosifiliogr*, 99(10):779–87, December 2008. ISSN 0001-7310. 129, 132

[20] T Gambichler, R Matip, G Moussa, P Altmeyer, and K Hoffmann. In vivo data of epidermal thickness evaluated by optical coherence tomography: effects of age, gender, skin type, and anatomic site. *J Dermatol Sci*, 44(3):145–52, December 2006. ISSN 0923-1811. 112

[21] I Georgakoudi, M G Nichols, and T H Foster. The mechanism of photofrin photobleaching and its consequences for photodynamic dosimetry. *Photochem Photobiol*, 65(1):135–44, January 1997. ISSN 0031-8655. 114

[22] M J P Gerritsen, T Smits, M M Kleinpenning, P C M van de Kerkhof, and P E J van Erp. Pretreatment to enhance protoporphyrin ix accumulation in photodynamic therapy. *Dermatology*, 218(3):193–202, 2009. ISSN 1421-9832. 116

REFERENCES

[23] P Gholam, K Denk, T Sehr, A Enk, and M Hartmann. Factors influencing pain intensity during topical photodynamic therapy of complete cosmetic units for actinic keratoses. *J Am Acad Dermatol*, June 2010. ISSN 1097-6787. 131

[24] T Glanzmann, C Hadjur, M Zellweger, P Grosiean, M Forrer, J P Ballini, P Monnier, H van den Bergh, C K Lim, and G Wagnières. Pharmacokinetics of tetra(m-hydroxyphenyl)chlorin in human plasma and individualized light dosimetry in photodynamic therapy. *Photochem Photobiol*, 67(5):596–602, May 1998. ISSN 0031-8655. 113

[25] S Grapengiesser, M Ericson, F Gudmundsson, O Larkö, A Rosén, and A-M Wennberg. Pain caused by photodynamic therapy of skin cancer. *Clin Exp Dermatol*, 27(6):493–7, September 2002. ISSN 0307-6938. 131

[26] S H Ibbotson, C Jong, A Lesar, J S Ferguson, M Padgett, M O'Dwyer, R Barnetson, and J Ferguson. Characteristics of 5-aminolaevulinic acid-induced protoporphyrin ix fluorescence in human skin in vivo. *Photodermatol Photoimmunol Photomed*, 22(2):105–10, April 2006. ISSN 0905-4383. 130

[27] E W Jeffes, J L McCullough, G D Weinstein, R Kaplan, S D Glazer, and J R Taylor. Photodynamic therapy of actinic keratoses with topical aminolevulinic acid hydrochloride and fluorescent blue light. *J Am Acad Dermatol*, 45(1):96–104, July 2001. ISSN 0190-9622. 113

[28] G B E Jemec. A simple method for routine measure of photodynamic therapy-associated pain. *Photodermatol Photoimmunol Photomed*, 26(1):51–2, February 2010. ISSN 1600-0781. 131

[29] Claire Johnson. Measuring pain. visual analog scale versus numeric pain scale: What is the difference? *J Chiropr Med*, 4 (1):43–4, 2005. ISSN 1556-3707. 118, 131

[30] A Juzeniene, P Juzenas, L W Ma, V Iani, and J Moan. Effectiveness of different light sources for 5-aminolevulinic acid photodynamic therapy. *Lasers Med Sci*, 19(3):139–49, 2004. ISSN 0268-8921. 113

[31] G B Langley and H Sheppeard. The visual analogue scale: its use in pain measurement. *Rheumatol Int*, 5(4):145–8, 1985. ISSN 0172-8172. 118

[32] H J Laubach, S K Chang, S Lee, I Rizvi, D Zurakowski, S J Davis, C R Taylor, and T Hasan. In-vivo singlet oxygen dosimetry of clinical 5-aminolevulinic acid photodynamic therapy. *J Biomed Opt*, 13(5):050504, 2008. ISSN 1083-3668. 113

[33] A Marti, P Jichlinski, N Lange, J-P Ballini, L Guillou, H J Leisinger, and P Kucera. Comparison of aminolevulinic acid and hexylester aminolevulinate induced protoporphyrin ix distribution in human bladder cancer. *J Urol*, 170(2 Pt 1):428–32, August 2003. ISSN 0022-5347. 130

[34] N McLoone, R F Donnelly, M Walsh, O M Dolan, McLoone, K McKenna, and P A McCarron. Aminolaevulinic acid diffusion characteristics in 'in vitro' normal human skin and actinic keratosis: implications for topical photodynamic therapy. *Photodermatol Photoimmunol Photomed*, 24(4):183–90, August 2008. ISSN 1600-0781. 113

[35] J Moan, L W Ma, and V Iani. On the pharmacokinetics of topically applied 5-aminolevulinic acid and two of its esters. *Int J Cancer*, 92(1):139–43, April 2001. ISSN 0020-7136. 130

[36] C Morton, S Campbell, G Gupta, S Keohane, J Lear, I Zaki, S Walton, N Kerrouche, G Thomas, and P Soto and. Intraindividual, right-left comparison of topical methyl aminolaevulinate-photodynamic therapy and cryotherapy in subjects with actinic keratoses: a multicentre, randomized controlled study. *Br J Dermatol*, 155(5):1029–36, November 2006. ISSN 0007-0963. 113

[37] C A Morton. Methyl aminolevulinate (metvix) photodynamic therapy - practical pearls. *J Dermatolog Treat*, 14 Suppl 3: 23–6, 2003. ISSN 0954-6634. 113, 116

[38] C A Morton, S B Brown, S Collins, S Ibbotson, H Jenkinson, H Kurwa, K Langmack, K McKenna, H Moseley, A D Pearse, M Stringer, D K Taylor, G Wong, and L E Rhodes. Guidelines for topical photodynamic therapy: report of a workshop of the british photodermatology group. *Br J Dermatol*, 146 (4):552–67, April 2002. ISSN 0007-0963. 130

[39] H Moseley. Light distribution and calibration of commercial pdt led arrays. *Photochem Photobiol Sci*, 4(11):911–4, November 2005. ISSN 1474-905X. 118

[40] M J Niedre, C S Yu, M S Patterson, and B C Wilson. Singlet oxygen luminescence as an in vivo photodynamic therapy dose metric: validation in normal mouse skin with topical amino-levulinic acid. *Br J Cancer*, 92(2):298–304, January 2005. ISSN 0007-0920. 113

[41] B Ortiz-Policarpio and H Lui. Methyl aminolevulinate-pdt for actinic keratoses and superficial nonmelanoma skin cancers. *Skin Therapy Lett*, 14(6):1–3, 2009. ISSN 1201-5989. 113, 130

[42] D Pariser, R Loss, M Jarratt, W Abramovits, J Spencer, R Geronemus, P Bailin, and S Bruce. Topical methyl-aminolevulinate photodynamic therapy using red light-emitting diode light for treatment of multiple actinic keratoses: A randomized, double-blind, placebo-controlled study. *J Am Acad Dermatol*, 59(4):569–76, October 2008. ISSN 1097-6787. 113, 130

[43] D M Pariser, N J Lowe, D M Stewart, M T Jarratt, A W Lucky, R J Pariser, and P S Yamauchi. Photodynamic therapy with topical methyl aminolevulinate for actinic keratosis: results of a prospective randomized multicenter trial. *J Am Acad Dermatol*, 48(2):227–32, February 2003. ISSN 0190-9622. 112, 113, 116

[44] Q Peng, T Warloe, K Berg, J Moan, M Kongshaug, K E Giercksky, and J M Nesland. 5-aminolevulinic acid-based photodynamic therapy. clinical research and future challenges. *Cancer*, 79(12):2282–308, June 1997. ISSN 0008-543X. 112

[45] P J F Quaedvlieg, E Tirsi, M R T M Thissen, and G A Krekels. Actinic keratosis: how to differentiate the good from the bad ones? *Eur J Dermatol*, 16(4):335–9, 2006. ISSN 1167-1122. 111

[46] D J Robinson, H S de Bruijn, N van der Veen, M R Stringer, S B Brown, and W M Star. Fluorescence photobleaching of ala-induced protoporphyrin ix during photodynamic therapy of normal hairless mouse skin: the effect of light dose and irradiance and the resulting biological effect. *Photochem Photobiol*, 67(1):140–9, January 1998. ISSN 0031-8655. 113, 132

[47] S J Salasche. Epidemiology of actinic keratoses and squamous cell carcinoma. *J Am Acad Dermatol*, 42(1 Pt 2):s4–s7, January 2000. ISSN 0190-9622. 111

[48] C Sandberg, B Stenquist, I Rosdahl, A M Ros, I Synnerstad, M Karlsson, F Gudmundson, M B Ericson, O Larkö, and A M Wennberg. Important factors for pain during photodynamic therapy for actinic keratosis. *Acta Derm Venereol*, 86(5):404–8, 2006. ISSN 0001-5555. 118, 131

[49] C Sheng, P J Hoopes, T Hasan, and B W Pogue. Photobleaching-based dosimetry predicts deposited dose in ala-ppix pdt of rodent esophagus. *Photochem Photobiol*, 83 (3):738–48, 2007. ISSN 0031-8655. 114, 132

[50] M Asif A Siddiqui, Caroline M Perry, and Lesley J Scott. Topical methyl aminolevulinate. *American Journal of Clinical Dermatology*, 5(2):127–37, 2004. 113

[51] T Smits, C A Robles, P E J van Erp, P C M van de Kerkhof, and M J P Gerritsen. Correlation between macroscopic fluorescence and protoporphyrin ix content in psoriasis and actinic keratosis following application of aminolevulinic acid. *J Invest Dermatol*, 125(4):833–9, October 2005. ISSN 0022-202X. 131

[52] T Smits, A I M van Laarhoven, A Staassen, P C M van de Kerkhof, P E J van Erp, and M-J P Gerritsen. Induction of protoporphyrin ix by aminolaevulinic acid in actinic keratosis, psoriasis and normal skin: preferential porphyrin enrichment in differentiated cells. *Br J Dermatol*, 160(4):849–57, April 2009. ISSN 1365-2133. 130

[53] R Sørensen, V Iani, and J Moan. Kinetics of photobleaching of protoporphyrin ix in the skin of nude mice exposed to different fluence rates of red light. *Photochem Photobiol*, 68(6): 835–40, December 1998. ISSN 0031-8655. 132

[54] M Stücker, A Struk, P Altmeyer, M Herde, H Baumgärtl, and D W Lübbers. The cutaneous uptake of atmospheric oxygen contributes significantly to the oxygen supply of human dermis and epidermis. *J Physiol*, 538(Pt 3):985–94, February 2002. ISSN 0022-3751. 114

[55] R M Szeimies, R T Matheson, S A Davis, A C Bhatia, Y Frambach, W Klövekorn, H Fesq, C Berking, J Reifenberger, and D Thaçi. Topical methyl aminolevulinate photodynamic therapy using red light-emitting diode light for multiple actinic keratoses: a randomized study. *Dermatol Surg*, 35(4):586–92, April 2009. ISSN 1524-4725. 113

[56] M Tarstedt, I Rosdahl, B Berne, K Svanberg, and A M Wennberg. A randomized multicenter study to compare two treatment regimens of topical methyl aminolevulinate (metvix)-pdt in actinic keratosis of the face and scalp. *Acta Derm Venereol*, 85(5):424–8, 2005. ISSN 0001-5555. 113

[57] N van der Veen, H S de Bruijn, R J Berg, and W M Star. Kinetics and localisation of ppix fluorescence after topical and systemic ala application, observed in skin and skin tumours of uvb-treated mice. *Br J Cancer*, 73(7):925–30, April 1996. ISSN 0007-0920. 130

[58] A Virgili, F Osti, C Maranini, and M Corazza. Photodynamic therapy: parameters predictive of pain. *Br J Dermatol*, 162 (2):460–1, February 2010. ISSN 1365-2133. 118

[59] X L Wang, H W Wang, Z Huang, H Stepp, R Baumgartner, C Dannecker, and P Hillemanns. Study of protoporphyrin ix (ppix) pharmacokinetics after topical application of 5-aminolevulinic acid in urethral condylomata acuminata. *Photochem Photobiol*, 83(5):1069–73, 2007. ISSN 0031-8655. 130

[60] C B Warren, L J Karai, A Vidimos, and E V Maytin. Pain associated with aminolevulinic acid-photodynamic therapy of skin disease. *J Am Acad Dermatol*, 61(6):1033–43, December 2009. ISSN 1097-6787. 131

[61] S R Wiegell, I M Stender, R Na, and H C Wulf. Pain associated with photodynamic therapy using 5-aminolevulinic acid or 5-aminolevulinic acid methylester on tape-stripped normal skin. *Arch Dermatol*, 139(9):1173–7, September 2003. ISSN 0003-987X. 130, 131

[62] S R Wiegell, J Skiveren, P A Philipsen, and H C Wulf. Pain during photodynamic therapy is associated with protoporphyrin ix fluorescence and fluence rate. *Br J Dermatol*, 158 (4):727–33, April 2008. ISSN 0007-0963. 116, 118, 129, 131

[63] S R Wiegell, M Haedersdal, and H C Wulf. Cold water and pauses in illumination reduces pain during photodynamic therapy: a randomized clinical study. *Acta Derm Venereol*, 89(2): 145–9, 2009. ISSN 0001-5555. 118, 131

[64] B Wilson, M Patterson, and L Lilge. Implicit and explicit dosimetry in photodynamic therapy: a new paradigm. *Lasers in Medical Science*, 12(3):182–199, 1997. doi: http://dx.doi.org/10.1007/BF02765099. 113

[65] V A Yantsos, N Conrad, E Zabawski, and C J Cockerell. Incipient intraepidermal cutaneous squamous cell carcinoma: a proposal for reclassifying and grading solar (actinic) keratoses. *Semin Cutan Med Surg*, 18(1):3–14, March 1999. ISSN 1085-5629. 111, 131

[66] T C Zhu and J C Finlay. The role of photodynamic therapy (pdt) physics. *Med Phys*, 35(7):3127–36, July 2008. ISSN 0094-2405. 113

Conclusions and Future Prospects

12

Conclusions

In this thesis, we focused on three projects in the field of photomedicine. The common, long term goal was to find methods and tools allowing for a better control of the parameters for the corresponding light-based treatment, in order to reduce, as much as possible, the inter- and intra-patient variations in the treatment's outcome.

Substantial differences existed in the technical and human environment of these three projects. Finally, it was interesting to find that occasionally economical interests or issues of intellectual property could also influence the approache token. In the CAM study (Part II), the measured values of tissular oxygen consumed during PDT, as determined by measuring the DF of the PS, were found to be, as expected, nicely correlated with the induced PDT vascular effects, suggesting a method for monitoring, controlling, and possibly adapting the light dose during PDT treatments. Similarly, in the actinic keratosis study (Part III), the measured amount of photobleaching of the photosensitizer was also found to be, correlated with the clinical outcome of the treatment, again suggesting a method for optmizing this treatment. However, in the infrared thermal laser therapy study (Part I), we could *not* find, with our setup, the hypothesized correlation between the eye fundus reflectance, and the occurence of retinal burns, and could *not*, therefore, propose this method as a monitoring solution.

But in all three experiments, exploring the complexity of the corresponding, detailed biotechnical situation, was a mind-stimulating experience, which in addition to the positive results, found in two out of three studies, has led us to formulate some suggestions for future research and applications, as detailed hereunder.

13

Future Prospects

For the *HRL "subthreshold" thermal treatment* study, we propose a strategy where the laser delivery device would be combined with an optical coherence tomograph, allowing for real-time monitoring of the reflectance of a selected structure in the chorioretinal volume. Thus, during the infrared laser therapy, the denaturation of proteins, which causes changes in the tissue reflectance, could be detected, and, by monitoring the reflectance of a specific deep seated structure, it may be possible to optimize the light dose administered to the eye fundus.

From a clinical point of view, HRL therapy still needs to be more extensively assessed by a scientific study, comparing its clinical outcome with the results of another standard therapy. The study should be focused on those pathologies where HRL seams to be more efficient than other standard therapies (*e.g. Retinitis Pigmentosa*). To support the current clinical use of HRL, to support the fact that the applied laser shots must be at the upper limit of the subthreshould regime, deeper insight on the processes initiated by the thermal laser need to be gained.

In the *in vivo CAM oxygen measurement* study, our measurements were affected by large error bars. One possible cause may reside in the gradient in tissular oxygen concentration, existing within the studied CAM region. The oxygen concentration, at a specific CAM location, probably depends on the distance to the nearest artery. We therefore propose to work with larger CAM surface zones ($\approx \varnothing 2 - 4\ mm$ zones, rather than $\approx \varnothing 500\,\mu m$ zones probed in the present experiments), to effectively average out these inhomogeneities. Another interesting possibility, would be to quantify the existing oxygen gradient, in the space between artery and vein. Such measurements could confirm that the observed errors are indeed linked to

pO_2 inhomogeneities in the CAM, and, possibly, be used to verify the differences in oxygen consumption between normal, hyperplastic, dysplastic, and malignant tissues.

Referring to the delayed fluorescence measurement method applied in the above study, an identical strategy could be applied when using photosensitizers other than PpIX. Verteporfin (BPD-MA, Visudyne®), used in ophthalmology for the treatment of choriodal neovascolarization in the case of wet AMD, is an interesting candidate. Here too, measuring the tissular pO_2 and adapting the light dose accordingly, could yield valuable information and lead to an improved PDT efficacy and possibly early detection of the disease.

Regarding the delayed fluorescence measurement setup used, by substituting the single optical fiber, used as a probe, by an optical fiber *bundle*, we could increase the fraction of collected photons. For example, by using one of the fibers in the bundle to excite the sample, and by then collecting the luminescence with the entire bundle, we could increase the collection fraction by about a factor of 3. This would also allow us to reduce the probing laser excitation intensity, thus further reducing the perturbation induced by the measurement in the probed tissue. As a possible, additional benefit, replacing the single probing fiber by an optical fiber bundle, and adapting the time-resolved spectrofluorometer so as to sequentially inject the excitation light in the different fibers of the bundle, it would be possible to *draw a 2D map of the oxygen distribution* in the inspected sample.

Regarding the *Actinic Keratosis outcome evaluation* study, let us first note that confirmation of the preliminary clinical outcome evaluation, at 1 year from the treatment, is scheduled to take place between September 2010 and January 2011. To verify the conclusions drawn from the present study and broaden its field of application, further clinical studies could be designed. For example, to explore if the clinical outcome would be indeed more stable if the *the drug light interval is individualized* in function of the lesion fluorescence measured just before illumination.

The photobleaching of the photosensitizer could be measured in function of the clinical result, when treating deeper seated lesions such as nodular BCCs, or during the treatment of deeper skin structures (sebaceous glands, hair bulbs). This would allow to verify if the results found in this study could be applied to the treatment of non superficial targets. Finally the same developed imaging apparatus, could be adapted and used as a simple and quantitative Wood's lamp to *quantify a skin pigmentation defect*(*e.g.* in vitiligo) or evaluate the efficacy of various existing treatments for the menagement of pigmentation disorders.

Acknowledgements

14

Acknowledgements

The present thesis is a patchwork of different projects in the interdisciplinary field of biomedical optics. Therefore, the 5 years of my PhD thesis are characterized by strong interactions with several different experts in medicine, biology, chemistry and physics. Actually, by fairly subdividing the present work into the contributions brought by every single person involved in the different projects, we would probably realize that my part is just marginal. In the following paragraph, I would like and I would try to thank all of you. First I will start with all my colleagues at the EPFL and then I will cite all the colleagues working in the clinics.

I thanks Prof Hubert van den Bergh who gave me the opportunity to be a PhD student in his laboratory. I appreciate the proven interest in the work developed during this period, the enthusiasm and his availability. In the same time, I would like to remember Jean-Pierre Ballini who was always ready to help, advise, discuss and propose new idea to solve any kind of problem. Jean-Pierre's scientific approach has been and it is still a reference example for many different aspects. Eddy Forte strongly helped me particularly at the end of my thesis period. He was charged to correct my awful English and transform the dyslexic phrases in real sentences (You have probably already realized that this final paragraph was not corrected...). Out of this unpleasant task, Eddy has been fundamental to discuss, clarify and finalize the results and the conclusions of the developed projects. My thesis director was Dr Georges Wagniéres.

A special thank to Blaise Lovisa who was always ready to listen and discuss ... the same topics; Tanja Gabrecht with a rich knowledge in many fields; Anna Maria Novello who actually performed all the CAM in-vivo measurements (Grande Anna!); Senthil Rajendran who transform egg hatching in art; Bernadette Pegaz who, without success, tried to hide her real

name; Elodie Debefve pédalo world champion; Jerôme Barge unfortunately suffering from chaetophobia since several years; Patrycja Nowak-Sliwinska the nice Polish girl ready for the war; Véronique Bauler, Stefania Tartaglia and Roxane Mischler who make the group running smoothly. Finally, I would like to thanks Flavio Comino for the excellent handcraft skills and the team of André Fattet work their excellent work in the design and realization of the mechanical part used in the different projects.

As already mentioned part of this thesis were accomplished in clinics, in direct collaboration with secretaries, technical staff, nurses and medical doctors. The team of Dr Vezzola's medical practice: Roberto Perotti who performed all the measurements in the frame work of the opthalmologic study; Patrizia Velardita who was always present to solve organizational issues; Sharra Dashamir; Serena Rubinelli; Stefania Tonoli; Costantino Centillo and Elena Ponciroli. A special thanks to Dr Edoardo Vezzola who welcome me to his medical practice took the time to explain me many different medical aspects. In the frame work of the same project I would like to thank also the team of Dr Sickenberg's medical practice with which we actually initiated the project. A special thanks to Dr Michel Sickenberg for his patience and for the enriching discussions.

In the frame work of the dermatological study I would like to thank all the staff of the "Service de dermatologie et vénéréologie - HUG": Yvette Armand who helped me a lot for all the bureaucratic and organizational issues; Carmen Cuesta, Catherine Lemarquis and Ana Deschenaux who were taking care of all the patients and controlled that the clinical protocol was correctly followed. A special thanks to Dr Behrooz Kasraee who actually performed all the fluorescence and clinical measurements with high precision and care. Without his professionalism and tenacity this clinical study would probably not end with such interesting results! Finally I am really grateful to Dr Denis Salomon for giving me the opportunity to work in his team and profit of his knowledges.

To conclude I would like to thank my family and friends for their support, their care and their patience. I would not have made it without you all. La famiglia *SalcioK*: Dado, Marco, Gianni, Chiaretta, Diego, Lüis, Davide, Riki, Roby, Livia, Graziella, Gaby, John, Micki, Poma, Desche, Oli, Ori, Crick, Fla, Gio, Leo, Piero, Luisella, Ale, Johnny, Seba, Shampo lassativo, Godo, Tanika ...I *dinosauri* del Poly: Gamba, Desche, Shrutha, Rajnish, Katia, Thomas, Skuro, Sam, Baffuz, Sebi, Nano, Charlie, LOliver, Fomy ...

Appendices

Appendix, Part II

II.A PpIX's Luminescence and Signal Processing

The luminescence emitted by a fluorochrome (PpIX in our case) is actually consequence of energy relaxation leading the electrons being in the excited electronic state to be transfered in a lower energetic state. The desexcitation probability of this excited population is found to be proportional to itself. Therefore, by integration of the excited population over time, the emitted luminescence results to follow an exponential decay.

In a more general situation, a real system maybe composed by different fluorochromes conformations (aggregates), different environments surrounding the studied fluorochromes and different possible deexcitation pathway. Thus, the emitted luminescence would be characterized by a sum of exponential decays (see Equation 1).

$$L(t) = \sum_i L_i e^{-t/\tau_i} \tag{1}$$

where $L(t)$ is the total luminescence, L_i are the specific intensities of each emissive contribution at $t = 0$, and τ_i are the characteristic lifetimes.

In our case, the PpIX's luminescence is recorded by mean of a transducer, a photo multiplier tube (PMT) which transforms the emitted photon into an analog electrical signal which is successively digitalized and exported in an ASCII format by a digital storage oscilloscope (DSO). Thus, the recorded signal is analyzed and fitted by a multi-exponential mathematical scheme to model the emissive phenomenon.

Non-linear regression by least squares estimation (NLS) is a well known and approved method to efficiently fit the recorded data $[y_i]$ to a mathematical model. The strategy used to estimate the regression function $f(\vec{t};\vec{\beta})$ is based on the minimization of the sum of the

squared residuals, *i.e.* the sum of the squared deviation between the observed data $[y_i]$ and the estimated model $[f(\vec{t_i};\vec{\hat{\beta}})]$ (see Equation 2).

$$Q = \sum_{i=1}^{n} [y_i - f(\vec{t_i};\vec{\hat{\beta}})]^2 \tag{2}$$

To iteratively minimize the residuals, different algorithms can be employed, the most reliable and most commonly used is the Levenberg-Marquardt computational method. During the fitting process, the estimated model's parameters $(\hat{\beta}_0, \hat{\beta}_1, \ldots)$ are treated as the variables, and the independent variable values $(t_1, t_2, \ldots)$ are treated as coefficients of the regression function. To successfully fit the recorded data initial estimates of each model's parameter $(\hat{\beta}_0, \hat{\beta}_1, \ldots)$ must be provided. Successively, the algorithm adjusts and update those parameter's to minimize the residuals (see Equation 3) and therefore produces a better mathematical fit to the measured data.

$$dQ(\beta_i) = 0 \tag{3}$$

During this process, it is very important to provide a precise initial estimate to assure the conversion of the algorithm to the real minimum of the residual function $(Q(\beta_i))$ and not to local minimum that would produce unacceptable solutions. Additionally, to further enhance the regression quality, the recorded data are unevenly weighted to increase the contribution of these data points that are less affected by the noise, thus giving to the points with a lower variance a greater statistical weight (See Equation 4).

$$Q = \sum_{i=1}^{n} w_i \, [y_i - f(\vec{x}_i;\vec{\hat{\beta}})]^2 \tag{4}$$

II.B Algorithm Performances

The results of a fitting calculation are regretfully influenced by the initial parameters fed to the algorithm. The ability to provide a stable mathematical solution with only weak sensibility to the initial parameters is a very important characteristic of a fitting algorithm. The algorithm performances need to be tested with simulated experimental data, where the exact solution is known, and therefore the fitting process and the performance of the algorithm can be deeply and precisely analyzed. Preliminary PpIX *in vitro* and *in vivo* measurements show that molecule relaxation is characterized by a bi-exponential phenomena with lifetime in the μs range. To have a more realistic situation the simulated data $S(t)$ were artificially created with a bi-exponential mathematical decay model to which was added a certain amount of random noise (see Equation 5). Different scenarios were taken into account to simulate different possible experimental data and evaluate the influence of several different parameters over the fitting quality. The goal of these simulations was to test the limits and the working range where the fitting solution can be considered accurate.

$$S(t) = A_1\, exp^{(t/\tau_1)} + A_2\, exp^{(t/\tau_2)} + rnd(k) \tag{5}$$

With exception of the initial estimated model's parameters (A_i and τ_i, see Equation 5), the quality of the fitting was studied by changing three important algorithm's parameters:

1. The standard error added to the simulated data $rnd(k)$ ($\mu_{rnd} = 0$, $\sigma_{rnd} = [1 \times 10^{-4}$ - $5 \times 10^{-3}]$).

2. The delay between the laser excitation pulse and the beginning of the signal's analysis (See ΔD in Figure II.B).

3. The period T over which the signal was analyzed.

The simulations were carried out by considering always the same exponential decay ($A_1 =$ 0.5 Volt, $\tau_1 = 40\ \mu s$, $A_2 = 2$ Volt, $\tau_2 = 10\ \mu s$) and by an indipendent evaluation of the effects of each studied parameter. Therefore, the simulated experimental data were fitted 100 different times, the fitting solution's variation was recorded and analysed. The goal was, in fact, to precisely define the parameters range that will permit to obtain an accurate fit minimizing, at the same time, the errors over the evaluated lifetimes.

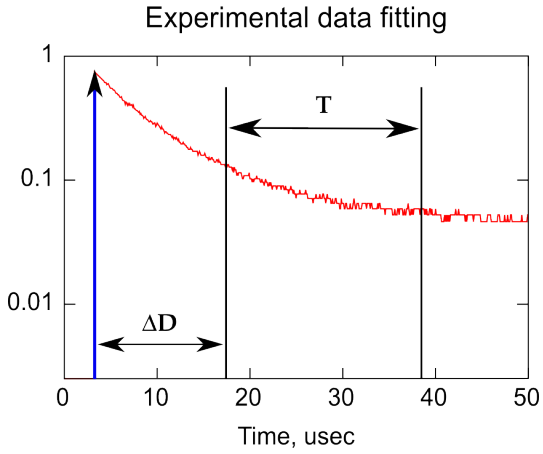

Figure 1: Illustrative figure for the definition of two parameters considered for the analysis of the algorithm's solution. ΔD is the signal analysis delay from the excitation pulse, T the signal analysis period.

The influence of the added random error is of main interest, in particular to evaluate the accuracy of the solution when real data are analyzed. In fact, by knowing the relation between dispersions of the algorithm's solution in function of the simulated data error, we are able, by measuring the dispersion between the recorded data and the algorithm's solution, to precisely define the error over the solution found. As a consequence, the dispertion over the simulated signal intensity needs to be smaller than $2\,mV$ to obtain a fitting solution with a lifetime error smaller that 5% (see table II.B).

Table 1: Errors of the fitting process in function of the standard deviation (σ_{rnd}) of the random error added to the simulated data

Standard deviation of the random error (σ_{rnd})	$E_{A_1}[\%]$	$E_{\tau_1}[\%]$	$E_{A_2}[\%]$	$E_{\tau_2}[\%]$
1×10^{-4}	18.12	0.01	4.92	0.06
1×10^{-3}	17.98	0.013	5.50	1.75
2×10^{-3}	18.24	0.01	4.43	3.94
3×10^{-3}	15.92	1.65	13.90	26.80
4×10^{-3}	17.13	0.48	7.96	15.43
5×10^{-3}	16.89	1.06	10.04	22.07

The delay between the laser excitation pulse and the beginning of the signal's analysis, affects only marginally the fitting process. We could, anyway conclude that this delay ΔD has

to be smaller than the shortest lifetime. (see table 2). Finally, we observed that the fitting quality is not dramatically dependent on the analysis period T. Nevertheless, the analysis period T should not be smaller than the half of the longest lifetime 3. Moreover, by considering very long analysis periods, we observed the efficacy of the algorithm (variance based weighted data) to ponderate the experimental data and therefore consider only the data not dramatically affected by a strong error. II.B

Table 2: Errors of the fitting process in function of the delay (ΔD) form the excitation source

Delay form the excitation, ΔD $[\mu s]$	$E_{A_1}[\%]$	$E_{\tau_1}[\%]$	$E_{A_2}[\%]$	$E_{\tau_2}[\%]$
1	9.59	0.04	2.16	0.20
2	18.10	0.08	5.37	0.74
3	25.47	0.34	9.06	2.48
4	33.06	0.09	9.14	0.22
5	39.60	0.23	10.71	0.87
10	62.73	0.69	24.06	3.25
14	78.54	79.50	16.82	9.29

Table 3: Errors of the fitting process in function of the analysis period (T)

Analysis period, T $[\mu s]$	$E_{A_1}[\%]$	$E_{\tau_1}[\%]$	$E_{A_2}[\%]$	$E_{\tau_2}[\%]$
20	17.77	0.25	6.34	1.93
50	18.13	0.01	4.85	0.02
100	18.13	0.01	4.87	0.02
300	18.12	0.0	4.89	0.01
500	18.13	0.01	4.85	0.02

The performances of the algorithm where also studied in function of the guessed parameters entered. The stability of the solution is tightly bind to the local minima present in the residual function. The algorithm typically converge to the correct solution even if the guessed parameters are one order of magnitude away from the real solution. As general rule, to reach in a fast way an accurate approximated solution the guessed parameters should be close as much as possible to those of the real solution.

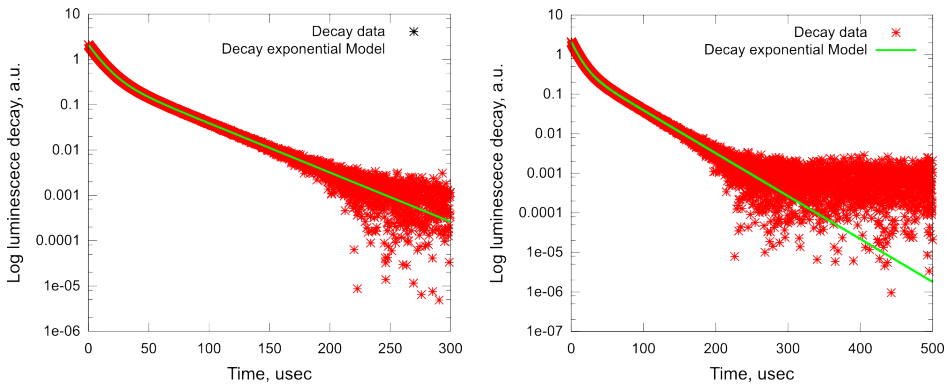

(a) Logaritmic decay $300\,\mu s$ (b) Logaritmic decay $500\,\mu s$

Figure 2: Data error at the of the signal do not affect at all the fitting results

Appendix Part III

III.A Nikon-D90 Sensor Linearity

In the following paragraph we will describe the experience used to verify the linearity of the optical sensor, please refer the bracketed numbers and letters to Figure 1.

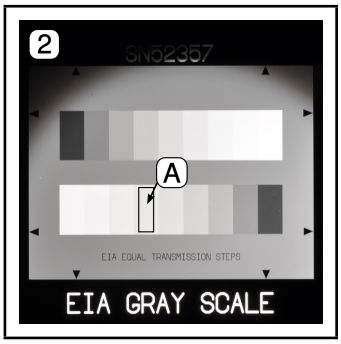

(a) Edmound® - EIA gray scale pattern slide, (A) Region of interest where the trasmitted light was measured

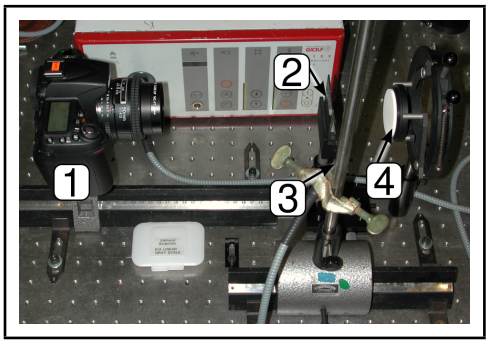

(b) Setup used to measure the linearity of the CMOS sensor

Figure 1: Verification of the linearity of the sensor of a Nikon®- 90D photo camera

The linearity of the CMOS-sensor of the photo camera ((1), Nikon®- 90D) was verified by recording the transmitted light through a standard gray scale pattern slide (GSP, (2), Edmound® - EIA linear transmission). The GSP is, in fact, characterized by nine different zones (see Figure 1(a)) with calibrated transmission. Therefore, by illuminating the GSP with a diffused excitation source and by measuring the average pixel value, of a defined surface (A), the linearity of the sensor was verified. With more details, a white light, fiber based, light source ((3), Richard Wolf®-IP20) was directed on a white reflecting coating ((4), SphereOptics

Hoffman® SRM-99H) to generate an homogeneous illumination of the GSP. Successively, to further reject the inhomogeneities of the intensity distribution of this illumination the GSP was translated horizontally. As a consequence the light transmitted through the 9 different zones was measured completely independently of the intensity distribution of the illumination. A very good linearity was observed, see Figure 2.

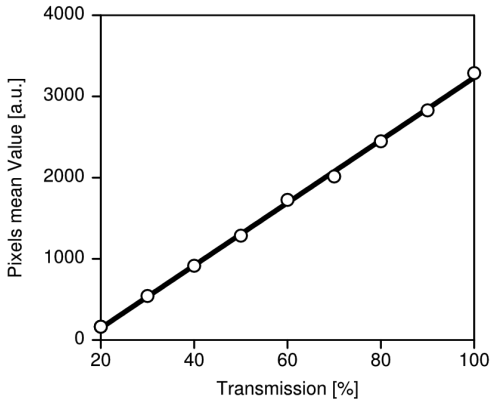

Figure 2: Linearity of the CMOS photo camera sensor

III.B Quantitative Light Measurements with Consumer Grade Photo Cameras

Consumer grade cameras, compared to scientific cameras, are much cheaper and additionally not designed for quantitative measurements. The main problem, with consumer grade camera, is that the manufacturing companies do not supply precise specifications of the specific optical components used. For instance, the exact transmission of the red-green-blue (RGB) filter and the spectral sensitivity of the sensor are unknown. Moreover, as a general rule, all these camera have an integrated image precessing unit that modify automatically the recorded pixels to improve the appearance and reduce the dark noise of the recorded scene, thus loosing the quantitative information of the amount of light reaching the camera sensor.

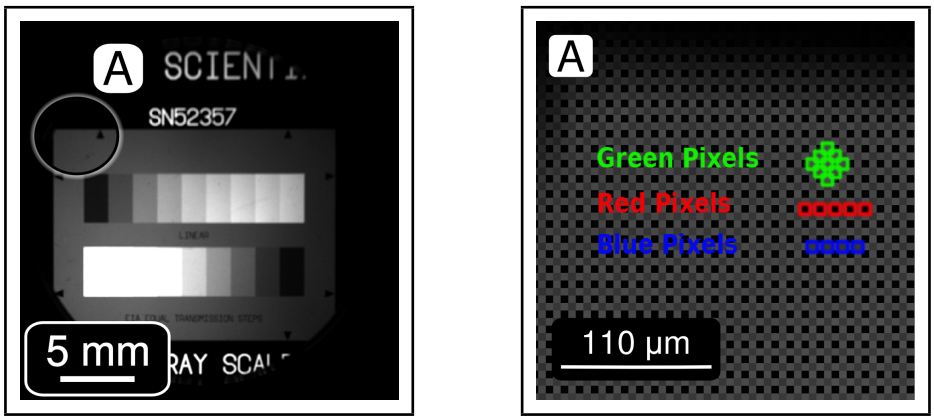

(a) Standard gray scale pattern slide, (A) Region of interest

(b) Red-Green and Blue pixels of the zoom area (A)

Figure 3: Non-interpolated - RAW values, recorded by the CMOS sensor

Modern semi-professional and professional camera allow the user to record unprocessed images (i.e. RAW image) which claim to be the rigorous digital transformation of the accumulated charges on the camera sensor (see Figure 3). Therefore, by appropriately analyzing "RAW images" and by calibrating the photo camera, quantitative measurement are also accessible with these less expensive devices. As a consequence the "RAW images" were transformed, without any data distrotion, into a more user friendly image format (Portable Pixel Map (ppm)) to be able to analize the 12-bit (dynamic range: 0 - 4096) values recorded in the three separately channels. The image transformations (*i.e.* "the developing a raw image", by analogy with the

process of film development) was realized with the help of a standard tool *dcraw* program. For all quantitative analysis we developed the RAW images with the following command:

```
dcraw -4Dh foo.NEF foo.ppm
```

Where the options of the command:

- 4: Linearly transformation of the 12 bit recorded images into the 16 bit computer compatible format. This option will also fix the picture gamma to 1. To verify these operations we analyzed a saturated images and we observed that the maximal value was still 4096;
- D: Transform the RAW data without pixel interpolation (see Figure 3) and do not scale the channels to compensate the inhomogeneous CMOS sensitivity.
- h: Create an half-size color image by grouping the red and blue pixels (see Figure 3) avoiding any value interpolation. Hereupon, for the green pixels, the average of two successive pixel has been evaluated to create an half-size image. This operation enable to rigorously analyze the pixel values of the red and blue channels (the PpIX fluorescence emission is in fact almost exclusively recorded within the red channel)

Curriculum Vitae

Filippo Piffaretti

Av. de Collonges 1, CH-1004 Lausanne

filippo.piffaretti@epfl.ch

Education

2005-Present	**Federal Institute of Technology, Lausanne** (EPFL) *PhD Student in Photomedicine*
1999-2004	**Federal Institute of Technology, Lausanne** (EPFL) *Microtechnical engineer* EPF (dipl.Micro.Ing EPF) Master's Level in Robotics and Techniques of Production
2000	**Liceo Lugano 1**, Ticino High school diploma Type C (Scientific & math)

Professional Experience

2005-2010	**EPFL Biomedical Photonic Group** Graduate Research Assistant
2004-2005	**EPFL Laboratory of Robotic Systems**, Switzerland Teaching Assistant
2004	**Texas A&M University**, USA Biomedical Engineering Department, Gradaute Research Assistant
Jul-Oct 2002	**Lappennranta University of technologies (LUT)**, Finland Laboratory of Nuclear Engineering, Scientific Trainee

Publications and award

Author or co-author of 3 submitted peer-reviewed publications, 3 oral presentations, 4 posters.

Languages

Italian (mother tongue), English (B2), French (B2), Spanish (B2), German (B1)

Hobbies

Sport activites: rowing, alpine touring ski, paragliding